

McGill University

MORPHOLOGY, SEDIMENTARY FACIES AND PROCESSES OF
THE NORTHWEST ATLANTIC MID-OCEAN CHANNEL
BETWEEN 61° AND 52°N, LABRADOR SEA

by

Sung Kwun Chough

A thesis submitted to the Faculty of Graduate Studies and
Research in partial fulfillment of the requirements
for the degree of Doctor of Philosophy in
the Department of Geological Sciences

Montreal, Quebec
Canada
February, 1978

ABSTRACT

Continuous seismic reflection profiling, echosounding and a core sampling program carried out by and in cooperation with Bedford Institute of Oceanography have provided new information on the morphology, sedimentary facies and processes, and the history of development of the Northwest Atlantic Mid-Ocean Channel of the Labrador Sea.

A sequence of layered sediments approximately 500 m thick consisting predominantly of terrigenous turbidites accompanies the Northwest Atlantic Mid-Ocean Channel (NAMOC) as a broad band and marginally interfingers with the acoustically transparent pelagic and contourite facies of the Labrador Sea. The meandering channel is a depositional-erosional feature formed by submarine mass flows dominated by turbidity currents.

The channel has a meandering talweg and appears to have remained relatively stable for a long time. There is little evidence for extensive lateral channel migration. The talweg is associated with a sequence of subdued submarine point bars which consist of lenticular, discontinuous bodies of thick bedded, coarse-grained turbidites and sand and gravel layers (channel-fill facies).

Natural levees flank the channel for its entire length merging with broad flood plain-like features that extend laterally up to a hundred kilometers. This spill-over facies comprises thin bedded, fine-grained turbidites dominated by thinly laminated muds. A layer-by-layer correlation of a sequence of spill-over turbidites is possible between two adjacent levee cores which are 70 km apart.

Individual units of parallel laminated muds result from single turbidity currents overtopping the channel banks. Each unit consists of laminae

of granular material alternating with laminae of flocculated clayey material a tenth of a millimeter to a few millimeters thick. Upward thickness variation of pairs of granular and flocculated laminae shows a logarithmic relationship with the granular laminae decreasing logarithmically upward in thickness and the flocculated laminae increasing logarithmically upward. This logarithmic thickness variation results from deposition through the viscous sublayer of dilute turbidity currents by mechanisms of sorting and differential settling which are not yet understood in detail.

The thinly laminated spill-over turbidites differ from laminated contourites recovered from Eirik Sedimentary Ridge, off the southern tip of Greenland by the high degree of bioturbation and mottling, and by the predominantly biogenic pelagic and terrigenous ice-rafted constituents of the latter.

The dominant sediment source for the NAMOC was on the northeastern Canadian continental margin, especially in the region off Hudson Strait, to which glaciers supplied a large volume of terrigenous sediments.

Turbidity current activity in the channel probably started with the onset of glaciation at about Mid-Pliocene time. During the end of the last glaciation turbidity current activity in the NAMOC was apparently concentrated in a period of a few thousand years and ceased at about 7,100 y B.P. when deglaciation was rapidly proceeding. Averaged over the period between 20,000 and 7,000 y the episodes of large-scale turbidity currents that overflowed the channel banks probably recurred about every 230 years. The average sedimentation rate of the levee turbidites during the Late Pleistocene is about 13 cm/1000 years. During much of the glacial episodes the northwestern Labrador Sea was covered with sea ice.

Voluminous spill-over muds with relatively high organic carbon content (av. 0.8%) and associated coarse-grained channel-fill sediments of buried deep-sea channels may under suitable diagenetic conditions become targets for future petroleum exploration in the deep-sea.

RESUME

Un programme de profilage par réflexion sismique continu, de sondage ultrasonore et de carottage entrepris avec la collaboration de l'Institut d'océanographie Bedford a permis de recueillir de nouvelles données sur la morphologie, les faciès et l'activité sédimentaires, et l'historique du développement du Chenal médio-Océanique du nord-ouest de l'Atlantique, dans la mer du Labrador.

Une séquence de sédiments stratifiés d'environ 500 m d'épaisseur composée essentiellement de turbidites terrigènes borde le chenal et s'interdigite avec les faciès de contourites et les faciès pélagiques acoustiquement transparents de la mer du Labrador. Le chenal, méandriforme, est une structure d'érosion-déposition formée par des écoulements de masse sous-marins dominés par des courants de turbidités.

Le chenal possède un talweg lui aussi méandriforme et semble être demeuré relativement stable depuis longtemps. Il y a peu d'évidences d'une migration latérale importante. Le talweg est associé à une séquence de barres sous-marines mineures consistant en corps lenticulaires et discontinus de turbidites épaisses et grossières et de lits de sable et de graviers (faciès de remplissage de chenal).

Des levées flanquent le chenal sur toute sa longueur et se perdent dans ce qui semble être une grande plaine d'inondation pouvant s'étendre sur une centaine de kilomètres. Ce faciès de débordement comprend de minces et fines turbidites et, principalement, des boues finement laminées. Une corrélation de lit-à-lit d'une séquence de turbidites de débordement est possible entre deux carottes adjacentes prises dans les levées et situées à 70 km l'une de l'autre.

Chacune des unités des boues laminées résulte d'un courant de turbidité dépassant les rives du chenal. Chaque unité consiste en laminae de matériel granuleux alternant avec des laminae de matériel argileux floculé d'un dixième de millimètre à quelques millimètres d'épaisseur. Il y a relation logarithmique dans la variation verticale de l'épaisseur des couplets de laminae granuleuses et floculées, l'épaisseur des couplets de laminae granuleuses diminuant logarithmiquement vers le haut, et celle des laminae floculées augmentant logarithmiquement vers le haut.

Ces variations logarithmiques d'épaisseurs sont attribuées à une déposition à travers l'horizon laminaire de courants de turbidités de faible concentration où entrent en jeu des mécanismes de tri et de sédimentation différentielle qui ne sont pas encore compris en détail.

Les minces turbidites de débordement se distinguent des contourites recueillies sur la Crête Sédimentaire d'Eirik, au large de l'extrémité méridionale du Groënland, par le degré élevé de bioturbation et de bariolement et par la prédominance de constituants biogènes pélagiques et d'éléments terrigènes dérivés de glaces flottantes qui caractérisent les contourites.

Les sédiments du Chenal médio-océanique du nord-ouest de l'Atlantique ont pour source dominante la plate-forme continentale canadienne, surtout au large du Détroit d'Hudson, qui a reçu des glaciers des apports importants de sédiments terrigènes.

La présence de courants de turbidités actifs dans le chenal remonte probablement à l'établissement de conditions de glaciation vers le milieu du Pliocène. Vers la fin de la dernière glaciation, l'activité de courants de turbidités semble avoir été concentrée à l'intérieur de quelques milliers d'années et cessa vers 7,100 a B.P. lorsqu'une rapide déglaciation eut lieu.

En moyenne, au cours des 20,000 à 7,000 dernières années, les épisodes de courants de turbidités à grande échelle capables de déborder des rives du chenal se produisaient à peu à tous les 230 ans. Le taux moyen de sédimentation des turbidites dans les levées pendant le Pléistocène supérieur est d'environ 13 cm/1,000 ans. Pendant la plus grande partie des épisodes glaciaires, le nord-ouest de la mer du Labrador était couvert de glace.

Des volumes importants de boues de débordement avec un contenu de carbone organique relativement élevé (en moyenne 0.8%) associés à des sédiments grossiers de remplissage de chenaux abyssaux et enfouis dans des environnements diagénétiques adéquats pourraient devenir des cibles intéressantes pour les futures explorations pétrolières en eaux profondes.

CONTENTS

	Page
ABSTRACT	i
RÉSUMÉ	iv
LIST OF FIGURES	x
LIST OF TABLES	xi
LIST OF PLATES	xii
LIST OF APPENDICES	xiii
NOTATIONS	xiv
 <u>CHAPTER I - INTRODUCTION</u>	
Field Work and Data Acquisition	7
 <u>CHAPTER II - MORPHOLOGY</u>	
Channel Position	10
Cross Sectional Profile	10
Longitudinal Profile	12
Channel and Talweg Meandering	14
Submarine Point Bars	17
 <u>CHAPTER III - SEDIMENTARY FACIES</u>	
Facies Distribution	21
Channel-fill Facies	23
Occurrence	23
Sedimentary Structures and Texture	26
Spill-over Facies	28
Occurrence	28
Sedimentary Structures and Texture	28
Crudely Laminated Sand-Silt-Clay division (T_{an})	31
Graded or Massive Sand and Sandy Gravel Division (T_a)	33
Parallel Laminated Sand Division (T_b)	33
Cross-Laminated Silt Division (T_c)	33

	Page
Parallel Laminated Mud Division (T_d)	36
Homogeneous Mud Division (T_e)	38
Pelagic Facies	39
Occurrence	39
Characteristics	39
Secondary Sedimentary Structures (Bioturbation) and Texture	41
• Contourite Facies	46
Occurrence	46
Sedimentary Structures and Texture	49
Sequential Analysis of Structure Divisions	50
 <u>CHAPTER IV - PETROGRAPHIC AND MINERALOGIC COMPOSITION</u>	
Gravel Components	53
Sand Fractions	54
Heavy Minerals	54
Light Minerals	55
Silt- and Clay-sized Fractions	56
Ice-rafted Debris	60
Ice-rafted Tephra	61
Organic Carbon	63
 <u>CHAPTER V - CORRELATION AND STRATIGRAPHY</u>	
Correlation of Individual Cores	67
Longitudinal and Lateral Variations	69
Stratigraphy	70
 <u>CHAPTER VI - SEDIMENTARY PROCESSES</u>	
Channel Processes	76
Comparison Between the NAMOC and Subaerial Meandering Channels	78
Turbidity Current Processes in the NAMOC	81
Spill-over Processes	87
Deposition of Laminated Turbidite Muds	92
Levee Turbidites vs. Contourites	97

	Page
Source of Sediment	100
History of Channel Development	102
Paleoceanography	106
Sedimentological Effects of Ice Cover	106
 <u>CHAPTER VII - SUMMARY AND CONCLUSION</u>	
Channel Processes	110
Spill-over Facies	111
Source of Sediment	113
History of Channel Development	113
Suggestions for Further Research	114
 ACKNOWLEDGEMENTS	 115
REFERENCES	118

LIST OF FIGURES

	Page
1. Major Physiographic Features of the Labrador Sea	3
2. Bathymetric Chart of the Labrador Sea	5
3. Bathymetric and Seismic Survey Tracks and Core and Camera Stations	9
4. Transverse Profiles across the NAMOC	11
5. Longitudinal Profiles of the NAMOC	13
6. Ship Track and Meander Pattern of the Channel and Talweg	15
7. Bathymetric Profiles Across and Along the NAMOC Showing the Talweg	16
8. Meander Wavelength vs. Channel Width	18
9. Subbottom Reflectors from the Channel Floor	20
10. Sedimentary Facies Distribution	22
11. Main Sediment Types of Channel-fill Cores	24
12. Cumulative Granulometric Curves of Channel-fill and Spill-over Facies	29
13. Classification According to Grain Size of Spill-over Deposits	32
14. Analysis of the Laminated Spill-over Facies	35
15. Upward Thickness Variation of Pairs of Granular and Flocculated Laminae in Parallel Laminated Mud	37
16. Classification According to Grain Size of Pelagic Lutites and Contourites	40
17. Cumulative Granulometric Curves: Pelagic Lutites and Contourites	42
18. Surface and Bottom Currents in the Labrador Sea	48
19. Turbidite Structure Sequence of the Spill-over Facies	51
20. X-ray Diffractograms of Turbiditic and Pelagic Sediments	58

	Page
21. Vertical Variation in Mineralogical Composition	59
22. Correlation of Disseminated Tephra Particles in Pelagic Lutite	62
23. Organic Carbon Content Plotted Against Core Depth	64
24. Frequency Histogram of Organic Carbon Content	65
25. Correlation of Levee Cores	68
26. Variations of the Foraminiferal Fauna	73
27. Facies Model for the NAMOC	77
28. Head Spill-over Versus Body Spill-over Turbidites	90

LIST OF TABLES .

1. Types of Bioturbation	44
2. Radiocarbon Age Dates	71

LIST OF PLATES

	Page
1. Seismic Reflection Profiles across the Channel	132
2. Gravels of Channel-fill Facies	133
3. Channel-fill Sediments	134
4. Typical Sediments of Spill-over Facies	135
5. Typical Sediments of Spill-over Facies	136
6. Spill-over Sands on the Natural Levees	137
7. Typical Sediments of the Pelagic Facies	138
8. Bioturbation Structures	139
9. Continued	140
10. Continued	141
11. Continued	142
12. Bottom Photographs, NAMOC Floor	143
13. Bottom Photographs, NAMOC Channel Wall	144
14. Contourites from Eirik Ridge; Slightly to Moderately Bioturbated	145
15. Contourites from Eirik Ridge; Very Strongly Bioturbated	146
16. Contourites from Eirik Ridge; Completely Bioturbated and Mottled	147
17. Photomicrographs of the Slightly to Moderately Bioturbated Eirik Ridge Contourites	148
18. Layer-by-layer Correlation of Two Right Levee Cores	149
19. Continued	150
20. Continued	151

LIST OF APPENDICES

	Page
1. Deep-sea Channels of the World's Oceans	152
2. Morphology of the NAMOC and Associated Talweg	153
3. List of Cores Recovered from the NAMOC	154
4. Core Descriptions	155
5. Grain Size Parameters	160
6. Lithology of Channel-fill Pebbles	161
7. Frequency of Heavy Minerals	162
8. Abundance of Tephra and Ice-rafted Debris	163
9. Organic Carbon and Carbonate Contents	165
10. Method to Impregnate Mud for Thin Section Preparation . . .	167

NOTATIONS

α	The ratio of the drag on the upper surface of a turbidity current to the drag on the bottom
A	Positive constant of Bagnold's auto-suspension criterion
β	Bottom slope
β_c	Critical bottom slope
C_1	Keulegan's coefficient
C_b	Particle concentration in suspension
C_f	Drag coefficient
C_o	Initial sediment concentration
C_t	Mean sediment concentration at time t
δ	Thickness of viscous sublayer
D	Flow depth of turbidity current
E	Net ejection rate from viscous sublayer
Fr	Froude number
g	Acceleration due to gravity
h_1	Thickness of head of turbidity current
h_2	Thickness of body of turbidity current
ΔH	Difference in levee height
p	The probability of deposition for a particle from the boundary layer
ρ	Fluid density
ρ_t	Density of turbidity current
$\Delta\rho$	$\rho_t - \rho$
R	Radius of meander
R_d	Net rate of sedimentation from viscous sublayer

Re	Reynolds number
S	Rate of settling input to viscous sublayer
τ	Fluid shear stress
τ_o	Shear stress at bed
τ_c	Critical shear stress
τ_l	Limiting shear stress
ϕ	Latitude
u	Velocity of body of turbidity current
v	Velocity of head of turbidity current
ν	Kinematic viscosity
w	Fall velocity of sediment grains
W	Width of channel
Ω	Angular velocity of earth rotation

CHAPTER I - INTRODUCTION

Marine geological studies of submarine canyons and deep-sea channels have progressively revealed the importance of processes of submarine mass flow in the transport of coarse-grained terrigenous material to the base of slope and the deep ocean basins. These studies have also helped paleohydrodynamic and paleoenvironmental interpretations of ancient sedimentary deposits. Mass flow processes such as slumps, debris flows, grain flows and turbidity currents are not restricted to submarine canyons, fan valleys and deep-sea channels on the continental slope and rise, but also play a role on deep-sea trench plains (Piper et al., 1973), and on abyssal plains (Horn et al., 1971) and on the abyssal sea floor. On the latter some of the largest deep-sea channels occur known as mid-ocean channels. The longest of these channels is the Northwest Atlantic Mid-Ocean Channel of the Labrador Sea and northwest Atlantic Ocean.

Along the course of the Northwest Atlantic Mid-Ocean Channel (henceforth abbreviated as NAMOC) of the Labrador Sea a band of young coarse-grained terrigenous sediments floors the central Labrador Basin, dissecting the blanket of pelagic and hemipelagic sediments. Much of these young sediments were deposited when the Quaternary glaciers extended far out on the northeast Canadian continental shelf. Identification of end moraines and other glacial landforms implies that much of the shelf was covered by the Laurentide ice sheet during the Wisconsinan. Seaward penetration and retreat of the glaciers have deposited large volumes of sediments on the shelf as ground moraines when the sea-level stood lower or as submarine glacial drift under the ice sheet in the deeper outer shelf (Fillon, 1975). Submarine canyons at the shelf edge were the loci of submarine mass flows

which originated from these piles of sediments on the shelf. Especially, the shelf edge off Hudson Strait was a locus for supply of terrigenous material, for the ice lobes flowing out of Hudson and Davis Straits coalesced here (van der Linden et al., 1976).

Different from other continental margins where submarine mass flows in submarine canyons on the slope result in the formation of deep-sea fans at the base of the slope the flows generated off Hudson Strait in the northwestern Labrador Sea apparently bypassed the base of the slope, not forming a deep-sea fan where it would be expected to occur. Instead these flows were guided southward across the deep Labrador and Newfoundland Basins by the NAMOC (Figure 1) which acted as an enormous funnel way for these glacial terrigenous sediments. Individual flows have probably travelled for the entire length of the channel or about 3,800 km. Transport of large amounts of sediment through the channel has probably involved alternating and repeated phases of erosion and deposition, erosion dominating in the channel to keep it clear from excess sediment, and deposition occurring predominantly on the channel banks forming broad natural levees.

Conceivably the submarine mass flows were initiated from the piles of glacial sediment deposited on the shelf edge. This concept, however, leads to a number of questions related to the mechanisms of initiating such flows. What were the mechanisms involved? Did the flows start in the form of subglacial melt water underflows? Did they result from sediment instability due to excessive glacial deposits on the outer shelf? Or were they triggered by more catastrophic events such as earthquakes? Were the flows largely generated under the ice sheet during glacial advance? Or were they mainly generated during the retreat of glaciers from the shelf? What was the volume of individual flows? At what frequency did they occur? Why did

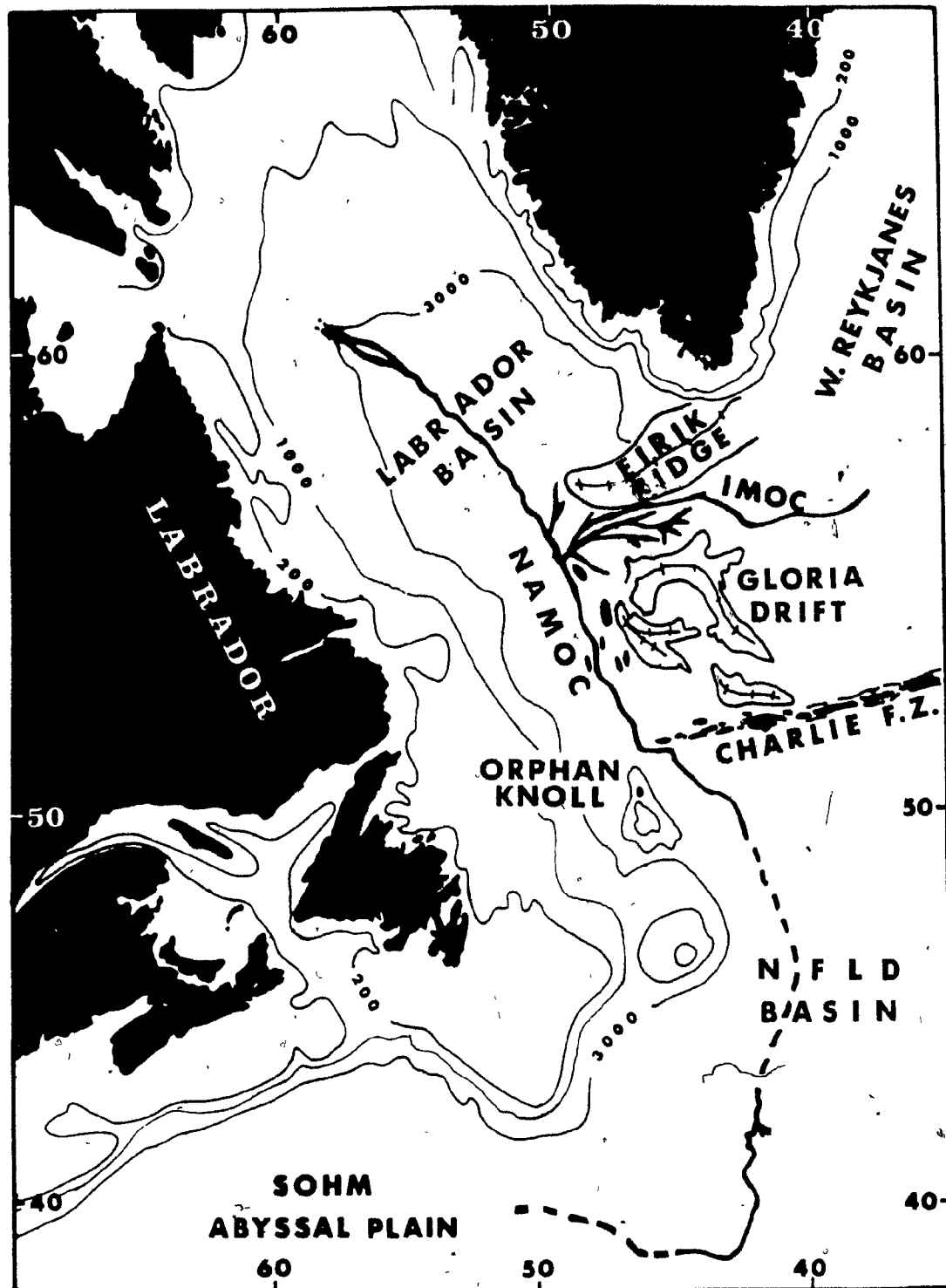


Figure 1. Major physiographic features of the Labrador Sea, modified after Heezen *et al.* (1969) and Egloff and Johnson (1975). NAMOC = Northwest Atlantic Mid-Ocean Channel, IMOC = Imarssuak Mid-Ocean Channel. Contours in meters. Broken line: Detailed position of the NAMOC undetermined.

they bypass the base of the slope?

Current models of deep-sea channel sedimentation based largely on results from the northeast Pacific (Nelson and Kulm, 1973) have emphasized certain analogies to sedimentation along subaerial fluvial channels, such as the differentiation between coarser-grained channel deposits and finer-grained, thin bedded overbank or natural levee deposits. Also meandering or braided channel patterns have been found or inferred for deep-sea channels in various ocean basins. On the other hand, individual continuous turbidite layers were traced for long distances in Cascadia Channel blanketing a flat channel floor (Griggs et al., 1969), unlike most river channels. How does the NAMOC match those different models? To what extent does it resemble subaerial river channels? In what respect is it different?

On rapid deglaciation of the continental shelves with subsequent eustatic rise of sea level the glacial sediments on the shelf probably no longer reached a position at the shelf edge suitable for the generation of submarine mass flows. It appears that the NAMOC is at present inactive as an avenue for mass flows. When did the activity cease? In the northeast Pacific, activity of channel processes decreased markedly in Holocene time, as shown by a sharp decline in the number, thickness, and coarseness of turbidites (Nelson and Kulm, 1973). Does the same hold for the NAMOC as well?

It has been generally recognized that bottom water circulation plays a significant role in transporting fine-grained abyssal sediments. In the periphery of the Labrador Basin contour-following bottom currents, intermittently generated by Norwegian Sea Water overflows, are believed to be responsible for building up sedimentary ridges, composed of contourites, such as Eirik Ridge off the southern tip of Greenland. Few criteria have been



Figure 2. Bathymetric chart of the Labrador Sea, modified after Johnson et al. (1971) and Egloff and Johnson (1975). Depth in fathoms (uncorrected) at an assumed sound velocity of 800 fm/s.

proposed to distinguish contourites from distal turbidites (e.g. Bouma and Hollister, 1973; Piper and Brisco, 1975). How do contourites on Eirik Ridge compare with other fine-grained terrigenous deep-sea sediments, for example those on the NAMOC levees? What are the principal differences between fine-grained distal turbidites or levee turbidites and contourites?

Beside the terrigenous facies and the contourite facies, pelagic sediments and abundant ice-rafted debris in the deep Labrador Basin constitute an additional distinct facies. The quantity of pelagic carbonates and ice-rafted debris in deep-sea sediments has been used as a paleoclimatic indicator. The relationship between rate of sedimentation and climate is complex and influenced by a number of factors. During climatic deterioration sea ice formation in the high latitudes precludes the supply of ice-rafted debris and markedly lowers surface productivity, whereas abundant ice-rafting and high carbonate production are associated with warmer periods (Keany et al., 1976). Much of the present northwestern Labrador Sea is seasonally covered with sea ice for a considerable period each year. What were the paleoceanographic conditions of the Labrador Sea during glacial stages? To what extent did the paleoceanographic conditions affect the distribution of ice-rafted debris and surface productivity?

A considerable volume of terrigenous sediments funnelled through the NAMOC system covers the axis of the central Labrador and Newfoundland Basins. Fine-grained levee deposits with relatively high organic carbon content abut sands and gravels of the channel facies. These would possibly represent suitable source and reservoir deposits for hydrocarbons if subjected to favorable diagenetic conditions. The occurrence of a 9 m thick coarse sand layer cored near Imarssuak Mid-Ocean Channel at Deep-Sea Drilling Project (DSDP) site 113 (Laughton et al., 1972) shows that such layers are not

restricted to the younger deposits of the Labrador Sea. Does this imply a theoretical petroleum potential of older deposits of the central deep basin?

One of the important questions related to the deposition of terrigenous sediments along the NAMOC concerns the source of these materials. This question has remained unanswered since the channel was first discovered in the early 1950's, due to the lack of adequate bathymetric information and core samples from the channel head area. Do the terrigenous sediments of the NAMOC originate predominantly from the Canadian or the Greenlandian coasts or are they derived from both sides?

In the foregoing paragraphs some of the basic problems of sedimentation in a small ocean basin in high latitudes have been outlined. Among the small ocean basins the Labrador Sea is perhaps unique as a single mid-ocean channel system profoundly influences the sedimentary facies distribution. Obviously a detailed study of some of these long-standing problems was warranted.

Field Work and Data Acquisition

Field work for this study was done in cooperation with Bedford Institute of Oceanography (BIO) aboard C.S.S. Hudson. It was started in 1974 and continued during the summer of 1975. During the 1974 cruise (Hudson 74-026-Phase IV) bathymetric profiles across the upper reaches of the channel were obtained. Due to unfavorable weather conditions in September and October, 1974 only a limited number of cores and grab samples was recovered (for stations see Figure 3 and Appendix 3). During the 1975 cruise (Hudson 75-009-Phase IV) a detailed bathymetric study, an extensive coring program and deep-sea photography were carried out in a selected area over the middle reaches of the NAMOC between 52° and $57^{\circ}30'$ N (for ship tracks, core and

camera stations see Figure 3 and Appendix 3).

Bathymetric and seismic reflection profiles across the NAMOC north of 56°N equally spaced at 30 km intervals were obtained by M/V Minna in 1974 (Macnab and Srivastava, 1975) and C.S.S. Hudson in 1975 (cruise 75-009-Phase V) and made available for this study, courtesy Dr. S.P. Srivastava, BIO. Seven additional seismic profiles across the NAMOC between 55°N and Charlie Fracture Zone were run by USNS Lynch in 1972 (Egloff and Johnson, 1975). Copies of the original profiles were kindly provided by Dr. J. Egloff, U.S. Naval Oceanographic Research and Development Activity, Bay St. Louis, Miss. Access to additional piston core samples recovered from the NAMOC and its vicinity by R/V Vema was made possible by Lamont-Doherty Geological Observatory, Palisades, N.Y. Subsamples of core materials from sites 112 and 113, Leg 12, of the Deep-Sea Drilling Project (DSDP) were made available by Drs. W.A. Berggren and U. Franz.

Three cores taken from Eirik Ridge during the 1975 cruise (Hudson 75-009-Phase IV) were made available for this study, courtesy Dr. R.H. Fillon, BIO.

Exploration History of the Northwest Atlantic Mid-Ocean Channel

The Northwest Atlantic Mid-Ocean Channel was discovered in 1949 by B.C. Heezen aboard R/V Atlantis in the abyssal plain east of Newfoundland. In 1952, the existence of the channel was confirmed by a survey with more than 80 crossings aboard Kevin Moran and R/V Atlantis in the Newfoundland Basin between 52° and 38°N (Ewing et al., 1953; Heezen et al., 1959).

In the Labrador Sea between 52° and 60°N the channel was further traced by Drake et al. (1963), Rvachev (1967) and Johnson et al. (1969). Jezek (1972) compiled echosounding profiles obtained from the Labrador Sea north of 60°N by Danish Hydrographic Service, Canadian Hydrographic Service, U.S. Naval Oceanographic Office and the U.S. Coast Guard in an attempt to establish possible northern extensions of the channel.

Prior to the present study which was started in 1974, a bathymetric map of the central Labrador Sea (Figure 2) was prepared through various echosounding and continuous seismic reflection profiles that were obtained by the U.S. Naval Oceanographic Office (Johnson et al., 1971), the Bedford Institute of Oceanography (C.S.S. Hudson cruise 72-025, van der Linden and Srivastava, 1974) and aboard USNS Lynch (Egloff and Johnson, 1975). These studies have also established the general channel morphology and postulated the possible depositional-erosional origin of the channel by turbidity currents (Heezen et al., 1969; Egloff and Johnson, 1975).

A sediment core from the floor containing fine sand and two silty lutite cores from the levees of the channel near 39°N were also considered evidence for the sedimentary origin of the channel by strong currents flowing from north to south (Ewing et al., 1953; Heezen et al., 1969). Sediment cores from the floor and associated levees of the channel in the north of 52°N were casually obtained during various R/V Vema cruises during the period between 1961 and 1969. These core materials were previously not studied and thus included in the present study, courtesy of Lamont-Doherty Geological Observatory.

It was obvious that a detailed sedimentological study including channel morphology, the sediment source, sedimentary facies and processes of sediment transport and deposition was warranted.

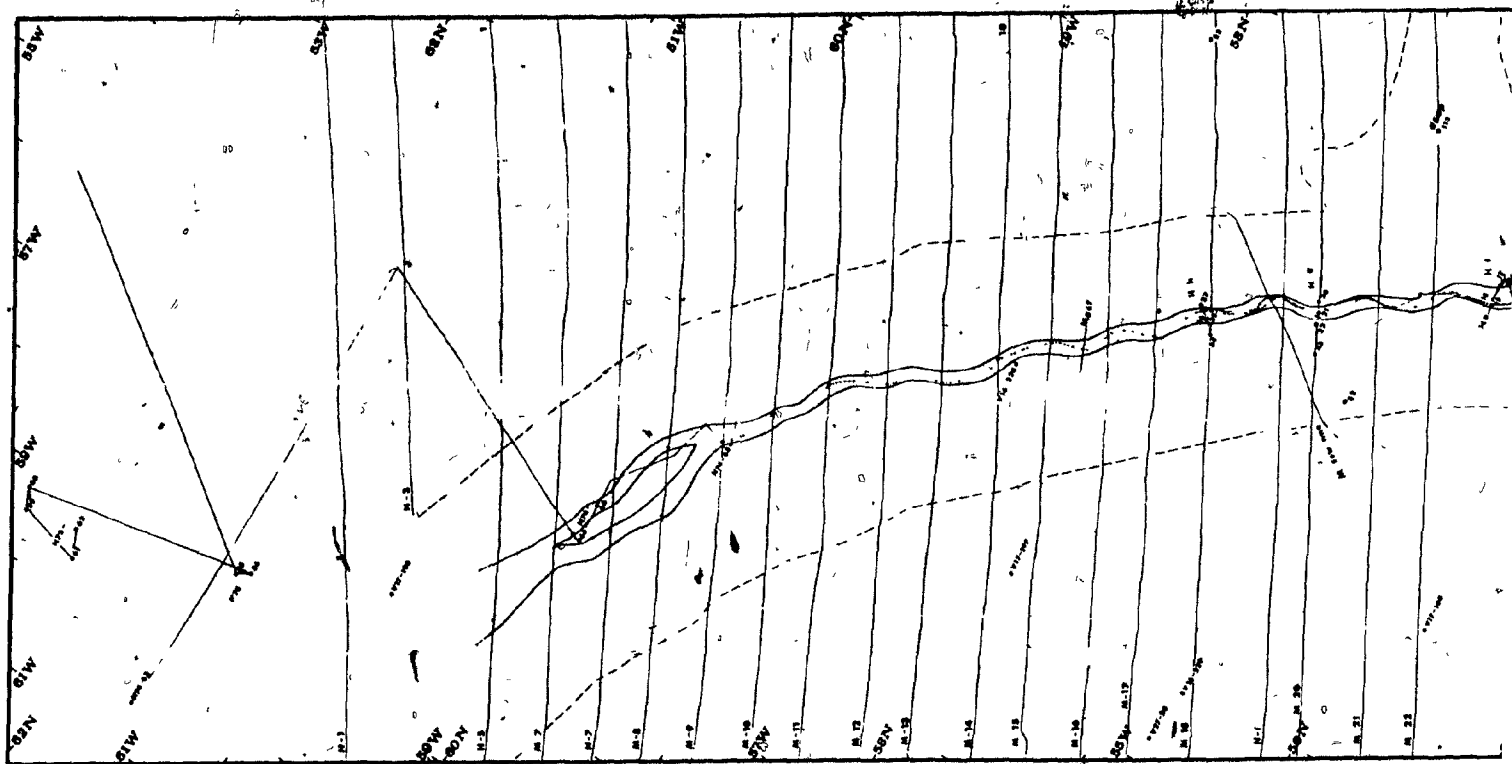
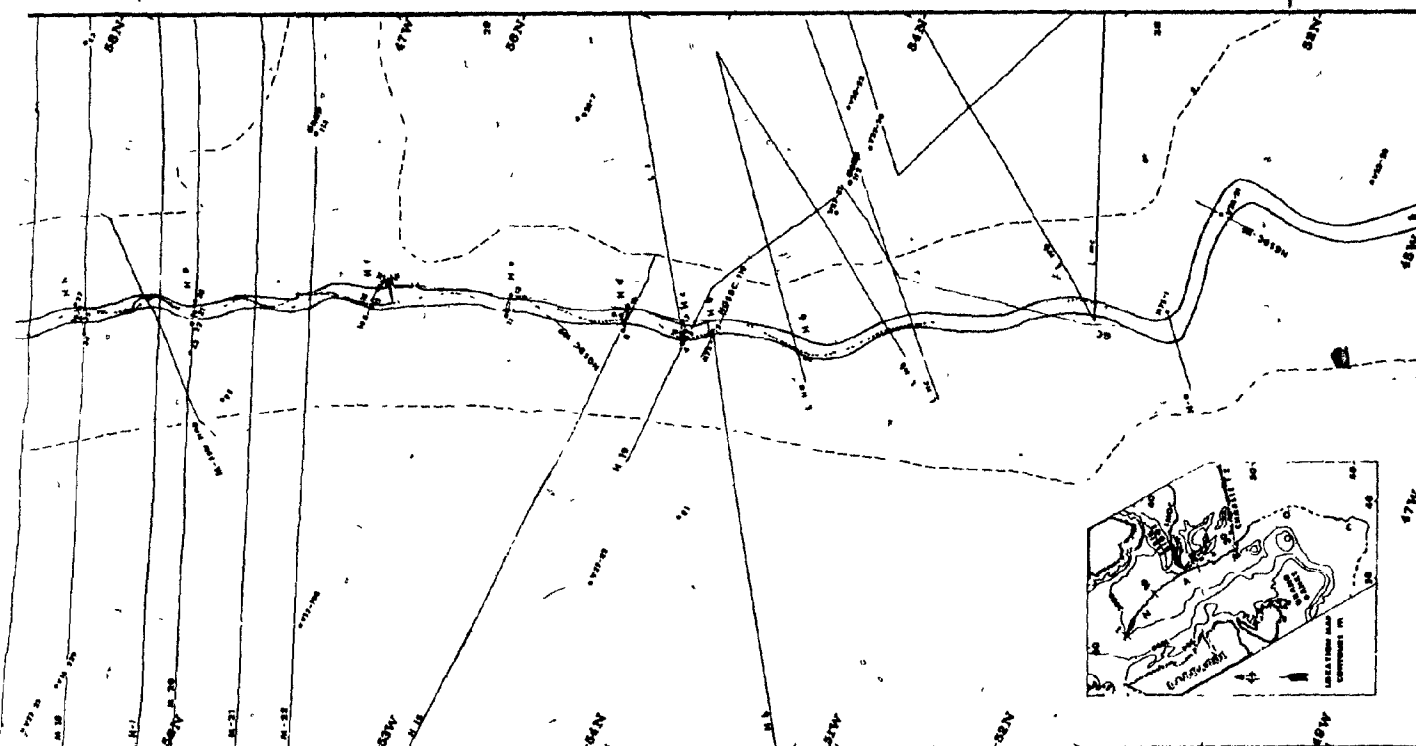


Figure 3. Bathymetric and seismic survey tracks across and along the NAMOC in the study are Hudson, USNS Lynch, R/V Mariposa, R/V Glomar Challenger, and National Geophysical and Solar-Terre DSDP represent R/V Vema, C.S.S. Hudson, R/V Eltanin and Deep-Sea Drilling Project core stations, by double stippled lines. Two broken lines on both sides of the channel indicate the extent of



along the NAMOC in the study area; M, H, L, Ma, GC and NGSDC -- represent M/V Minna, C.S.S. Geophysical and Solar-Terrestrial Data Center survey lines, respectively; V, H, E and drilling Project core stations, respectively. The meandering talweg of the channel is shown. The channel indicate the extent of spill-over facies, modified after Egloff and Johnson (1975).

CHAPTER II - MORPHOLOGY

Channel Position

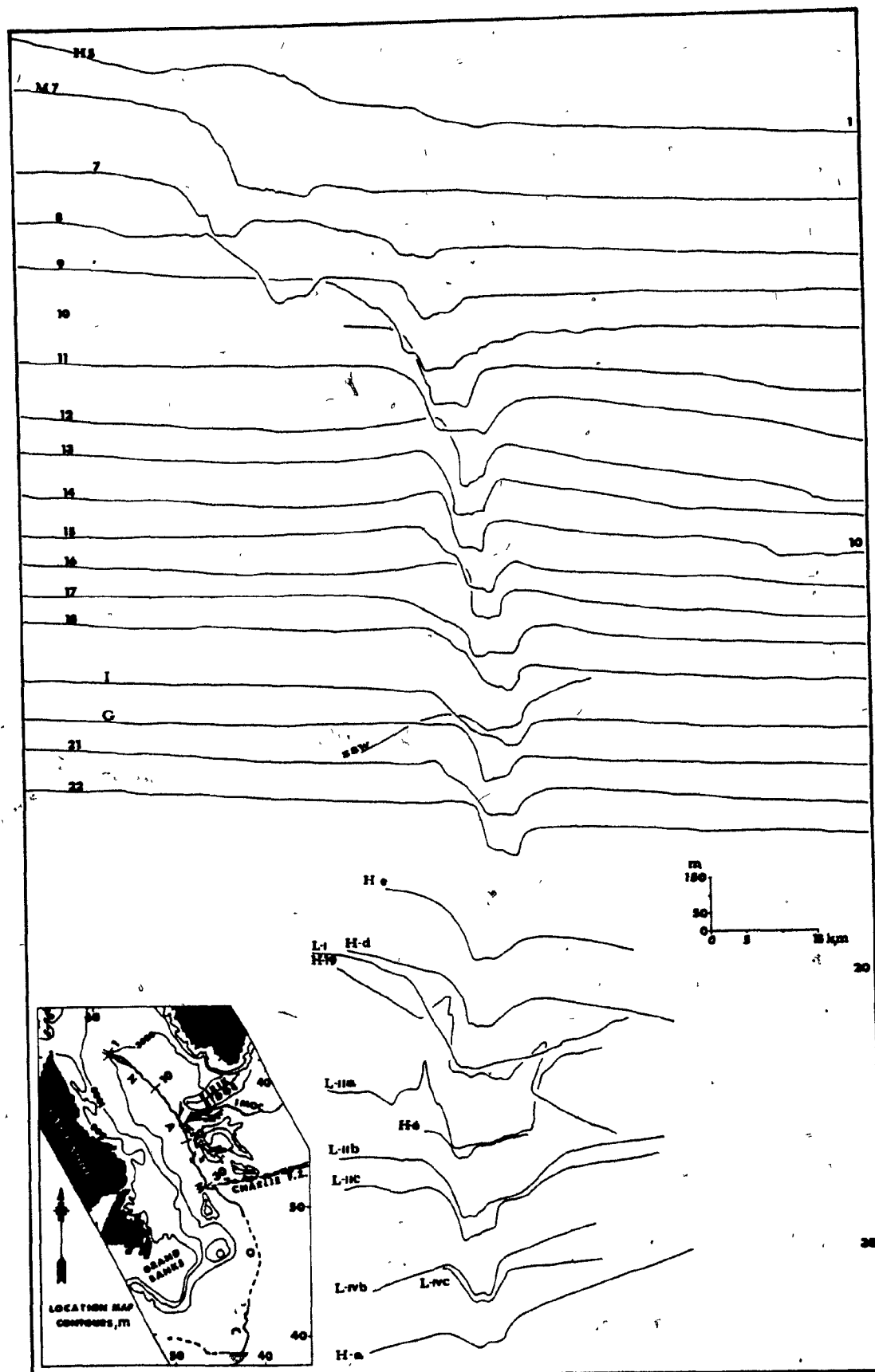
The NAMOC extends for more than 3,800 km, from about 60°30'N off Hudson Strait to about 39°N, where it merges with Sohm Abyssal Plain (Figure 1). It traverses the Labrador Basin approximately along its median line until it turns east north of Orphan Knoll at 52°N. The channel trends east for about 90 km along the Charlie Fracture Zone (Egloff and Johnson, 1975), then it enters the Newfoundland Basin to the south. At about 39°N the channel swings westward entering Sohm Abyssal Plain where it eventually becomes morphologically indistinct. The NAMOC has two eastern tributaries between 56° and 57°N (Figure 1). One, the Imarssuak Mid-Ocean Channel (IMOC), which originates in the West Reykjanes Basin on the southeast side of Greenland (Egloff and Johnson, 1975), joins the NAMOC near 56°N. It cascades onto the NAMOC with a 40 m drop of its braided floor. The other tributary near 57°N appears to be a minor one which does not extend far to the northeast.

In the following sections morphological data for the NAMOC are discussed.

Cross-sectional Profile

In vertically exaggerated cross-sectional profiles (Figure 4) the NAMOC appears to be generally box-shaped with a flat floor and relatively steep walls. A detailed survey of an approximately 180-km-long stretch of the middle channel between 56° and 57°30'N shows a rather specific channel morphology. On most crossings the channel displays an asymmetric shape with the right (west) wall being consistently steeper (average slope of 4.3°)

Figure 4. Transverse profiles across the NAMOC from the channel head to Charlie Fracture Zone; M, H, and L - numbers represent M/V Minna, C.S.S. Hudson, and USNS Lynch surveys, respectively; I and G are also Hudson profiles; numbers on the right-hand side serve for location of the lines in the inset. Vertical exaggeration 100:1. Scale bar applies to Minna profiles; for those profiles oblique to the Minna profiles the scale bar should be rotated.



than the left (east) wall (average slope of 3.2°). The channel floor is slightly inclined with an angle between 0.2° and 1.5° sloping either toward southwest or northeast. At the deepest point the channel is entrenched by 0.5 to 10 m over a 0.5 to 1.5 km wide area. This observation was the first hint that the NAMOC may possess a talweg and that this deepest part of the channel may be meandering, a feature comparable to subaerial channels.

The NAMOC is between 2 and 5 km wide at the floor and 100 to 200 m deep. Measured at the crests of the levees channel width is between 6 and 19 km. Natural levees accompany the channel for its entire length and develop laterally into broad flood plain-like areas up to a hundred kilometers wide. They are built up to an average height of 60 m above the adjacent plains. The right (west) levee is consistently up to 90 m higher and 5 to 10 km wider than the left (east) levee. The slope gradient of the levees away from the channel is higher on the right levee (average slope of $11'$) than on the left levee (average slope of $8'$). Both gradients gradually decrease downcurrent.

Longitudinal Profile

A 1,200 km longitudinal profile from the head region to Charlie Fracture Zone was constructed from 31 transverse profiles. It shows three major segments of the NAMOC (Figure 5) in this region: an upper, middle, and lower segment, with slope gradients of 0.002, 0.001, and 0.0005, respectively.

The upper segment of the channel consists of two branches in the region between $60^\circ 10'N$ and $59^\circ 40'N$ where the slope gradient of the floor is relatively high. The channel floor of the west branch is cut down by about 60 m deeper than in the east branch. A talweg is present in both branches

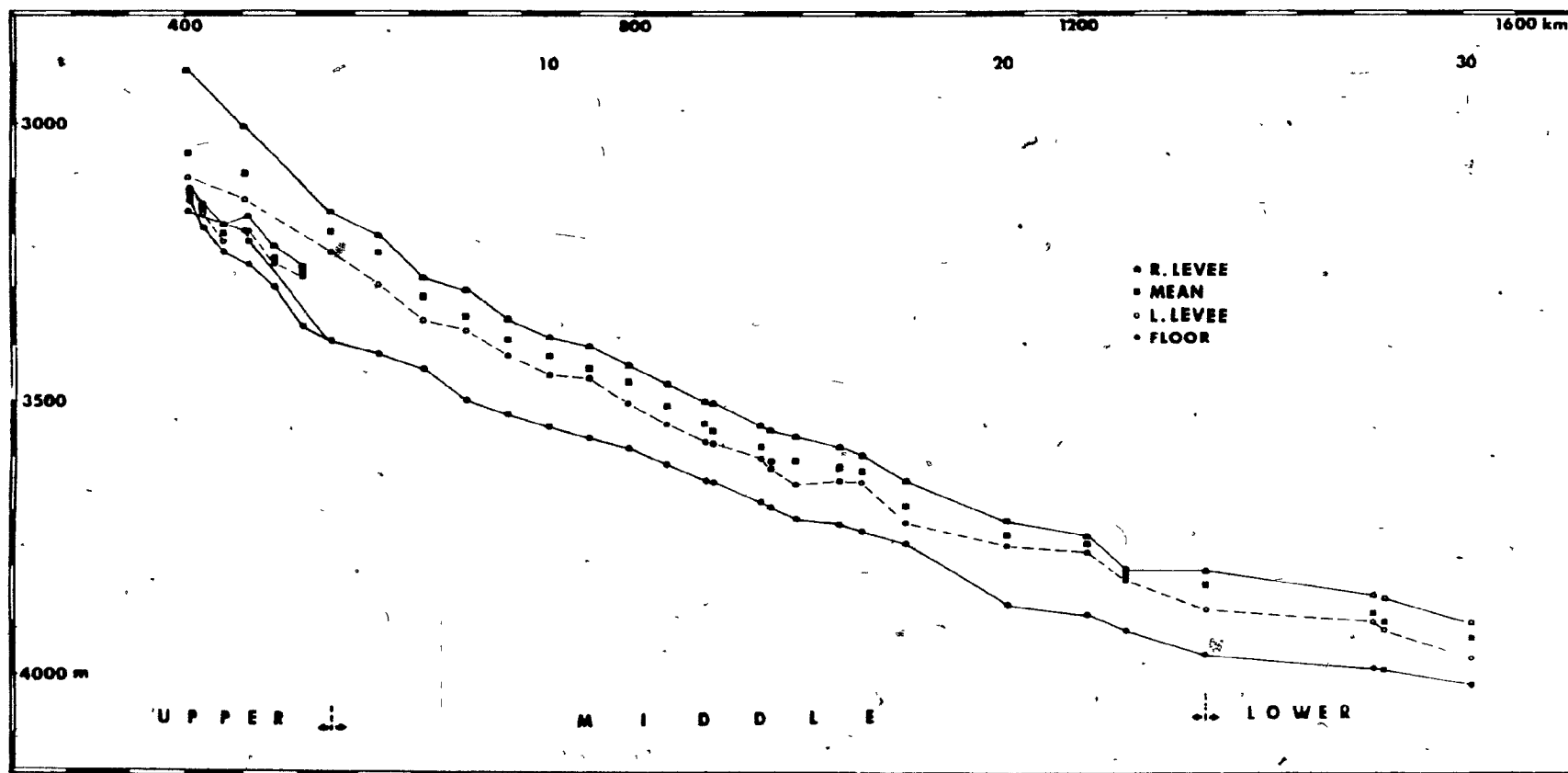


Figure 5. Longitudinal profile of the NAMOC from the head to Charlie Fracture Zone; numbers (10, 20 and 30) for location of data points in inset on Figure 4; ordinate: corrected water depth in meters; abscissa: distance from shelf edge off Hudson Strait in kilometers. The gradients of the upper, middle and lower reaches are 0.002, 0.001 and 0.0005, respectively. The difference between the mean and the floor indicates channel depth.

of the upper channel, but the east one appears to be the locus of much winnowing.

From the confluence of the two branches the middle segment extends to $54^{\circ}30'N$ with a gradual decrease in slope gradient. In this segment the channel attains its maximum relief and the average difference in height between the left and right levee (63 m) is greatest.

A downchannel gradient of 0.0005 and a less pronounced difference in levee height characterize the lower segment of the channel. Further downstream the gradient of the channel decreases slightly more. In the Newfoundland Basin the slope gradient of the NAMOC is as low as 0.00045 (Ewing *et al.*, 1953).

The significance of variations in the longitudinal gradient of the NAMOC with respect to levee height and their implication regarding both the expected flow characteristics of turbidity currents and the textural characteristics of their deposits is discussed in the sections on channel and spill-over processes.

Channel and Talweg Meandering

The meandering pattern of the channel and talweg was initially reconstructed from Precision Depth Records (PDR) on a ship-track of C.S.S. Hudson (cruise 75-009-Phase IV), across and parallel the channel in the middle reach between 56° and $57^{\circ}30'N$ (Figure 6). Positioning was by satellite navigation and Loran-C. Loran-C fixes were obtained every two minutes at a ship speed of less than 6 knots. The location of the talweg is apparent on the cross-channel records (Figure 7A, B). On some records parallel to the channel, the talweg could be determined with special precision at some outer meander bends where the talweg comes so close to the channel wall that side-echoes from the wall appear on the PDR records simultaneously

Figure 6. Ship track and meander pattern of the channel and talweg. B: Bold lines are locations of profiles shown on Figure 7. C: Diagonal hachures: portions of channel where side-echoes from channel walls were seen. Actual crossings of talweg by ship track shown as bold lines. For other information see Figure 3.

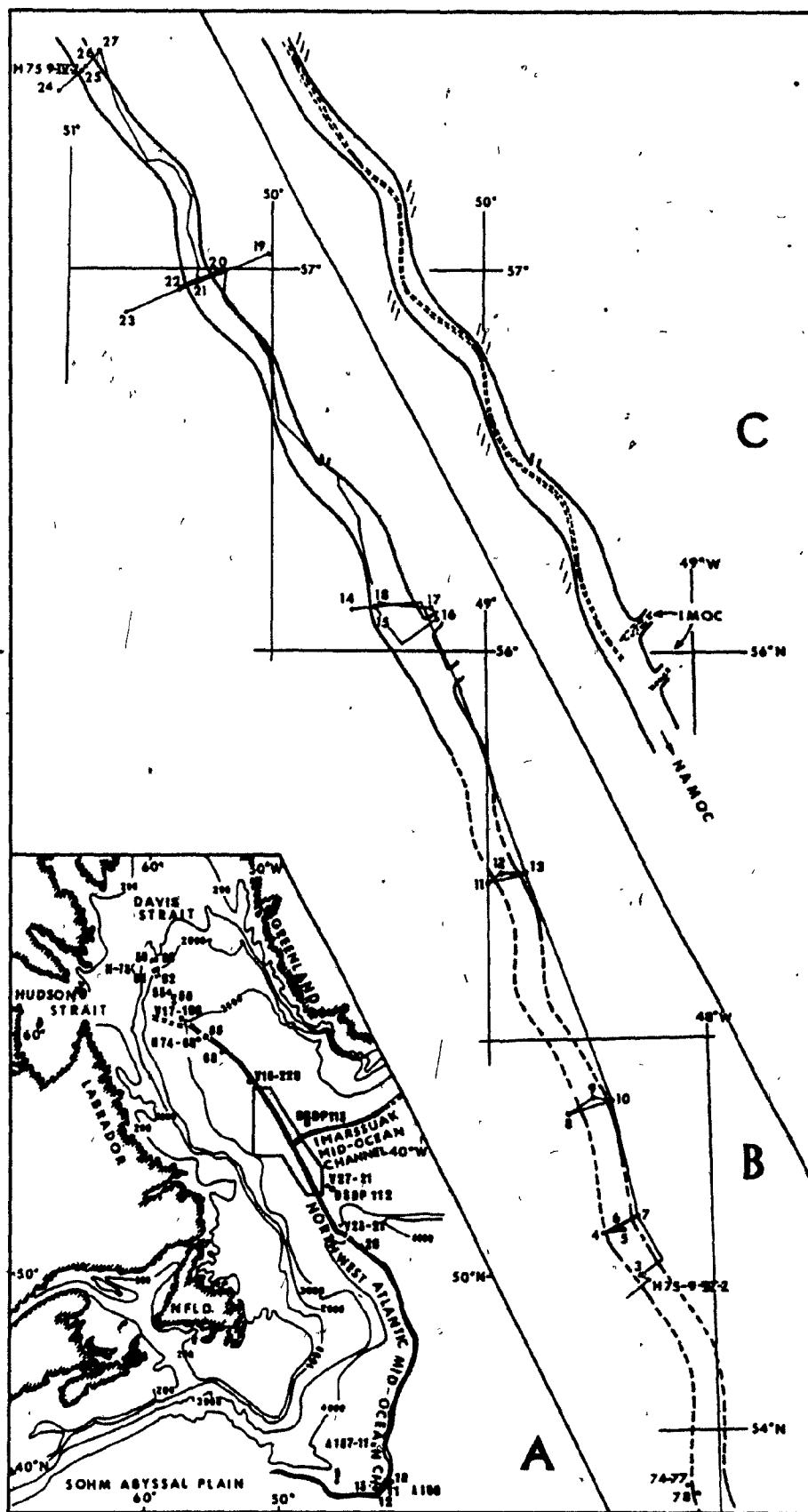
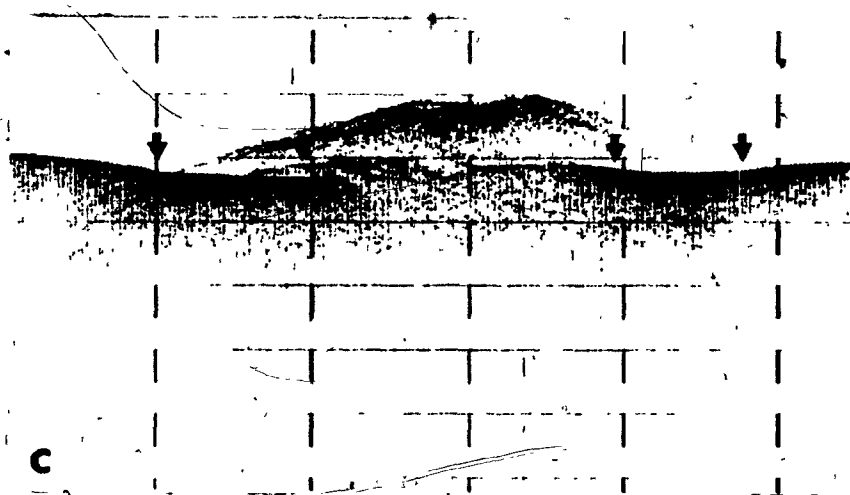
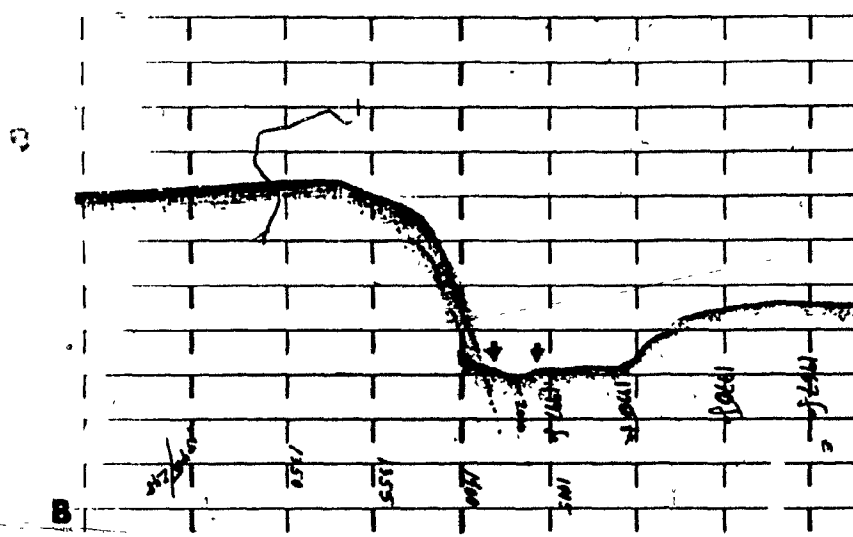
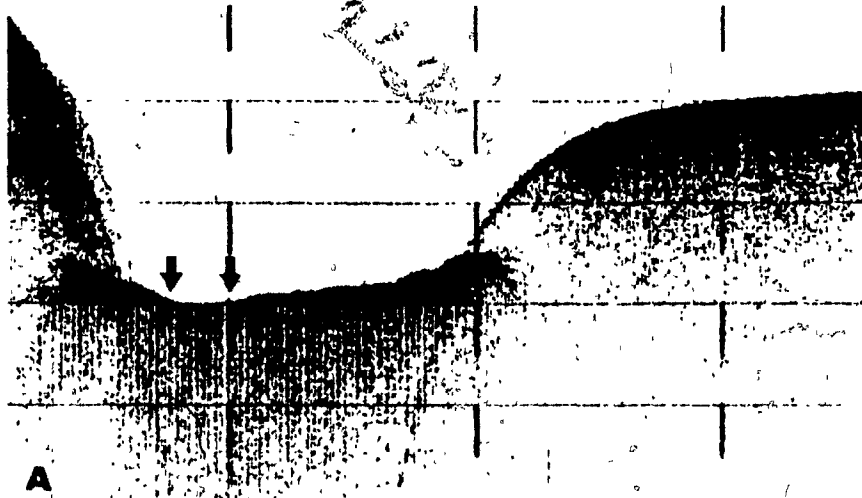


Figure 7. 20 kHz bathymetric profiles across and along the NAMOC showing the talweg (between arrows). Distance between horizontal lines is 20 fm; distance between vertical broken lines is approximately 1 nautical mile. For location of profiles, see Figure 6B, bold part of ship track. A: channel crossing at 56°57'N, 50°22'W with talweg near higher western levee; arrows indicate width of talweg of approximately 400 m; low reflectivity of talweg is probably due to pelagic sediment fill; corrected water depth is 3,731 m; depth of talweg is approximately 5 m; downcurrent direction pointing out of picture. B: channel crossing at 56°58'N, 50°22'W showing talweg near higher western levee; arrows indicate width of talweg of approximate 400 m; depth of talweg is approximately 2.5 m; corrected water depth is 3,730 m; subbottom reflectors in the upper 15 m on the right levee suggest internal stratification due to interlayering of sands and fine-grained turbiditic and pelagic muds. C: profile near eastern levee (appearing as side echo in center of picture) at 56°48'N, 50°00'W; ship's track intersects meandering talweg twice; inside the two central arrows the talweg runs midway between eastern levee (in background) and point bar (closest to viewer, about 8 to 10 m higher than talweg); downcurrent direction to the right; note relatively high reflectivity of talweg, which is indicative of coarse (channel-lag) sediments; corrected water depth is 3,738 m.



with the talweg (Figure 7C). With the limited data available the reconstructed meander pattern of the channel and talweg appears to be the best interpretation possible, although more closely spaced bathymetric lines might reveal a slightly different pattern in detail.

The talweg meanders with about the same wavelength (50 km) but slightly higher amplitude than the channel, i.e. 11 and 10 km, respectively (Figure 6C). These averages are based on the reconstructed meandering pattern of the channel and talweg for the entire reach between the head region and 54°N for which the closely spaced 1974 crossings by M/V Minna (Figure 3) were also available.

Figures 3 and 6B clearly show a relatively low sinuosity of the meandering channel and talweg. The sinuosity is the ratio of channel length to meander length. For most river channels there is a constant relationship of meander wavelength to channel width. On Leopold and Wolman's (1960) meander wavelength-channel width (L/W) diagram (Figure 8) the NAMOC plots below the 10:1 (L/W) line characteristic for subaerial rivers; i.e. its wavelength to channel width ratio is less than that typical for fluvial channels. This is in line with data from Maury Mid-Ocean Channel or the Gulf Stream which also have a smaller than 10:1 ratio of meander wavelength to channel width. It thus seems that hydrodynamic processes in large submarine channels differ systematically from those in subaerial ones as will be further discussed in the section on channel processes.

Submarine Point Bars

On most crossings the channel floor is slightly inclined toward the talweg with an angle between 0.2° and 1.5° (see Figure 7A, B) dipping alternately either toward southwest or northeast (Figure 9A, C).

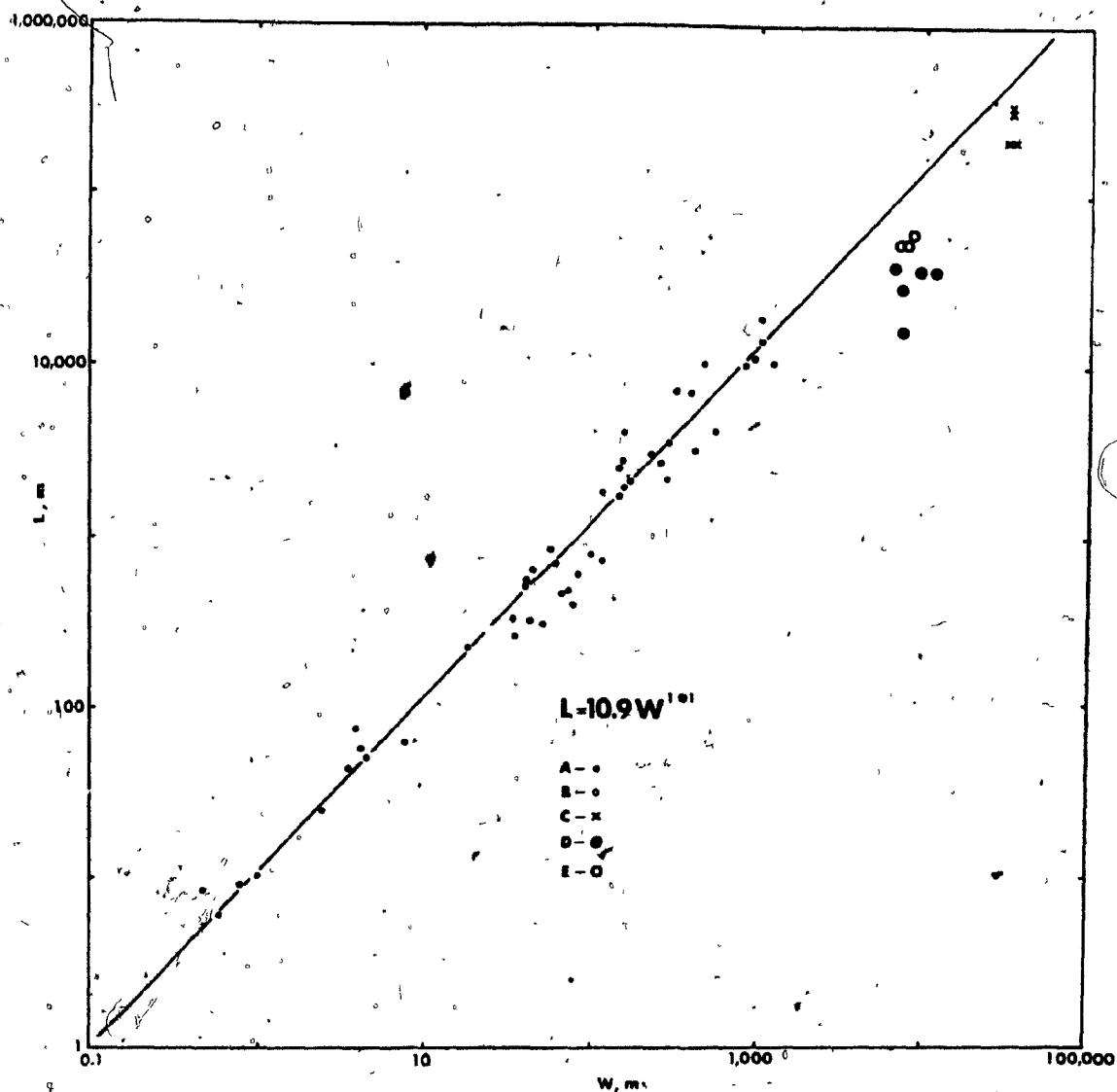


Figure 8. Relation between meander wavelength (L) and channel width (W), modified after Leopold and Wolman (1960) and Egloff and Johnson (1975). A: meanders in rivers and laboratory flumes; B: meanders on glacier ice. Note that the NAMOC plots (E) are below the 10:1 line characteristic for subaerial channels, as are the data points for Maury Mid-Ocean Channel (D) and the Gulf Stream (C).

Morphologically this change in direction of floor inclination toward the talweg may be interpreted as a sequence of point bars associated with the meandering talweg. This is apparent on the concave (inner) bend of the 4.0 km segment of the talweg meander shown in Figure 7C. Subbottom reflectors in the upper part of the sediment column on some channel profiles reveal oblique internal stratification supporting the interpretation as submarine point bars (Figure 9A). The same feature is also visible on a slow-scan profile obtained while the ship was drifting on station (Figure 9B, C). A short piston core at this station (H75-6) contains a layer of sand under a thin veneer of fine-grained pelagic lutites.

Figure 9. Subbottom reflectors from the channel floor at 54°33'N, 48°24'W (between stations 4 and 7) showing inclined strata dipping toward west and probably representing internal stratification in a submarine point bar; downcurrent direction pointing out of the Figure. A: distance between horizontal lines is 36 m, distance between vertical broken lines is about 200 m. B: distance between two vertical broken lines is approximately 20 m. Location approximately 400 m west of A. C: detailed subbottom stratification; total height of picture is about 40 m, width is approximately 20 m.



CHAPTER III - SEDIMENTARY FACIES

Facies Distribution

Four distinct sedimentary facies occur in the central Labrador Sea (Figure 10): a) the channel-fill facies of the NAMOC, b) the spill-over facies associated with the channel, c) the pelagic-hemipelagic facies and d) the bottom-current deposits (contourite facies).

The deposition of pelagic sediment results from particle-by-particle settling of biogenic components and terrigenous detritus. In the Labrador Sea the latter includes abundant ice-rafted debris. In the vicinity of the NAMOC pelagic sedimentation has been frequently interrupted by the rapid input of terrigenous sediments by channel processes resulting in an alternation of terrigenous and pelagic layers. The latter are limited in number and thickness. The terrigenous sediments cover an area up to a hundred kilometers wide on either side of the NAMOC comprising both the channel-fill facies within the confines of the channel and spill-over facies on the natural levees deposited by flows overtopping the channel walls. The channel-fill facies consists of thick bedded, coarse-grained deposits in contrast to the spill-over facies which is predominantly thin bedded and fine-grained. Bottom current deposits (contourites) consist of pelagic and hemipelagic sediments reworked by contour-following deep oceanic currents. In the Labrador Sea there are two contourite ridges; Eirik Ridge on the south Greenland continental rise, south of Cape Farewell and Gloria Drift in the central southern part of the Labrador Basin, respectively (Figure 10). These are piles of acoustically transparent sediments differentiated from the pelagic facies by their characteristic hummocky surface morphology, which yields wavy or hyperbolic reflections on echograms and seismic

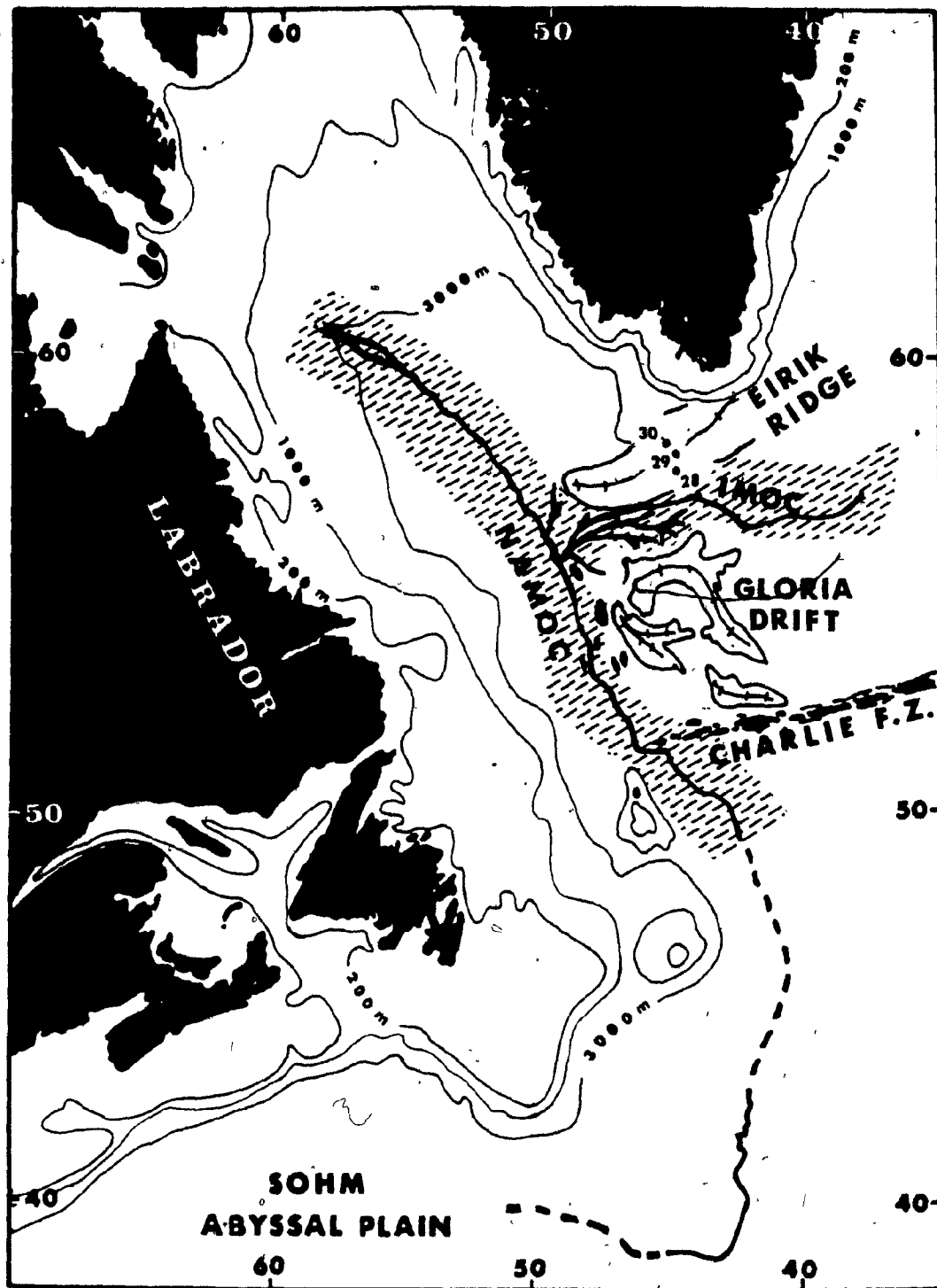


Figure 10. Schematic sedimentary facies distribution of the central Labrador Sea extrapolated to a subsurface depth of 500 m on the basis of seismic reflection profiles, partly after Egloff and Johnson (1975). Diagonally hatched pattern: spill-over facies of the NAMOC and IMOC. Sedimentary ridges with crest lines: contourite facies. (Nos. 28, 29 and 30 denote sediment cores from Eirik Ridge)

records (Davies and Laughton, 1972).

A tentative interpretation of the seismic profiles (Plate 1) suggests that approximately a 500 m thick sequence of alternating terrigenous and pelagic sediments was deposited in the central Labrador Basin under alternating regimes of predominant channel processes and subordinate pelagic sedimentation. In the following sections the diagnostic features of each facies, such as occurrence, sedimentary structures and texture and sequential analysis of structure divisions, revealed in the topmost 10 m of sediments, are discussed.

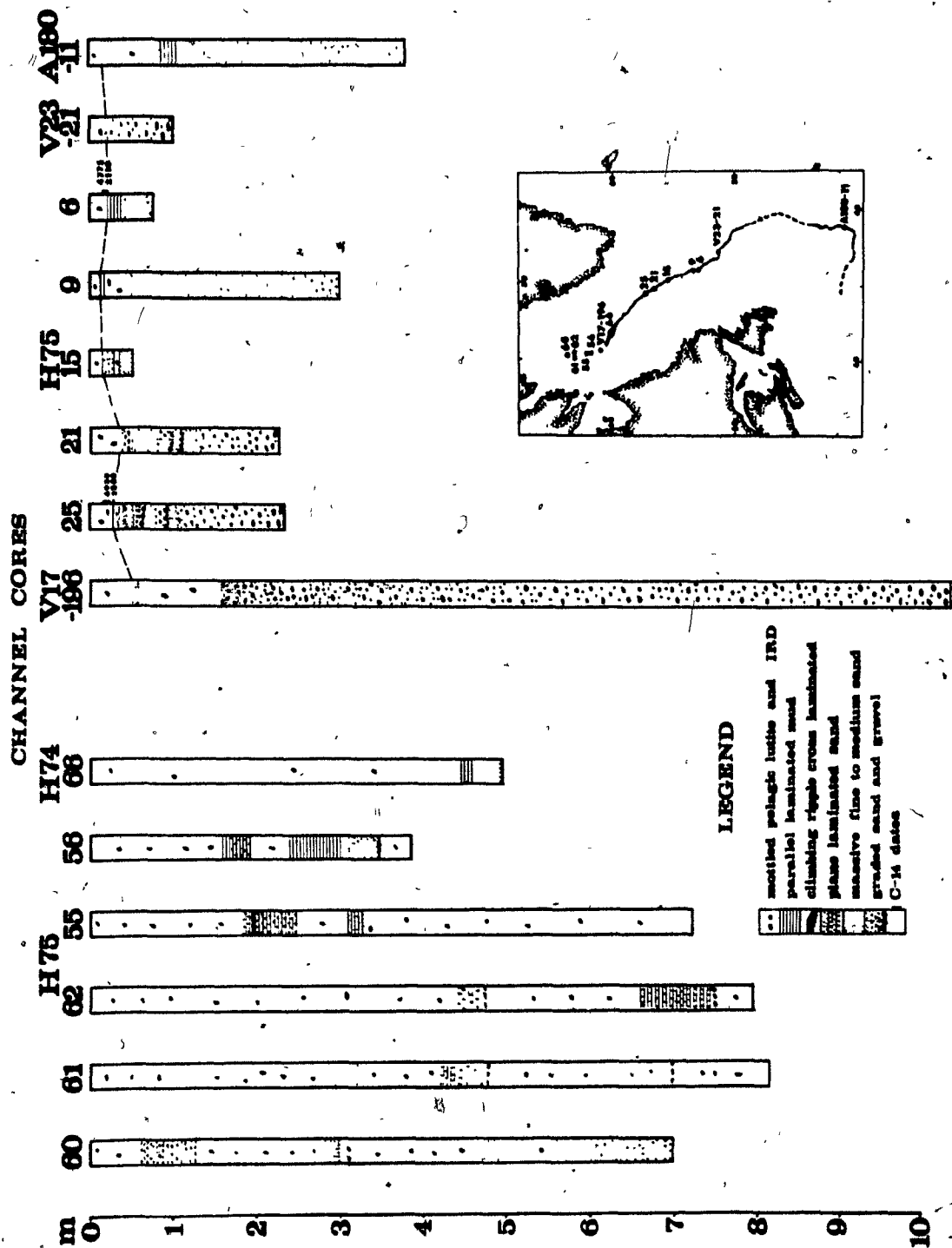
Channel-fill Facies

Occurrence

Coarse-grained deposits, layers of sand and gravel, extend along the length of the NAMOC floor; they were found in almost all of the channel cores taken from the head region down to the termination of the channel near 39°N (Figure 11; for descriptions of individual cores see Appendix 4). Layers are up to several meters thick and show distinct depositional units: graded or massive divisions bound at the base by a scour surface and sometimes being overlain by cross-bedded, cross-laminated and parallel laminated divisions.

Core V17-196 was recovered from near the northern limit of the study area near 60°44'N, where the channel is morphologically ill-defined. It contains an 8.7 m thick sandy gravel layer overlain by a layer of pelagic ooze. Individual pebbles are up to 60 mm in diameter (Plate 2C). Although the gravel layer is bottomed by pelagic lutite in the core catcher a substantial "flow-in" of materials during retrieval of the piston corer is

Figure 11. Main sediment types of channel-fill cores. Note discontinuity of sand and gravel layers which cannot be traced from station to station. Dashed line in cores V17-196, H75-25 and more southerly cores denotes lower boundary of uppermost pelagic layer. Cores on the left hand side of diagram are from the possible northern tributary of the NAMOC off Cumberland Sound. The pelagic sections of these cores are dominated by ice-rafted debris.



evident. Nevertheless, the occurrence of gravel and sand at this locality is of great significance for tracing the coarse channel-fill sediments toward their source.

Core H75-25 (Plates 2A, B and 3) was taken approximately 450 km farther south in water 3,600 m deep. Here, a 1.3 m thick sandy gravel layer underlain by a 10 cm thick parallel laminated mud grades upward into sand. It is, in turn, overlain by another graded layer of sandy gravel. A thin pelagic ooze layer is intercalated between the sandy gravel layers. The upper gravel layer is followed by a sequence of layers containing a basal division of graded gravel and sand, parallel laminated sand, cross-laminated and climbing ripple cross-laminated sand, parallel laminated mud, homogeneous mud, and at the top, a pelagic division.

Core H75-21 was recovered from the more or less flat channel floor, approximately 50 km downcurrent from core H75-25. It consists of a 1 m thick layer of sandy gravel at the base (which shows evidence for disturbance by flow-in). It grades upward into sand displaying divisions of the Bouma-sequence: parallel laminated sand and cross-laminated fine sand and silt.

In cores H75-15, 9 and 6 (Figure 11), which were taken approximately 700, 800, and 850 km away, respectively, from the channel head, sand layers with thin intercalated layers of pelagic ooze occur. These cores bottom in coarse-grained sediment, which was penetrated only superficially by the corer. At channel stations H75-2 and 5 no penetration was achieved.

Core V23-21 from the channel floor near Charlie Fracture Zone contains a sandy gravel layer (Plate 2D) within the lower 75 cm of a total length of 1 m. The top 25 cm consist of pelagic lutite. The core was taken approximately 1,600 km away from the possible source on the shelf edge

off Hudson Strait.

In core A180-11 (Heezen et al., 1969, p. 1445) a 2.4 m thick well sorted fine sand layer (parts of which probably represent flowed-in material) is overlain by 1.3 m of pelagic lutite. The core was recovered near 39°N at a distance of approximately 3,000 km from the channel head.

Core H74-66 was raised from the eastern branch of the upper channel whose floor is approximately 60 meters shallower than the western branch. Although this locality is proximal to the source, the core consists almost entirely of bioturbated, mottled pelagic lutite except for a 5 cm thick sand layer which is accompanied by parallel laminated mud.

Cores H75-60, 61, 62, 55 and 56 (Figure 11) were recovered from a northern tributary of the channel north of 61°N where the continuity of the channel morphology is not well established. The cores consist of mottled pelagic lutite with abundant ice-rafted debris and some intercalated coarse-grained layers.

Sedimentary Structures and Texture

Sedimentary structures of the channel-fill sediments were studied by visual examination of split cores and X-radiography of sediment slabs. For X-radiography 1 cm thick slabs of sediment were sliced from all core sections except for material coarser than gravel size. Slicing was done using thin wire and 29 cm long plastic containers. Thin sediment slabs for X-radiography rather than core halves or the entire core have the advantage of minimizing superposition of sedimentary structures and avoiding edge effects. All pictures were taken on Kodak Industrial AA2 Film with a Picker Mini Shot II X-ray unit at 50-60 KV, 3 mA, 10 seconds exposure time and source to sample distance of 53 cm.

The coarse-grained layers vary in thickness from a few centimeters to more than 9 m. As mentioned before the 9 m thick layer of coarse gravel and sand in core V17-196 most likely does not represent the true amount of penetration. The sediments were probably sucked in during retrieval of the corer. These thick layers are largely structureless except for grading (Plate 2A, B). The lack of structures is either a primary feature (massive basal division of turbidites, debris flow deposits) or the result of coring disturbance. Thin, usually less than 20 cm thick, sandy gravel layers intercalated between finer-grained cohesive sediments are usually less affected by coring disturbances and often show graded bedding (Plate 3B, C). In most cases the graded (or structureless) sandy gravel at the base (Bouma's A-division or T_a) is followed by parallel laminated sand (Bouma's B-division or T_b). Sometimes the B-division starts at or near the base. In some layers a thin division of cross-laminated and climbing-ripple laminated fine sand to silt (Bouma's C-division or T_c) follows on top of T_b , which, in turn, is sometimes overlain by the upper parallel laminated mud (Bouma's D-division or T_d , Plate 3A, B). Less frequently homogeneous turbiditic silt and clay (Bouma's E-division or T_e) and inter-turbidite pelagic ooze (F-division of turbidite-pelagite sequence) are found (Plate 3A, B and Appendix 4) in the channel cores. Turbidite sequences observed in the channel-fill facies can be summarized as follows: T_{abcde} , T_{abc} , T_{ab} with intercalated pelagic intervals. For a statistical analysis of the structure divisions the number of cores from the channel is insufficient.

The gravel and sand layers of the channel-fill facies are apparently lenticular and form discontinuous bodies, because the sequence of layers encountered do not match between cores, even if core stations are less than

than a few kilometers apart (Figure 11).

Grain size analyses were done according to standard granulometric techniques; i.e. sieving at $1/4$ phi intervals of the sand-sized (> 63 microns) material using a Fritsch-Analysette-3 sieving machine, and pipette analysis for the finer fractions following the procedure of Folk (1968). The standard grain size nomenclature of Shepard (1954) is used. In addition the term mud is used in this study for mixtures of terrigenous silt and clay, thus including clayey silt and silty clay.

Individual thin sandy gravel layers are poorly to very poorly sorted (Figure 12). Individual gravel components are subangular to subrounded and mostly equant or prolate in shape (Plate 2C, D). Some show surface striations which may indicate a subglacier origin. Numerical textural parameters for the gravel layers are given in Appendix 5.

Spill-over Facies

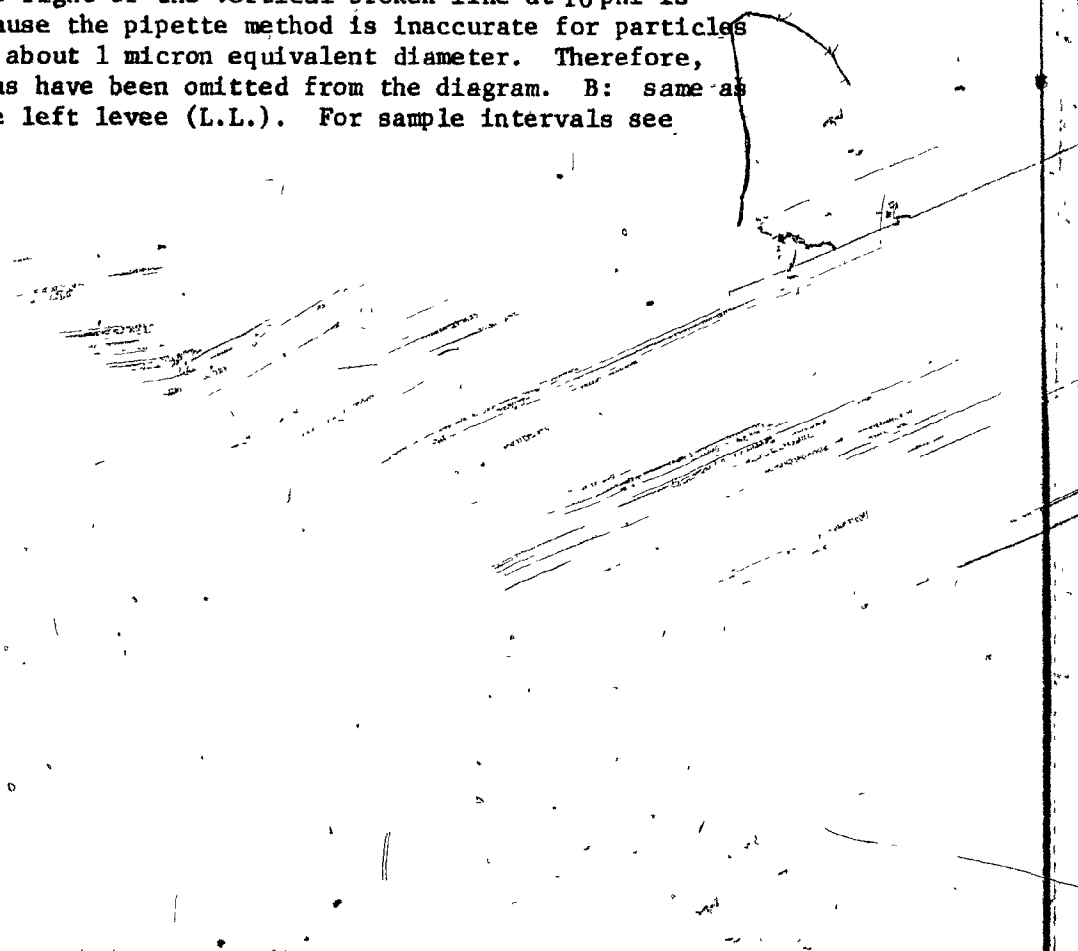
Occurrence

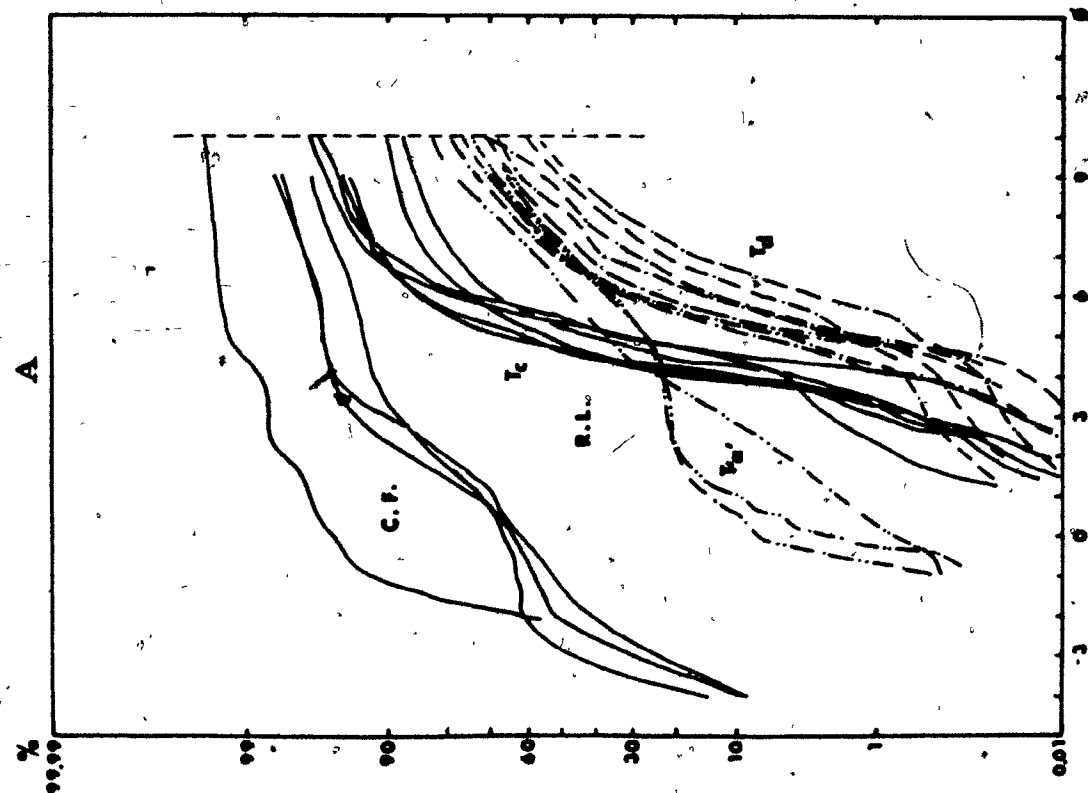
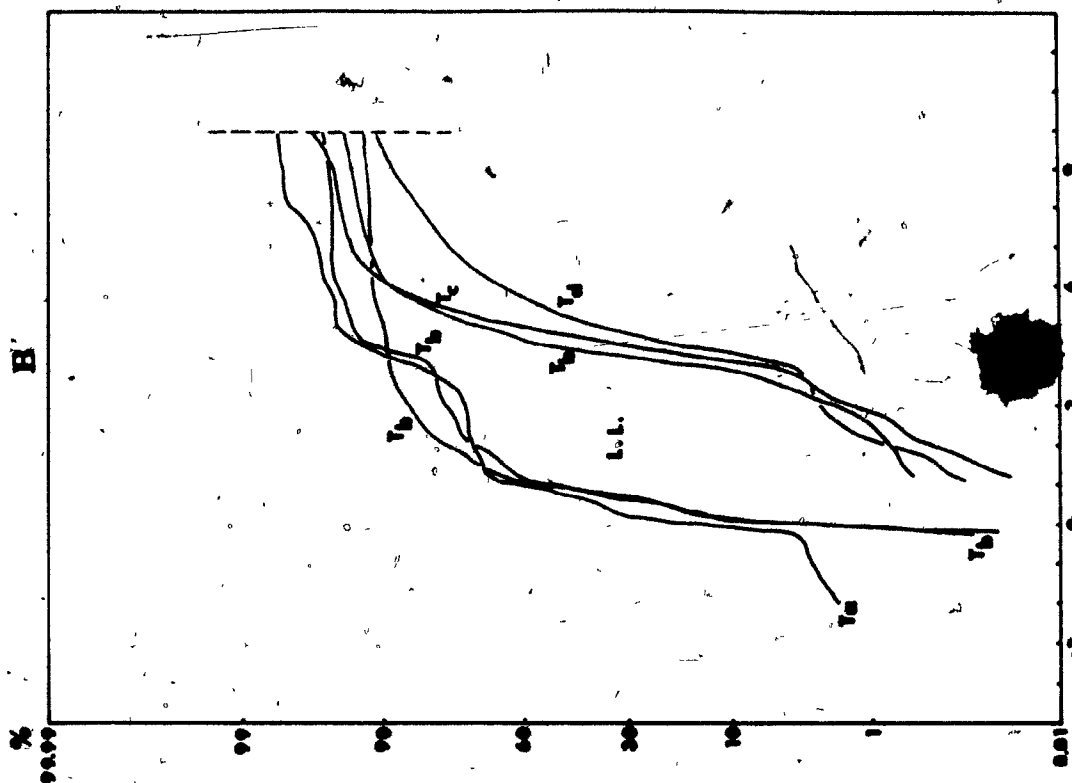
The spill-over facies occurs on the natural levees resulting from innumerable overflows of flows from the channel. In the Labrador Basin this facies extends laterally up to a hundred kilometers on both sides of the channel. According to Egloff and Johnson (1975) further downchannel in the Newfoundland Basin it widens to over 240 km. The spill-over facies is envisaged to marginally interfinger with the pelagic facies. It consists of thin bedded fine-grained sediments, usually finer than medium sand, which are devoid of bioturbation, except beneath some thin intercalated pelagic layers that are intensely bioturbated and mottled.

Sedimentary Structures and Texture

The most distinctive feature of the spill-over sediments is a monotonous

Figure 12A. Cumulative granulometric curves of channel-fill (C.F.) and spill-over facies (R.L. = right levee); $T_{a''}$, T_a , T_b , T_c and T_d indicate "A", A, B, C and D-structural divisions of turbidites, respectively, of the spill-over facies. "A" (or $T_{a''}$) denotes a non-typical turbidite structure unit which is characterized by its crude parallel laminations. The unit is tentatively called "A"-division because of its extremely poor sorting and scattered pebbles, which resemble the A-division. C.F., "A", A and B are very poorly sorted, whereas C and D are moderately to poorly sorted. Reliability of portions of the curves to the right of the vertical broken line at 10 phi is limited, because the pipette method is inaccurate for particles smaller than about 1 micron equivalent diameter. Therefore, these portions have been omitted from the diagram. B: same as A but for the left levee (L.L.). For sample intervals see Appendix 5.





repetition of thin parallel laminated units of terrigenous very fine sand and mud (clayey silt and silty clay). A set of tens of thin laminae forms an upward-fining unit between 0.2 and 9 cm thick (3 cm on the average). This parallel laminated unit often starts with a climbing micro-ripple or micro-cross-laminated very fine sand to silt division at the base and grades in most cases upward into unlaminated homogeneous mud (Plates 4 and 5).

The occurrence of climbing micro-cross-lamination at the base of many of the depositional units clearly indicates: a) the fine parallel laminations are current-generated, b) sediment supply was relatively rapid. These units are fine-grained turbidites as will be discussed in more detail in the section on spill-over processes.

The sedimentary structures of the spill-over facies can therefore be described in terms of Bouma's (1962) sequence of sedimentary structures established for "classical" turbidites with some minor modifications: 1a) crudely parallel laminated sand-silt-clay (designated here as "A"-division or $T_{a''}$), 1b) massive or graded medium to coarse sand division (Bouma's A-division or T_a), 2) lower parallel laminated division (Bouma's B-division or T_b), 3) climbing micro-ripple or micro-cross-laminated sandy silt, clayey silt and silt division (Bouma's C-division or T_c), 4) parallel laminated mud division (Bouma's D-division or T_d) and 5) homogeneous mud (Bouma's E-division or T_e). Some pelagic ooze layers (F-division of turbidite-pelagite sequences) are intercalated between some of the turbidite units.

Crudely parallel laminated "A"-divisions were observed in some cores from both levees (Plate 6). These units are more common in the upper and upper middle channel segments than in the lower segment. The massive or

graded A-division and the parallel laminated B-division occur only rarely in the spill-over facies. Most common among the sedimentary structures in the spill-over facies are the climbing micro-ripple or micro-cross-laminated and parallel laminated divisions, which occur ubiquitously on both levees. The unlaminated homogeneous mud (T_e) may be distinguished from the inter-turbiditic pelagic ooze by sediment composition (terrigenous components) and a lesser degree of bioturbation.

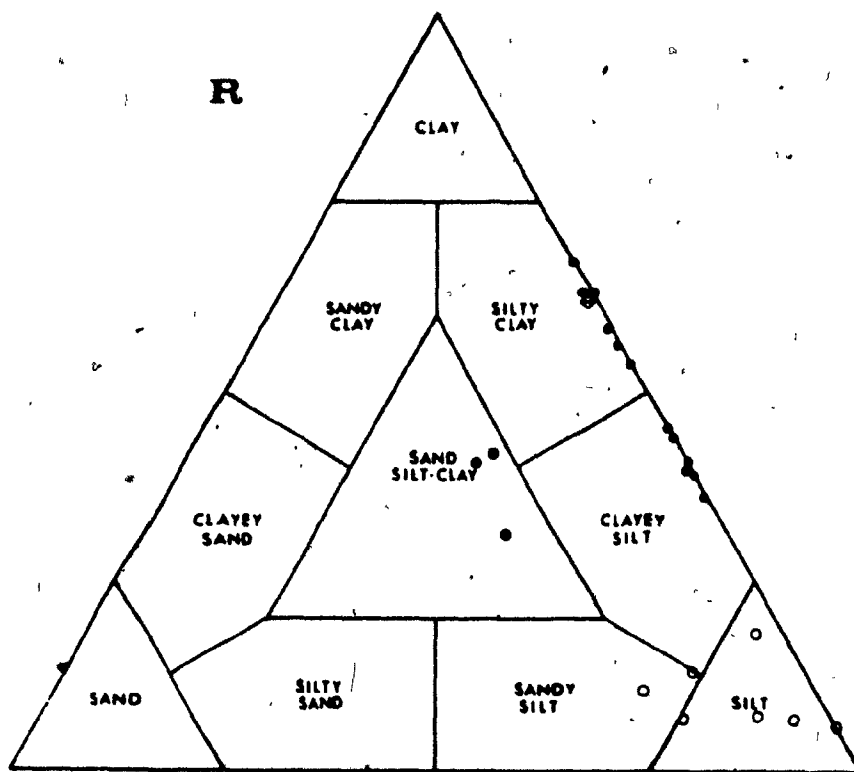
In the following sections individual sedimentary structures of the spill-over facies are discussed. Grain size distributions for various types of sedimentary structures are shown on Figure 13.

Crudely Laminated Sand-Silt-Clay Division ($T_{a,n}$)

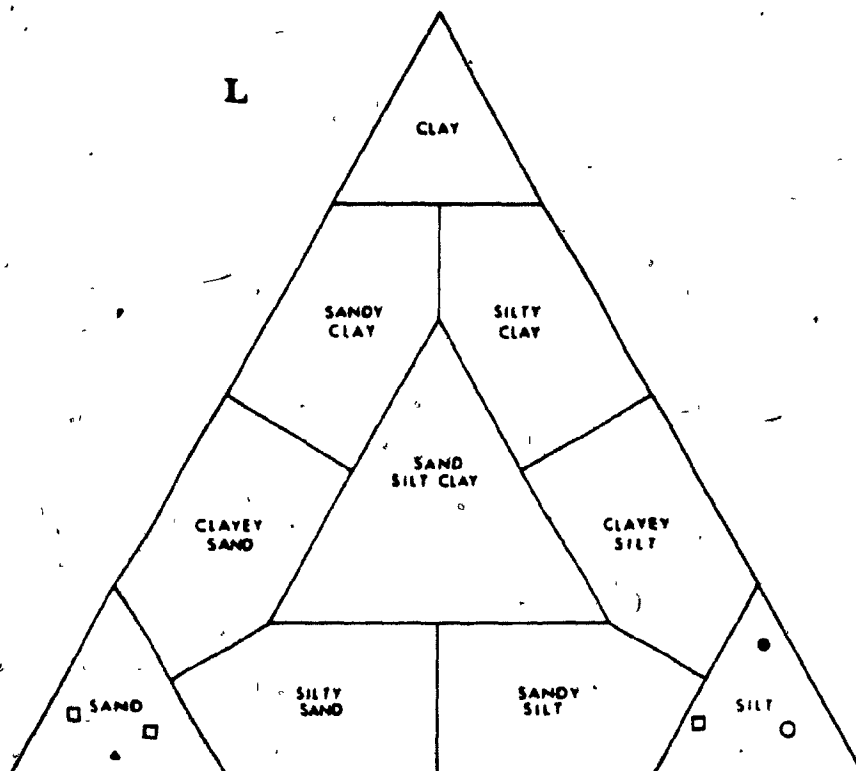
This unit is characterized by its crude parallel lamination and often by the presence of some pebbles which are in most cases scattered throughout the layer (Plate 6C). It consists of approximately equal proportions of sand-, silt- and clay-sized terrigenous material (Figure 13R) and is very poorly sorted. With the underlying mud the unit is bound by a sharp contact, which may be of erosional nature. With the overlying cross-laminated silt, parallel laminated or homogeneous mud it contrasts in sorting. The thickness of individual units rarely exceeds 6 cm. This unit is estimated to make up less than 5 percent by thickness of the spill-over facies in the core material.

Whereas the crude lamination mimics Bouma's (1962) B-division, the extremely poor sorting and existence of scattered pebbles suggest that it is equivalent to the A-division. Although no modern examples of such deposits have been reported elsewhere, similar, but much thicker examples are found in the basal unit (A-division) of some ancient turbidites

Figure 13. Classification according to grain size of spill-over deposits of the natural levees; nomenclature after Shepard (1954); R = right levee, L = left levee; "A", A, B, C, D and E denote the crudely laminated, the graded, the lower parallel laminated, the cross-laminated, the upper parallel laminated and the pelitic turbidite divisions (Bouma, 1962), respectively. "A" is more common on the right levee, whereas A and B were found only on the left levee; D, E and C are equally common on both levees. (From the left levee no samples of "A", D and E were analyzed.) For sample intervals see Appendix 5.



A-▲ B-□ C-○ D-● E-◊



(van der Lingen, 1969; Hesse, 1973; Rocheleau and Lajoie, 1974). Because of this similarity the unit is referred to as "A"-division (or $T_{a''}$).

The significance of the "A"-division with respect to levee height, the flow characteristics of overflows and the channel gradient will be discussed in the section on spill-over processes.

Graded or Massive Sand and Sandy Gravel Division (T_a)

Bouma's (1962) A-division occurs very rarely in the spill-over facies. Only three sequences were found that start with the A-division: a) a 40 cm thick massive medium to coarse sand on the right levee (core H75-14); it rests with an erosional contact on a parallel laminated mud; b) a 10 cm thick graded gravelly sand on the right levee (core H74-68); it is followed by subsequent turbidite divisions; c) a 5 cm thick obliquely stratified gravelly sand on the left levee (core H75-13, Plate 6A); the oblique stratification is accentuated by alternating placers of heavy minerals and coarse sand.

Parallel Laminated Sand Division (T_b)

The parallel laminated sand which corresponds to Bouma's B-division (or T_b) is also very rare. It consists of well sorted fine to medium sand. Grading, if present, is masked by parallel lamination. Two parallel laminated sand divisions followed by cross-laminated sandy silt divisions were found on the left levee (e.g. Plate 6A). The thickness of individual units is less than 4 cm.

Cross-Laminated Silt Division (T_c)

This unit includes micro-ripple cross-lamination, climbing micro-

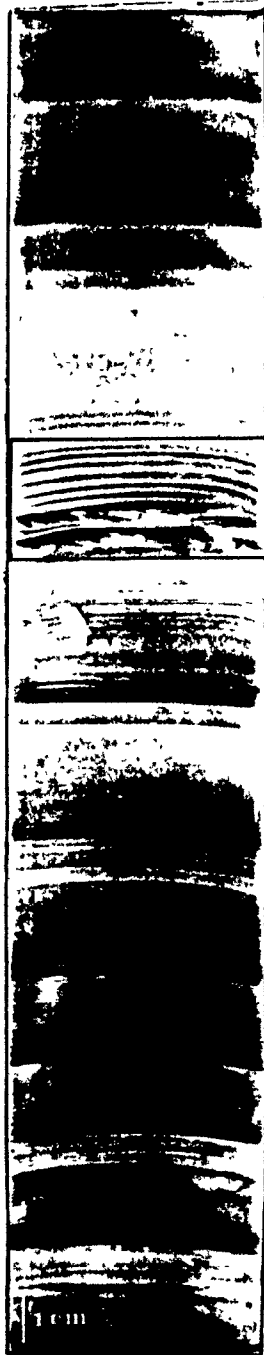
ripple lamination and some convolutedly laminated sandy silt, clayey silt and silt. It is generally medium olive grey in color (5Y 5/1), and consists dominantly of quartz together with detrital carbonates and other terrigenous grains. The thickness of individual units rarely exceeds 3 cm. It is estimated to make up less than 10 percent by thickness of the spill-over facies.

The cross-laminated and overlying parallel laminated divisions were studied in thin sections obtained from impregnated sediment samples. These were taken from the slabs used for X-radiography. The impregnation was done following a method modified after Foster and De (1971). A 1 cm thick slab of glass slide size was treated with chloroform and acetone in a desiccator in order to replace the pore water (Appendix 10). The sample was then impregnated with araldite resin, and a thin section was prepared from it.

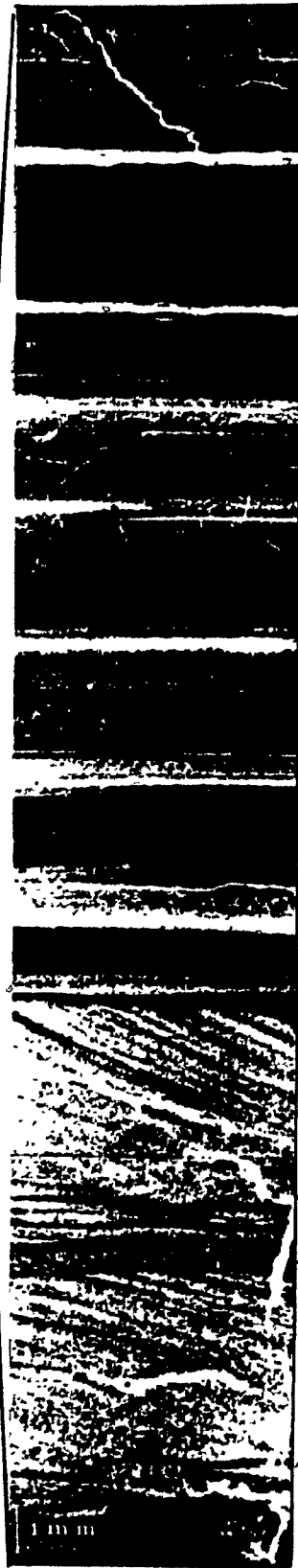
Under the microscope the micro-ripple laminated division shows alternating lee-side laminae (of heavy and light minerals) which are tabular (and rarely convex upward) in shape but become slightly concave near the base of the lee-side (Figure 14). The slope angle of the lee-side laminae ranges from 12° to 14° for different cosets. The level of the sedimentation surface remains nearly horizontal.

Some cross-laminated divisions are composed of climbing sets of lee-side laminae with or without preservation of stoss-side laminae (Plates 4 and 5). Also here, lee-side laminae are accentuated by the concentration of heavy minerals in alternating laminae. The angle of climb is generally less than 5°. The climbing ripples are useful for determining rates of sediment transport and deposition from unidirectional flows. In general, three types (A, B and S) of climbing ripples are distinguished by their

Figure 14. Analysis of the laminated spill-over facies; core H75-11, interval 354-382 cm. A: X-radiograph of a typical sequence of spill-over turbidites; B: photo-micrograph of 8th laminated unit from bottom, unit begins with micro-cross laminated fine sandy silt and silt (T_c) followed by parallel laminated and homogeneous mud; cross-lamination accentuated by placers of heavy minerals; in the parallel laminated division the light bands are dominantly composed of silty quartz (granular laminae = G), whereas the dark bands are composed of flocculated (F) clays. Numbers give thickness in millimeters of G and F laminae, respectively. Contraction of the columnar diagram C eliminates the voids due to cracks developed in the thin section during sample preparation. Grain size variations (in median diameter) of quartz grains in five consecutive laminae (nos. 4 to 8) are shown in D.

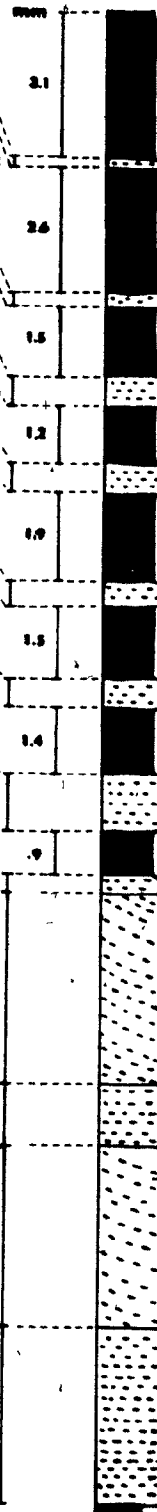


A



B

G F



C

D



preservation of stoss-side laminae, asymmetry of ripple profile and the angle of climb (Jopling and Walker, 1968; Allen, 1973). The climbing ripples of the NAMOC spill-over facies are of type A. They are characterized by a low angle of climb, preservation of stoss- and lee-side laminae and the micro-scale of the cosets (Plates 4 and 5).

At the upper contact the cross-laminated unit is always followed by the upper parallel laminated division. This transition occurs at a median sediment size of about 30 to 40 microns, below which no ripples form.

The significance of these ripple laminations with regard to flow regimes and rates of deposition from bed-load and suspension will be discussed in the section on spill-over processes.

Parallel Laminated Mud Division (T_d)

In terms of frequency of sedimentary structure divisions this is the dominant element in the spill-over facies, comprising more than 60 percent of all the structure divisions. It consists of medium olive grey (5Y 5/1) mud (clayey silt and silty clay). The division sometimes overlies the micro-ripple or cross-laminated division but in most cases it repeats itself. On the average it is 30 mm thick and consists of laminae hundreds of microns to a few millimeters thick. Similar deposits have been described from ancient and modern turbidites (e.g. Bouma, 1972b; Piper, 1972, in press; Rupke and Stanley, 1974). It corresponds to the upper parallel laminated division (D-division) of the idealized Bouma sequence. This division was originally defined for sand and silt sized material and still lacks an adequate hydrodynamic interpretation (Blatt *et al.*, 1972, p. 123).

Each unit begins with a lamina of granular material of medium to coarse silt size (30 to 40 microns), followed by a finer-grained lamina of

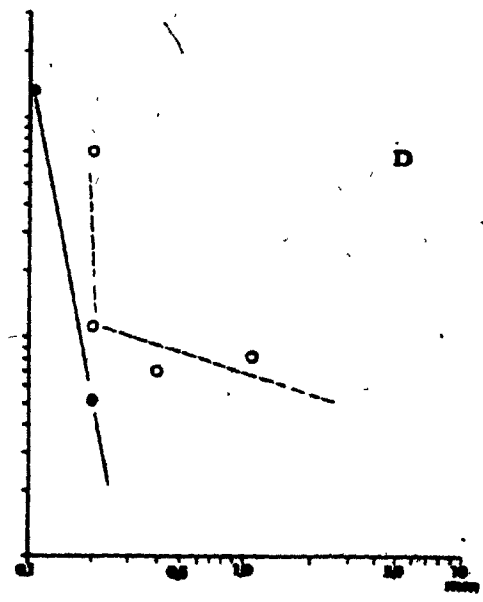
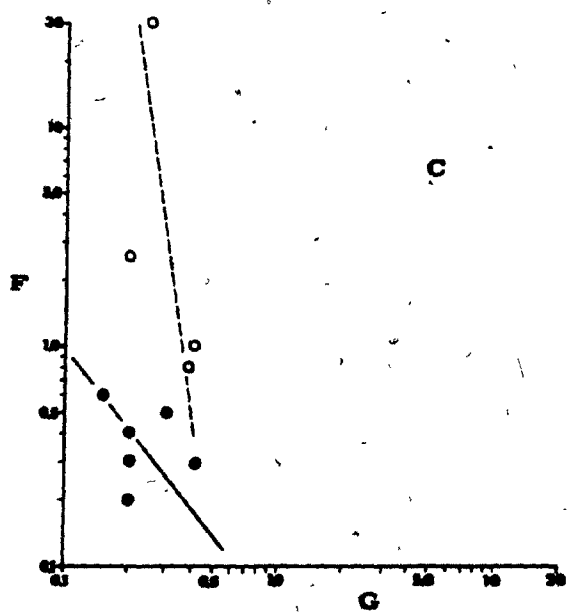
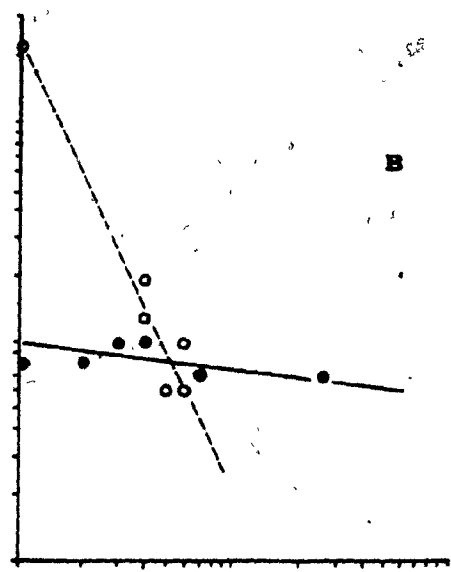
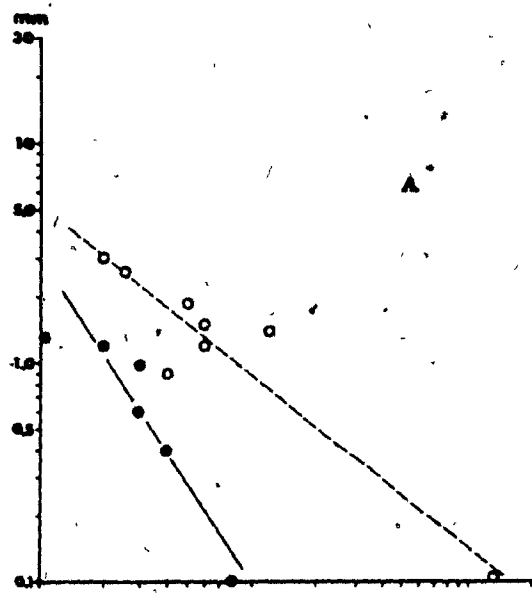
Figure 15. Upward thickness variation of pairs of granular (G) and flocculated (F) laminae in parallel laminated mud; abscissa: thickness of granular lamina (logarithmic scale); ordinate: thickness of flocculated lamina overlying granular lamina (logarithmic scale). Trends of upward decreasing thickness of G and corresponding increasing thickness of F display a nearly logarithmic relationship for samples shown in A, B and C.

A, open circle: H75-11, 362-365 cm
filled circle: H75-11, 373-374 cm

B, open circle: H75-11, 367-369 cm
filled circle: H75-11, 378-380 cm

C, open circle: H75-22, 244-245 cm
filled circle: H75-22, 239-242 cm

D, open circle: H75-22, 244-246 cm
filled circle: H75-22, 256-259 cm



non-granular flocculated clayey material. The results of a detailed analysis of one such unit are shown in Figure 14. The light and dark horizontal bands (Figure 14B, C) represent granular and flocculated laminae, respectively. Each granular lamina consists of well sorted quartz and other detrital grains with less than 10 percent of clayey matrix. The flocculated laminae contain only a few percent of quartz grains. The mean grain size of the granular materials in both types of laminae decreases upward (Figure 14D). Each unit ends with a lamina of flocculated clay at the top which attains the greatest thickness of all flocculated laminae. In many parallel laminated divisions the upward thickness variation of granular and flocculated laminae shows a logarithmic relationship. The logarithmic relationship is better displayed in some units than in others. Figure 15 shows the vertical thickness variation of successive pairs of granular laminae and flocculated laminae. The thickness of the granular laminae is plotted on the abscissa, the thickness of the corresponding flocculated lamina on the ordinate. The former decreases logarithmically upward, whereas the latter increases logarithmically. A discussion of the possible causes of this systematic variation follows in the section on deposition of laminated turbiditic mud.

Homogeneous Mud Division (T_e)

The top of the parallel laminated unit, which consists of flocculated clay is designated homogeneous mud. It is the equivalent of Bouma's (1962) pelitic or E-division (T_e). In X-radiographs this division is devoid of parallel laminae and thereby differentiated from the underlying laminated division. Its average thickness is about 10 mm. In terms of frequency of structural divisions of the spill-over facies it is the second most

frequent unit after the parallel laminated division. The unit is sometimes bioturbated (bioturbation of the E-division is treated together with pelagic sediments in section on secondary sedimentary structures of the pelagic facies).

Pelagic Facies

Occurrence

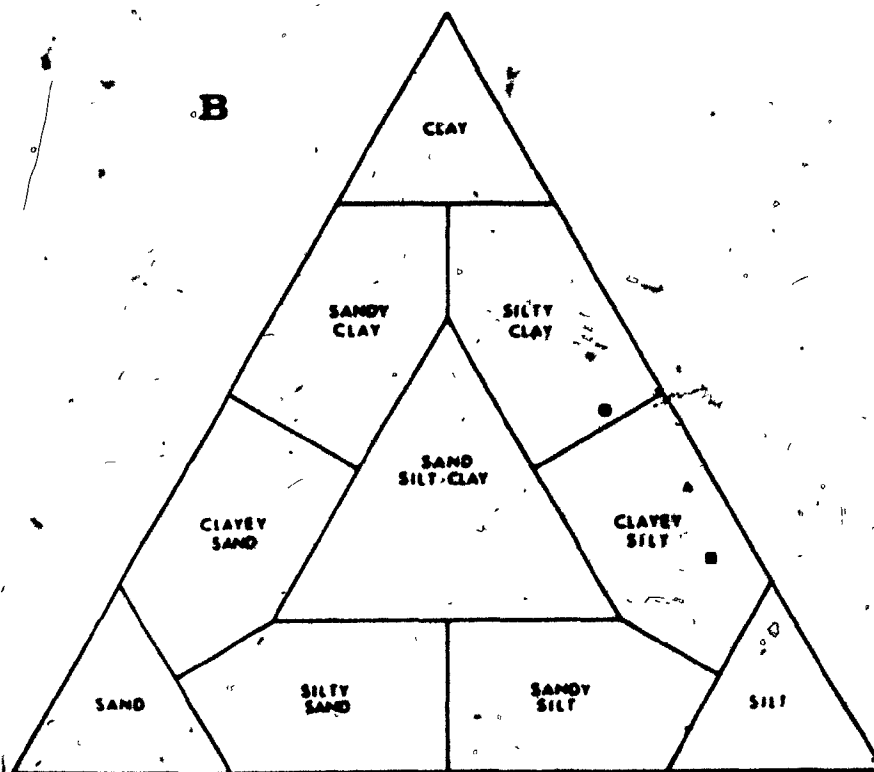
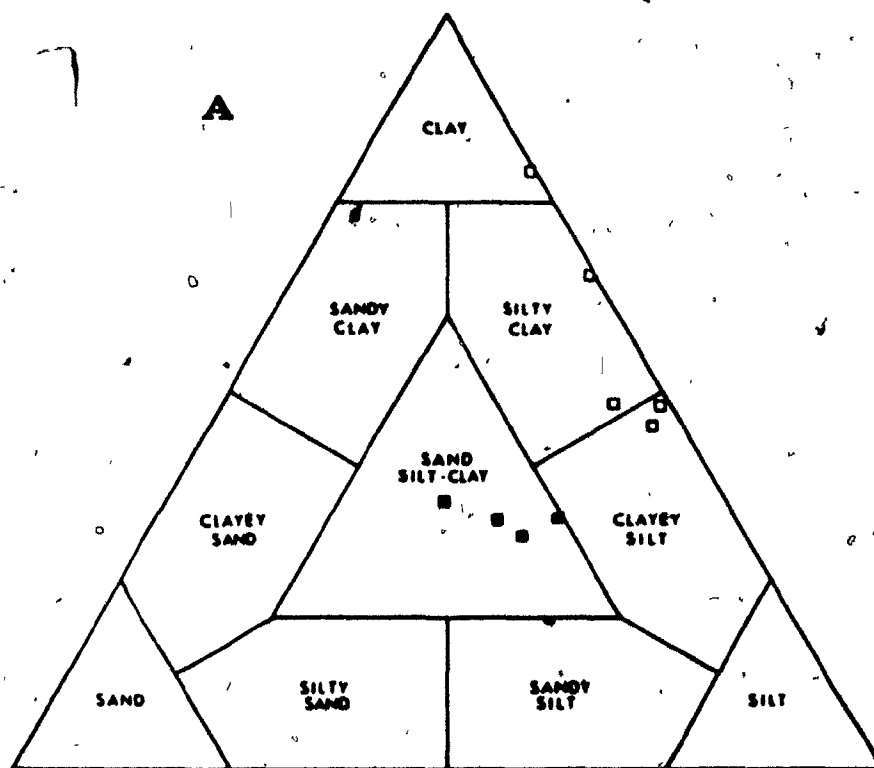
The present sea floor of the Labrador Sea is covered with pelagic and hemipelagic sediments with admixed ice-rafted debris, a facies that results from the slow particle-by-particle settling of biogenic and continental detrital materials through the water column. In the process of settling some of the fine-grained material is picked up by bottom currents or incorporated into diluted turbid suspensions often referred to as nepheloid layers. Surface currents also assume an important role in the distribution of fine-grained particles as well as ice-rafted debris including ice-rafted tephra particles.

This facies is interrupted by the broad band of terrigenous sediments along the course of the NAMOC in the central Labrador Basin. Within the terrigenous channel-fill and spill-over facies of the NAMOC the occurrence of pelagic sediments is limited in time and space. In the spill-over facies of the cores recovered the pelagic layers make up less than 3 percent of the total sediment thickness.

Characteristics

The biogenic materials of the pelagic facies are composed of the tests of foraminifera, diatoms, Radiolaria, coccoliths and sponge spicules. In the oxidation zone near the sediment surface, the sediment color is usually pale or moderate to dark yellowish brown (10YR 6/4, 10YR 6/2, 10YR 5/2) but

Figure 16. Classification according to grain size of (A): pelagic lutites (F), and (B): contourites; IRD = ice-rafted debris; X = slightly to moderately bioturbated, Y = very strongly bioturbated and Z = completely bioturbated and mottled contourites.



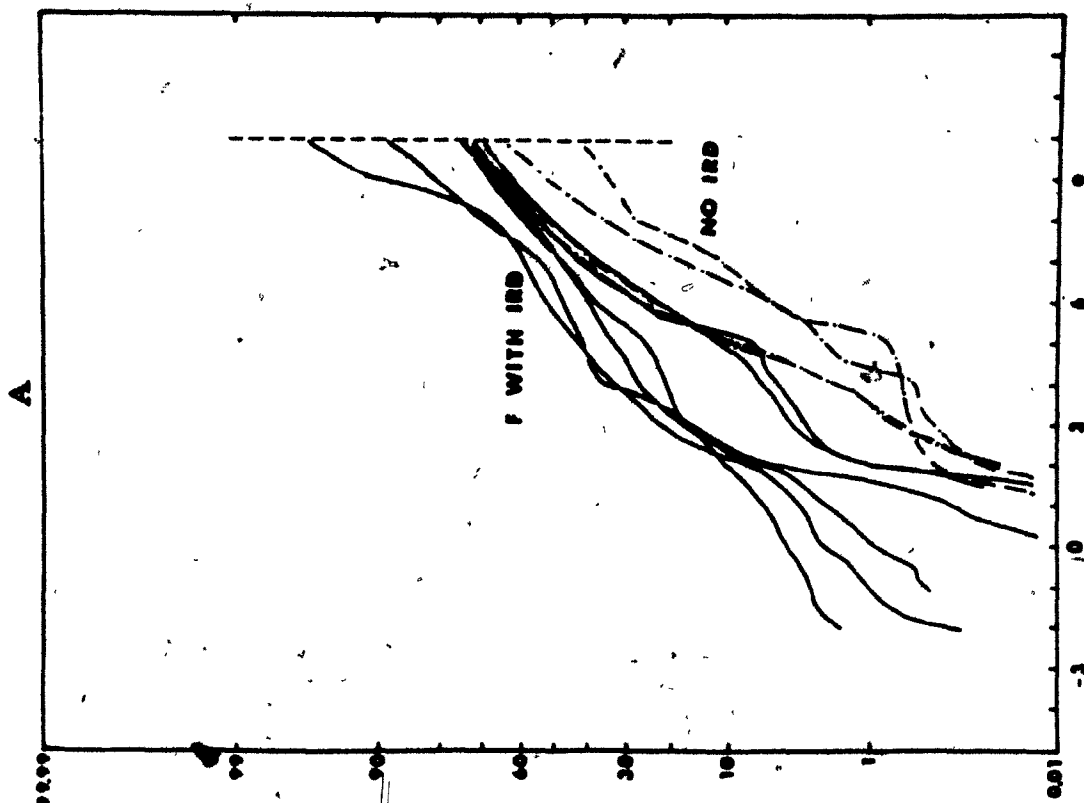
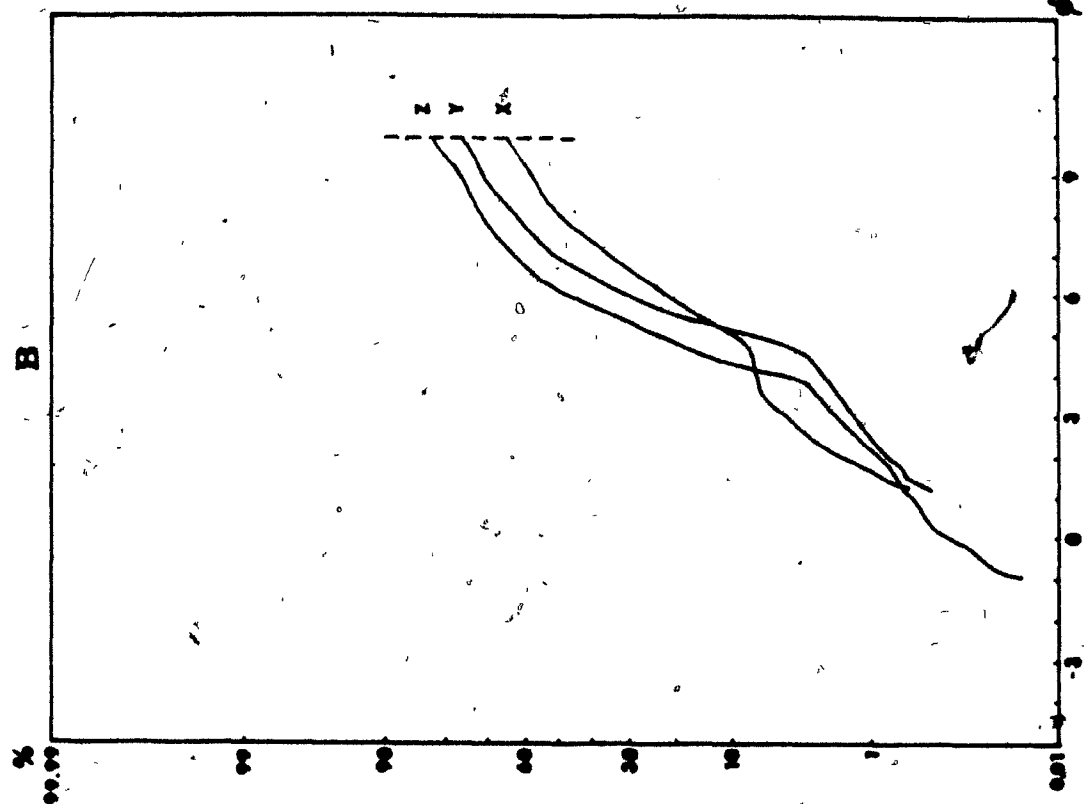
below 50 cm greenish or olive grey hues prevail. Ice-rafted debris form a significant constituent of the pelagic sediments in the Labrador Sea (Plate 7 and Figure 16A). Texturally this is expressed by the very poor sorting of these sediments (Figure 17A). Structurally the most important characteristic of the pelagic facies is the high degree of bioturbation (Plates 8 to 11). The ice-rafted debris include pebble and boulder sized rock fragments whose surfaces contain glacial grooves and striations. Although texturally these pebbly muds resemble debris flow deposits, the matrix composition (biogenic materials) is distinctly different from the terrigenous constituents of debris flows.

Secondary Sedimentary Structures (Bioturbation) and Texture

Bioturbation structures are biogenic secondary sedimentary structures that reflect the disruption of original stratification features or sediment fabrics by the activity of benthonic organisms. An ethological classification of bioturbation structures proposed by Seilacher (1964) is commonly used. It includes a) resting traces (cubichnia), b) crawling traces (repichnia), c) grazing traces (pasichnia), d) feeding structures (fodinichnia) and e) dwelling structures (domichnia). Most studies of bioturbation structures have focused on tidal flat and near shore environments which are easily accessible. In deep-sea sediments observations of bioturbation structures and burrowing organisms are comparatively few. Although photographs of the present deep-sea floor (see Heezen and Hollister, 1971) have revealed many details of the surface morphology of trace fossils and also living organisms, various burrow structures observed in deep-sea sediment cores remain still unclassified.

Bioturbation structures in the NAMOC sediments were observed both in

Figure 17. Cumulative granulometric curves: (A) pelagic lutites (F) and (B) contourites; IRD = ice-rafted debris; X = slightly to moderately bioturbated, Y = very strongly bioturbated, and Z = completely bioturbated and mottled contourites. Because reliability of portions of the curves to the right of vertical broken line at 10 phi is limited, these portions were omitted as on Figure 12.



vertical sections of core samples and on bottom photographs of the sea floor. They are most abundant in the pelagic facies.



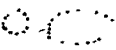

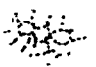

In Table 1 six types of burrows are distinguished according to their shape. It also records the orientation of burrows and their position with respect to the pelagic sediment/turbidite boundary.

(1) Tubular burrows, mostly produced by polychaete worms (Griggs et al., 1969; Piper and Marshall, 1969) are common in pelagic oozes and in the topmost (approximately 10 cm) of the underlying turbidite muds (Plates 8 and 10). The tubes are filled with sandy silt or mud. They measure between 1 and 5 mm in diameter and usually between 1 and 5 cm in length. A variety of shapes are observed including straight, bifurcated and dendritic ones.

(2) Subhorizontal burrows are found in pelagic lutites and underlying turbiditic muds. They are (sub-)horizontal and often display meniscus-shaped internal structures (Plate 8B). The meniscus-shaped linings are made up of reworked sandy silt and muddy sediment, probably representing excrements of sediments ingested by the organism. These burrows represent vertical sections of the conical and helical structure of Zoophycos. Zoophycos is formed by the burrowing of a sediment-feeder of uncertain affinity. The diameter of these burrows is close to 1 cm. The same type of burrows are described by van der Lingen (1973) and Piper and Schrader (1973) from deep-sea sediments in the Pacific.

(3) Oval to circular burrows are common in thick pelagic layers and in the top 10 cm of underlying turbidite muds (Plates 8A and 9). The burrows are filled with poorly sorted sand and mud. They are up to 20 mm in diameter. These burrows are believed to be formed by sediment feeders such as polychaetes, holothurians, molluscs, and echinoids (Piper and Marshall,

TABLE 1. TYPES OF BURROWS

Type	Shape	Characteristic	Length (L) Diameter(D)	Orientation	Occurrence	Assumed Burrower
1. Tubular		straight, bifurcated, dendritic, lined tubes	L=1-5 cm D=1-5 mm	vertical, oblique	Pelagic ooze, top of turbidite	polychaetes pelecypods ? crustaceans ?
2. Subhorizontal (Zoophycos)		meniscus-shaped or concentric internal structure	L=5 cm D=2-20 mm	horizontal to sub- horizontal	Pelagic ooze, turbidite	
3. Oval to circular		reworked sediment	small; D=1-8 mm large; D=8-20 mm	variable	Pelagic ooze, top 10 cm of turbidite	polychaetes holothurians echinoids ?
4. Needle- shaped		very small, straight, dendritic	L=2-5 mm D=1 mm	variable	Mainly turbidite	polychaetes
5. Mottled		completely reworked, no distinct structures			Mainly pelagic ooze	
6. Pyritized filament		very small	L=1-3 cm D=0.5 mm	variable	Pelagic ooze	worm tubes ? hyphae of marine fungi ?

1969).

(4) Needle-shaped burrows are oriented vertically or randomly and commonly occur in turbidites (Plates 9B, 10B and 11B). Where they occur in high concentration the original laminae are almost completely destroyed. They are sediment filled or open, as type 1, and one end of the burrow usually terminates with a circular outline, probably representing the intersection of the tube-shaped burrow with the face of the sediment slice. They are less than 1 mm in diameter and between 2 and 5 mm long.

(5) "Mottled" is the term used for sediments whose primary sedimentary structures have been disturbed so intensely that the individual bioturbation structure is not recognizable (Plate 7).

(6) Pyritized filaments are apparent on X-radiographs (Plates 7A and 16C) of thick pelagic oozes from the upper reaches of the NAMOC and of bottom current deposits on Eirik Sedimentary Ridge. They seem to be particularly abundant in sediments strongly affected by bioturbation, especially those of the contourite facies. Similar filaments have also been described from burrowed sediments in the Strait of Otranto, Mediterranean (Hesse et al., 1971), in burrowed turbiditic muds of the Alboran Sea, Mediterranean (Rupke and Stanley, 1974) and in mottled sediments from the Gulf of Mexico (Bouma, 1972a). They are interpreted as pyritized filaments of worm tubes or hyphae of marine fungi (Hesse et al., 1971).

Bottom photographs of the channel floor and walls of the NAMOC reveal numerous epibenthonic organisms, tracks, trails and excrements (Plates 12 and 13). The most common types of organism observed on these photos are polychaete worms and holothurians. Crustaceans and sea anemones are rare. Other animals such as annelids, ophiuroids, gastropods and pelecypods that have been reported from abyssal depths (Piper and Marshall, 1969; Griggs

et al., 1969; Heezen and Hollister, 1971) may be responsible for some of the structures described, although living specimens were not seen on the bottom photographs from NAMOC.

The amount of reworking of sediments by bioturbation is controlled by the number of organisms per unit volume of sediment and the rate of sedimentation. The depth of penetration of burrows into underlying turbidites appears to be also affected by the sedimentation rate of the overlying pelagic sediments and by the length of the time interval between successive turbidity currents. In other words, organisms penetrate deeper into turbidites when the overlying pelagic sediments accumulate more slowly and for a longer period of time.

Contourite Facies

Occurrence

Bottom current deposits (contourites) in the Labrador Sea delineated by Johnson and co-workers (Johnson and Schneider, 1969; Jones et al., 1970; Egloff and Johnson, 1975) include the Eirik Ridge on the continental rise off the southern tip of Greenland and the Gloria Drift in the central southern Labrador Basin (Figure 10). The Eirik Ridge is bordered by the terrigenous facies of the NAMOC to the west and the Imarssuak Channel to the south, whereas the Gloria Drift forms a loop bound on three sides by the NAMOC, the Imarssuak Channel and the Charlie Fracture Zone, respectively.

On echograms and seismic records contourites are distinguished from normal pelagic sediments by hyperbolic reflections indicative of wavy surface morphology; from turbidites by their relative acoustic transparency. According to Davies and Laughton (1972) contourites are further characterized by the fact that the "sediments are often heaped into piles and ridges

elongated in the direction of the bottom current and lying under the margin of the current"; and by the "presence of marginal channels or moats developed around basement highs or obstacles encountered".

The contourite ridges (or drifts) in the Labrador Sea are believed to be shaped by bottom currents that originate from intermittent overflows of the Norwegian Sea Water (Figure 18). The Eirik Ridge is due to the Northwest Atlantic Bottom (NWAB) Water overflowing intermittently through Denmark Strait. Flowing southwestward on the East Greenland continental slope and rise below 1200 m it turns northwestward at the southern tip of Greenland forming a counterclockwise gyre. On the periphery of the Labrador Basin, measured bottom velocities of the current exceed 20 cm/s (Rabinowitz and Eittrheim, 1974).

Norwegian Sea Water enters the Labrador Sea also through the Charlie Fracture Zone. Overflowing from the Norwegian Sea through the Faeroe Channel (Crease, 1965) this water mass, designated Northeast Atlantic Deep (NEAD) Water flows southward along the eastern flank of Reykjanes Ridge below 2,000 m. A significant portion of the NEAD Water is deflected westward through Charlie Fracture Zone (Worthington and Volkmann, 1965; Garner, 1972), then turning northeast in response to the Coriolis force and flowing northward along the western flank of Reykjanes Ridge. Here, the topography of the West Reykjanes Basin forces it to turn west- and southwestward, part of it overlying the NWAB Water. The Gloria Drift is believed to be formed by this WSW-moving counterclockwise gyral circulation within the southern basin.

In the following section sedimentary structures and textures of three cores obtained from Eirik Ridge are discussed.

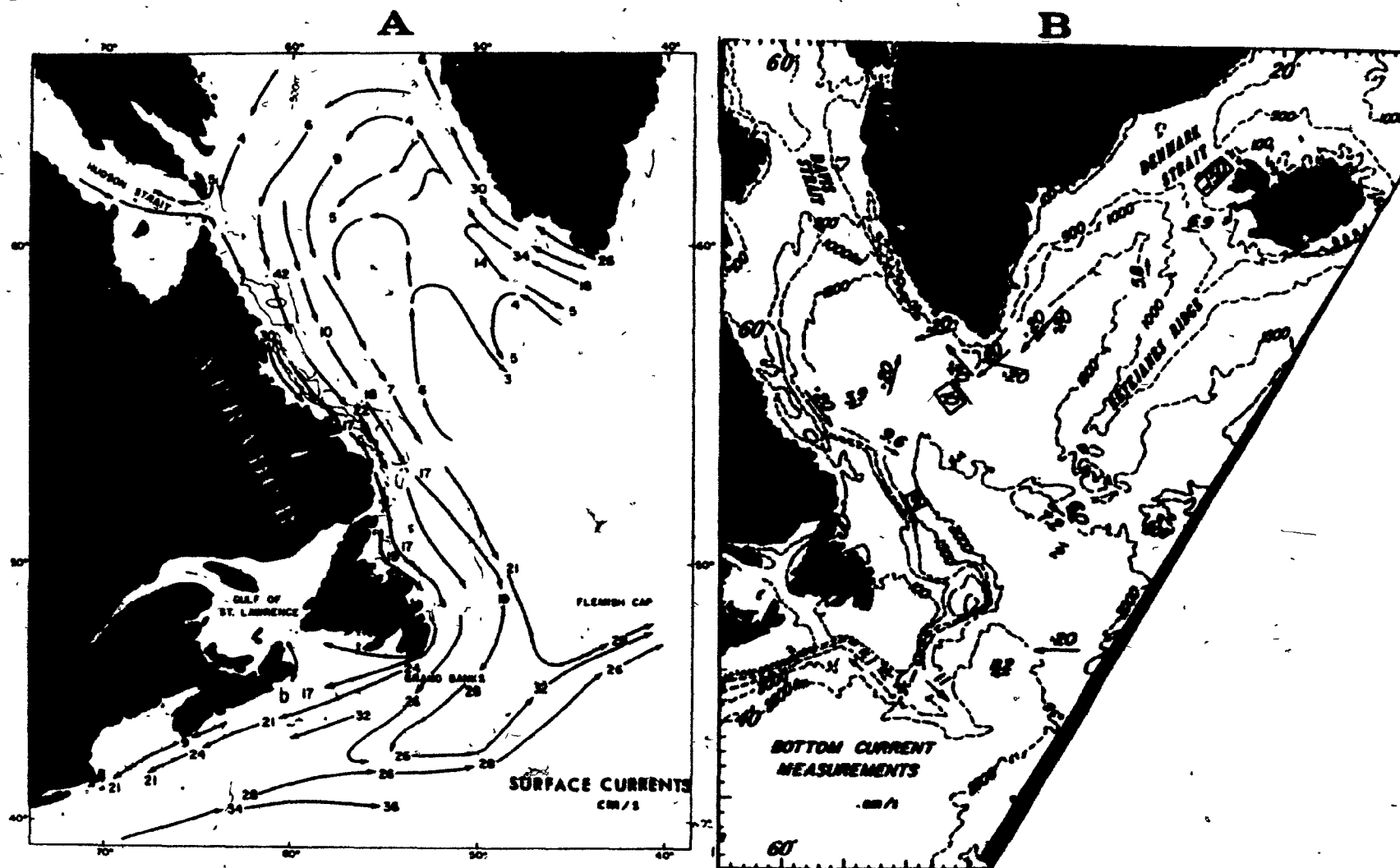


Figure 18. Surface and bottom currents in the Labrador Sea; velocities are in cm/s; A: modified after Dunbar (1951) and Anonymous (1965); B: after Rabinowitz and Eittrheim (1974).

Sedimentary Structures and Texture

Contourites of the Eirik Ridge studied in three cores are, in general, intensely bioturbated and mottled. Therefore, the former presence of primary sedimentary structures could not always be revealed with certainty. Intensity and types of bioturbation are similar to those of the pelagic facies discussed earlier. On the other hand, a very small portion of finely laminated contourites in these cores is virtually unaffected by burrowing. In this case burrows occur only sporadically. There are also some layers which are strongly bioturbated but are left with some traces of the original laminae or layers.

According to the scheme of Reineck (in Reineck and Singh, 1973) the various degrees of bioturbation in Eirik Ridge contourites correspond to the following three categories: a) slightly to moderately bioturbated (grade 1 of Reineck; degree of bioturbation, 1-5%), b) very strongly bioturbated but with some original bedding still being recognizable (grade 5; degree of bioturbation, 90-99%) and c) completely bioturbated and mottled (grade 6; degree of bioturbation, 100%) - the existence of original structures being uncertain.

More than 98 percent of the Eirik Ridge sediments examined belong to the grade 6 of bioturbation, i.e. they are completely bioturbated and mottled (Plate 16). Individual burrow types in sediments bioturbated to a lesser extent are the same as those discussed for pelagic sediments. Approximately one percent of the contourites is very strongly bioturbated (grade 5), and shows vague traces of original laminations (Plate 15). Less than one percent of the contourites show grade 1 bioturbation. Here, the lamination is nearly parallel but wavy and hummocky, clearly distinguishable

from the parallel lamination of the spill-over facies. It also lacks the systematic vertical change and gradation in thickness and grain size of the laminae within individual laminated turbidites (Plates 14B, C). Plate 14B also shows some wavy laminations of fine to medium sand which may have been produced by winnowing bottom currents.

Texturally most contourites studied are poorly sorted due to biogenic mixing and the presence of abundant ice-rafted debris (Figure 17B). The less disturbed finely laminated contourites are moderately to poorly sorted. Numerical textural parameters are given in Appendix 5.

Sequential Analysis of Structural Divisions

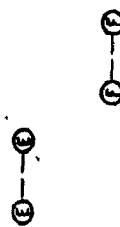
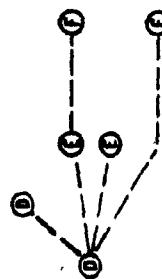
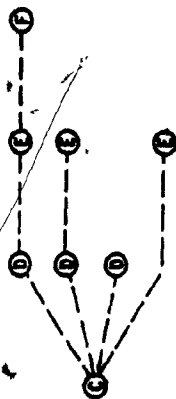
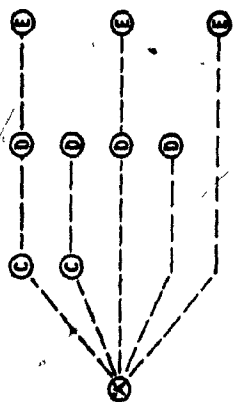
The monotonous repetition of fine-grained, parallel laminated turbidites is a distinctive feature of the spill-over facies.

In order to characterize the spill-over facies more precisely a quantitative analysis of vertical structure sequences was carried out by counting the number of transitions between the various structural divisions encountered on X-radiographs (Figure 19). Most levee cores used in the analysis are from the middle channel segment where the channel gradient is less than 0.002.

More than 95 percent of the turbidites in the spill-over facies start either with the D-division or less frequently with the C-division. Less than 5 percent begin with basal divisions such as the crudely laminated "A"-division, the graded or massive A-division and the B-division. The most frequent transition on both levees is from D to D (average of 55 percent of all transitions). It is followed by the transition D to E (about 20%). The transition E to E occurs with relative frequencies

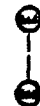
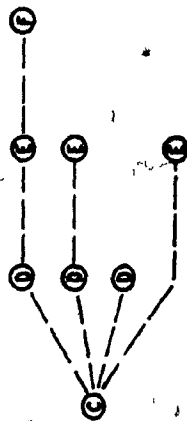
Figure 19. Turbidite structure sequences observed in the spill-over facies of (A), right levee, and (B), left levee; "A", C, D and E represent the turbidite structure divisions: crudely laminated basal division (T_a), cross laminated silt division (T_c), parallel laminated mud division (T_d), homogeneous pelitic mud division (T_e); F represents pelagic ooze or interturbidite. Because of insufficient occurrence, T_a and T_b divisions were omitted from the analysis. Broken lines connect structure sequences within individual turbidites deposited by spill-over of single turbidity currents over the channel walls. Self transition such as D-D indicates that a D-division is immediately followed by another one deposited from a second turbidity current of similar hydrodynamic characteristics.

Freq.	Z
2	0.38
2	0.38
3	0.58
12	2.30
7	1.30
2	0.38
9	1.70
33	6.20
3	0.38
206	53.80
11	2.07
107	20.10
2	0.38
52	9.80
1	0.20
532	100.00



A

Freq.	Z
1	1.10
2	2.20
1	1.10
1	1.10
1	1.10
1	1.10
51	50.00
21	23.90
3	3.40
6	6.80
88	100.00



B

of 10 and 7 percent on the right and the left levee, respectively. C to D transitions occur more frequently on the right levee (6 %) than on the left levee (1 %).

On the natural levees the D-division is predominant and is repeatedly followed by itself; i.e. the parallel laminated mud division is, in at least 50 percent of the overflows, the sole turbidite structure developed from each overflow. Occasionally, deposition from an overflow starts with micro-cross lamination. Often it terminates with unlaminated homogeneous clay.

Basal turbidite divisions are generally rare but occur more frequently in the upper part of the middle channel segment than in the lower part. They are more commonly followed abruptly by D- or E-divisions (4.2%) than by B- (0%) or C-divisions (0.8%). They are also more frequent on the left than on the right levee.

CHAPTER IV - PETROGRAPHIC AND MINERALOGIC COMPOSITION

Gravel Components

In order to trace the NAMOC sediments to their source a detailed analysis of gravel components of the channel-fill facies was made, aiming at the identification of pebbles characteristic for a specific source such as Paleozoic carbonates which have been known to occur only on the continental margins of northeastern Canada but not on the Greenlandian continental margins.

Mineralogy and petrology of gravel components (greater than 2 mm) were studied in thin sections of grain mounts embedded in araldite resin. Thin sections were prepared from samples of all gravel layers in the channel cores and counts of the total number of grains were used for estimating relative frequencies.

Of the more than 1,000 gravel components examined, 50 percent are carbonates, 37 percent granite and granite gneisses, 7 percent sandstones, 2 percent basalts, 1.8 percent gabbros, 1.7 percent amphibolites and less than 1 percent anorthosites (Appendix 6). Several ironstones and sillimanite-schist fragments were also found.

Carbonates are most common among the rock types encountered and consist of limestone and dolomite of various textures and composition. More than 80 percent of the carbonate pebbles are micrites and biomicrites. Fossils in biomicrite include crinoids, gastropods, brachiopods, bryozoa, molluscs and others. A number of samples also contained coral fragments. The coral fragments were identified as Paleofavosites of Late Ordovician to Middle Silurian age (C.W. Stearn, pers. comm.).

Granite gneisses include various types of granites, gneisses and related

rocks which are common in the Canadian Shield and also in Greenland. Sandstones include litharenites with angular grains, poorly sorted arkoses and quartzites.

Although only a few fragments of anorthosite were found the plagioclase composition in anorthosites is of particular importance for the identification of the source of the NAMOC material. The An-content of plagioclase in 7 anorthosite samples ranges from An₂₅ to An₄₅ (andesine-oligoclase). Anorthosites on the Canadian Shield are intermediate (An₄₀₋₆₀) whereas anorthosites from Greenland are higher in An-content of plagioclase (An₈₀₋₉₀) (Windley, 1969).

The abundance of carbonate pebbles and the plagioclase content in anorthosites indicates a Canadian source for the NAMOC sediments and is further discussed in the section on sediment source.

Sand Fractions

Heavy Minerals

Studies of heavy minerals have provided useful information on the provenance of sediments in many ancient and modern basins. Potentially useful provenance indicators are minerals unique to a localized sediment source as for example the alkali basalts of southwestern Greenland. For comparative purposes samples of beach sands from this region (courtesy F. Kalsbeek) were included in this study. Also studied were the coarse layers of sediment cores from the Imarssuak Mid-Ocean Channel area (DSDP site 113).

Standard methods were followed for heavy mineral separation (using bromoform with a specific gravity of 2.88 g/cm³) and sample preparation (Carver, 1971). To make results between samples comparable, two narrow

grain-size fractions (63-125 and 125-250 microns, respectively) were used. In each mount the total number of grains, 150 on the average, was counted.

The heavy mineral assemblage of the non-opaque, non-micaceous grains of the NAMOC and the Imarssuak Mid-Ocean Channel area is dominated by garnet and hornblende. Garnets include clear to pale pink and some salmon colored varieties. The hornblendes are dominantly green and blue-green with some brown varieties. Amounts of clinopyroxene, hypersthene, epidote, tourmaline and apatite are subordinate. Very small amounts of sphene, zircon, andalusite, rutile, sillimanite, zoisite, enstatite, kyanite and staurolite are present in varying proportions.

Percentages of individual heavy mineral assemblages of the NAMOC and the Imarssuak Mid-Ocean Channel are given in Appendix 7. Minerals characteristic for the alkali basalt province of southwestern Greenland such as chromite, eudialyte, arfvedsonite, aegirine and twinned hypersthene (Crömmelin, 1937; Kalsbeek, pers. comm.) are absent in the sediments of the two channels. Although the mineral assemblages are very similar in the two channels, the ratio of garnet to hornblende is greater in the NAMOC than in the Imarssuak Mid-Ocean Channel area. In addition, a small percentage of actinolite and tremolite is recorded from the latter.

Light Minerals

A detailed study of light minerals of the coarser layers was not made because the results were not expected to contribute significant information for the problems under investigation. For comparison with the coarser layers of the pelagic facies only a small number of samples were studied using the grain size fractions of 63-125 and 125-250 microns. For the

distinction between K-feldspar and plagioclase the grain mounts were stained according to the method of Bailey and Stevens (1960).

In decreasing order of abundance the light minerals include: quartz (50%), detrital carbonate (40%), plagioclase (5%), K-feldspar (3%), biotite (2%) and remainder (e.g. clay pellets, less than 1%).

Silt- and Clay-sized Fractions

Mineralogical composition of the fine-grained sediment fractions was studied in order to further characterize the differences between fine-grained turbidites of the spill-over facies and intercalated pelagic lutites.

Two sets of samples were analyzed: one for bulk mineralogy and one for clay mineralogy. For X-ray diffraction analysis of the bulk mineralogy samples were prepared by the smear-slide method (Gibbs, 1971) without removing carbonates. In the Labrador Sea the carbonate content serves as an additional means to distinguish between fine-grained turbidites and pelagic lutites.

The clay-sized fractions for X-ray diffraction were prepared according to the method of Griffin *et al.* (1968). A sample of approximately 10 g was treated with a solution of 10 percent H_2O_2 in distilled water to remove the organic carbon. The sample was then sieved through a 63-micron sieve and the fine fractions were collected in a 35 cm high, one-litre cylinder. Two grams of sodium metaphosphate (Na_3PO_4) were added to disperse the clay. The suspension was stirred and after four hours of settling, size fractions smaller than 2 microns were collected from the top 5 cm of the cylinder. Oriented slides were prepared for each sample; one untreated, the other treated with 25 percent HCl to remove the carbonates. All slides were treated with ethylene glycol overnight.

All X-ray diffraction analyses were performed with a Norelco diffractometer using Cu K α radiation and a nickel filter at a scanning speed of 1 2-theta/min. or 1/4 2-theta/min. Identification of the mineral phases and semi-quantitative analysis of clay minerals were carried out following the methods of Biscaye (1965), Carroll (1970) and Carver (1971). The result of a systematic X-ray diffraction study of two cores (Figure 21) was also provided by Dr. J. Müller, Technische University.

The minerals present include calcite, quartz, plagioclase, K-feldspar, dolomite and clay minerals. Both in turbidites and pelagic lutites, calcite along with dolomite are dominant over quartz and feldspar (Figure 21A, B). Detrital calcite and dolomite are more common in turbidites than in pelagic lutites (Figure 20; also compare A and B in Figure 21) which result in the high total carbonate contents (Figure 21).

Among the clay minerals the four major groups of clay minerals, i.e. illite, chlorite, montmorillonite and kaolinite are present. Turbidite muds are rich in illite with an average of 70 percent and contain less than 10 percent montmorillonite, whereas illite makes up 40 to 50 percent and montmorillonite 25 to 40 percent in the pelagic lutites, respectively (Figure 21). Kaolinite and chlorite make up less than 20 percent in both the turbidites and pelagic lutites.

The predominance of illite in the turbiditic muds reflects glacial erosion of weathered plutonic and high grade metamorphic rocks of the Precambrian Shield during the Wisconsinan. Piper and Slatt (1977) also found that illite was the dominant clay mineral contributed to northeastern Canadian shelves during Late Wisconsin time. Montmorillonite, on the other hand, is absent from the Baffin Island till and onshore in northeastern Canada but occurs offshore Labrador, where it is supposed to be derived from the underlying coastal plain strata (Piper and Slatt, 1977) and possibly from alteration of

Figure 20. X-ray diffractogram showing presence of abundant calcite and dolomite in turbiditic muds (1 and 2) whereas pelagic lutites (3 and 4) are free of or contain very little dolomite. Also shown is the contrast in the illite/montmorillonite ratio between the two, which is relatively high for the turbiditic muds and lower for the pelagic lutite; portion of diffractograms to the right of 27° : sample treated with 25 percent HCl and glycolated overnight; left portion: untreated sample. C = calcite, D = dolomite, Ch = chlorite, K = kaolinite, I = illite, M = montmorillonite, Q = quartz.

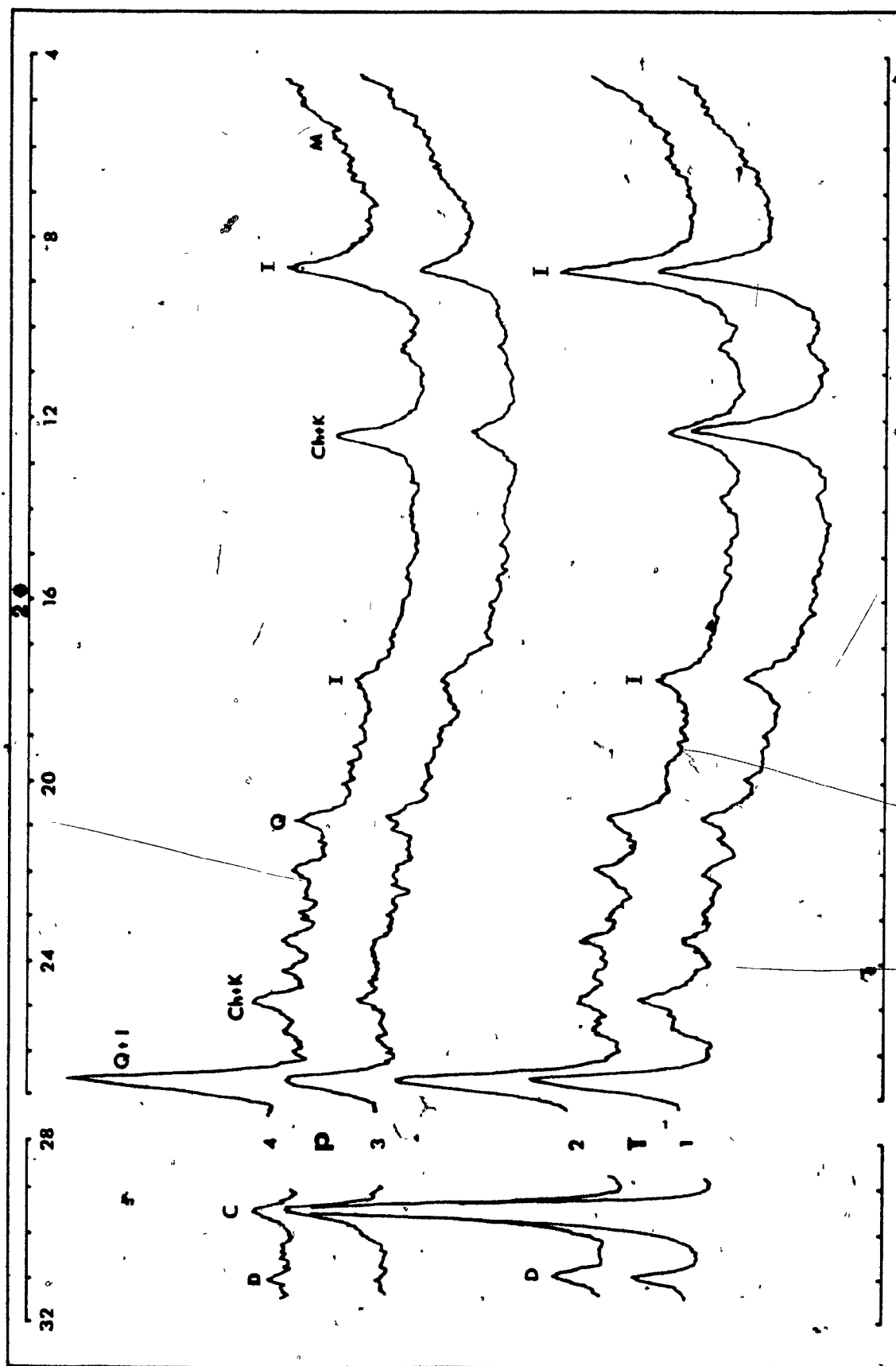
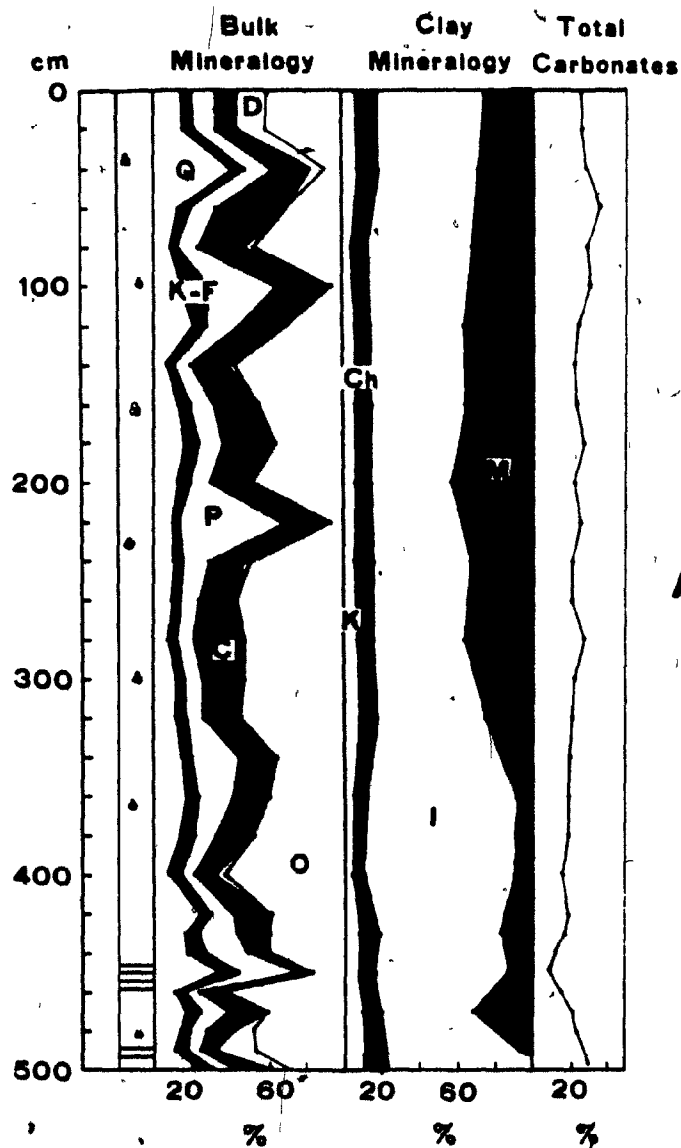
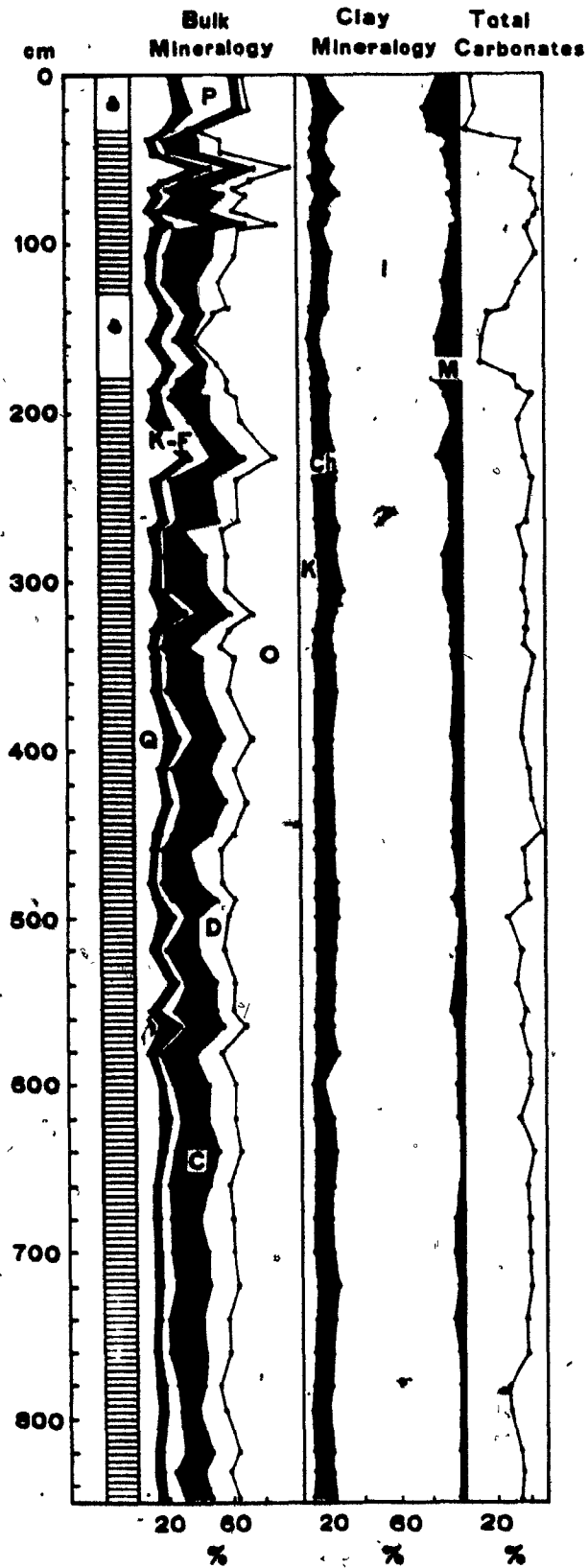


Figure 21. Vertical variation in mineralogical composition of two cores, H74-66 (A) and H74-68 (B); (J. Müller, unpublished data). In general carbonates are very common; detrital dolomites are more abundant in turbidites (most of B) than in pelagic lutites (most of A) resulting in a higher total carbonate content in the turbidites compared to the pelagic lutites. Also shown is the contrast in the illite/montmorillonite ratio between the two: it is higher for the turbidites and low for the pelagic lutites.

H74-66



H74-68



indigenous volcanogenic material originating from disseminated tephra of Icelandic origin.

Ice-rafted Debris

Paleoclimatic implications of ice-rafted debris in deep-sea sediments have been quantitatively studied in many parts of the high-latitude oceans. In an attempt to evaluate Late Pleistocene to Holocene paleoceanographic conditions of the central Labrador Sea ice-rafted debris in pelagic sediments were quantitatively analyzed.

Ice-rafted debris are recognized on X-radiographs as scattered sand- and pebble-sized clasts in pelagic lutite (Plate 6B, C). The majority of the larger ice-rafted components consists of angular to subrounded rock fragments, some of which contain glacial striations and grooves. On scanning electron microscope (SEM) photos of ice-rafted quartz grains typical features of glacial origin such as high relief, conchoidal fractures, chatter marks and lack of solution pits are common, as have been described in numerous previous studies of ice-rafted debris (e.g. Margolis and Kennett, 1971). Some ice-rafted quartz grains are frosted which according to Slatt (1973) is an indication of initial deposition in a beach environment. The distinction of these ice-rafted sediments from poorly sorted pebbly muds of debris-flow deposits, which may be similar texturally and structurally, is confirmed by the matrix composition being pelagic ooze rather than terrigenous mud.

Detrital grains larger than 63 μ in pelagic ooze were considered ice-rafted debris. Quantitative estimates were obtained with the method of Kennett and Brunner (1973). Layers identified as pelagic on the X-radiographs were sampled at intervals of 5 or 10 cm with an 11 cm³ cylinder. Samples were dried and weighed, then wet washed through a 63 micron sieve

and weighed dry again. The number of clastic grains was counted and converted to grains per gram of total sample. Estimates of the proportion of tephra grains were obtained in the same way except their abundance is expressed as number of grains per gram of material coarser than 63 microns.

There is no systematic latitudinal or temporal variation apparent in the abundance of ice-rafted debris during the last 23,000 years (Appendix 8). This is partly due to the limited number and thickness of pelagic layers^{*} but may also have been caused by a number of other factors such as seaward extent of glaciers, and shelf-ice development, ice surges, variations of preferred iceberg tracks, or transport by bottom currents that control the distribution of ice-rafted debris as explained by Keany et al. (1976).

Ice-rafted Tephra

Ice-rafted debris include sand-sized tephra particles disseminated in the pelagic ooze. Ice-rafting and also bioturbational mixing (Berger and Heath, 1968) are responsible for an extreme dissemination of these particles. They consist of brownish and dark pumice and tuff particles as well as rare grains of clear bubble-walled shards. Some grains are as large as 6 mm in diameter.

^{*}Similar tephra material was previously found in the North Atlantic in pelagic layers dated 9,300 (Ruddiman and McIntyre, 1973), 54,000 (W.F. Ruddiman, pers. comm. to R.H. Fillon) and 65,000 y B.P. (Bramlette and Bradley, 1941). They are assumed to have been transported by ice-rafting of volcanic material originating from Iceland (Ruddiman and Glover, 1972). The sand size of the tephra grains, their widespread distribution and great distance from volcanic centers eliminate any other possibilities of

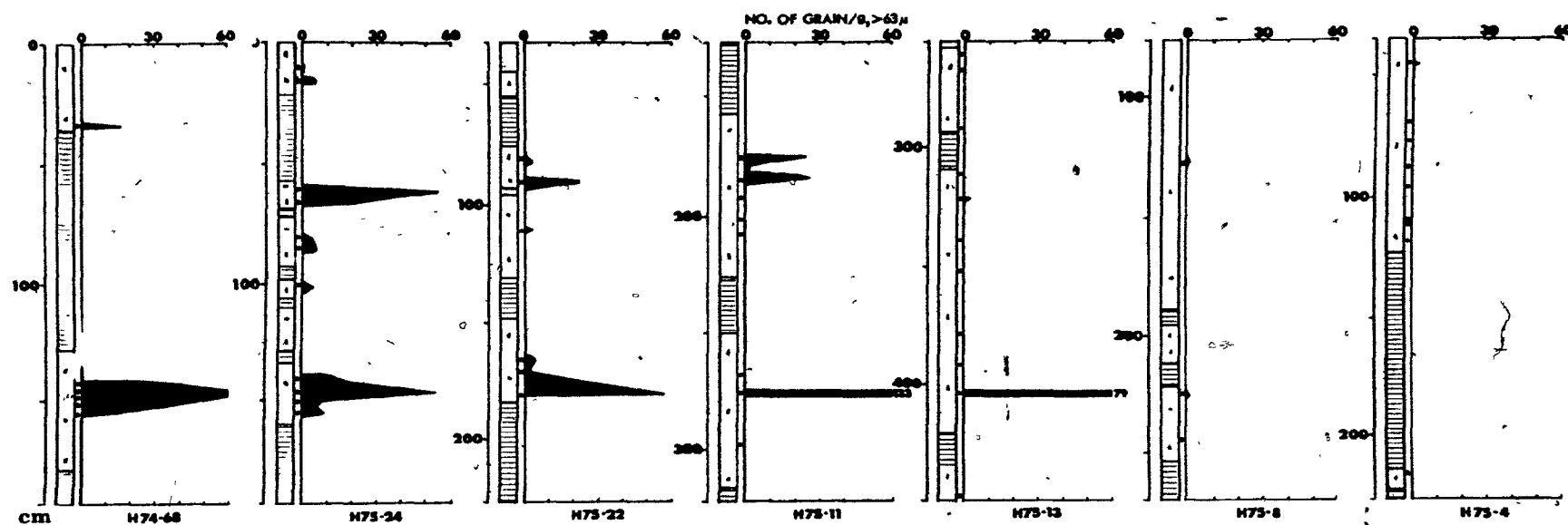


Figure 22. Correlation of disseminated tephra particles in pelagic lutite. Closely spaced horizontal lines represent parallel laminated turbidite mud; the rest for pelagic lutite that contains ice-rafted debris and ice-rafted tephra. Dots indicate sample points.

transport in water or the atmosphere. Tephra layers are assumed to have accumulated on the ice around Iceland within 200 to 400 km from volcanic vents during periods of extensive ice-cover (Fisher, 1964). Breaking of the ice during subsequent warmer periods caused redistribution of the tephra material, which was controlled by the prevailing surface currents.

A correlation of two discrete layers of disseminated tephra particles emerges from a systematic analysis of the levee cores (Figures 22 and 25), which will be discussed in detail in the section on stratigraphy.

Organic Carbon

The organic carbon content of the turbiditic muds and pelagic oozes was determined for selected intervals of the levee cores in which the two types of sediments can easily be distinguished by means of X-radiography, composition and other characteristics.

The organic carbon content was measured with a Leco induction furnace and a gasometric analyzer. Carbonate was removed by digestion in 50 percent HCl. Complete removal of carbonates was checked by XRD. The samples were then washed, dried and ground. A constant amount of material of 0.5 gram was used for analysis. Total carbon content was also determined by the same method, without HCl treatment (Appendix 9).

The organic carbon content of the turbiditic muds is on the average twice as high as that of the pelagic oozes (Figures 23 and 24). The high values of organic carbon in the turbiditic muds are attributed to rapid deposition of organic matter bearing sediments (see also Froelich *et al.*, 1971). This material comes from the continental margins where primary production and terrigenous input of organic matter bearing sediment are high (Griggs *et al.*, 1969; Heezen *et al.*, 1955). Lower organic carbon in

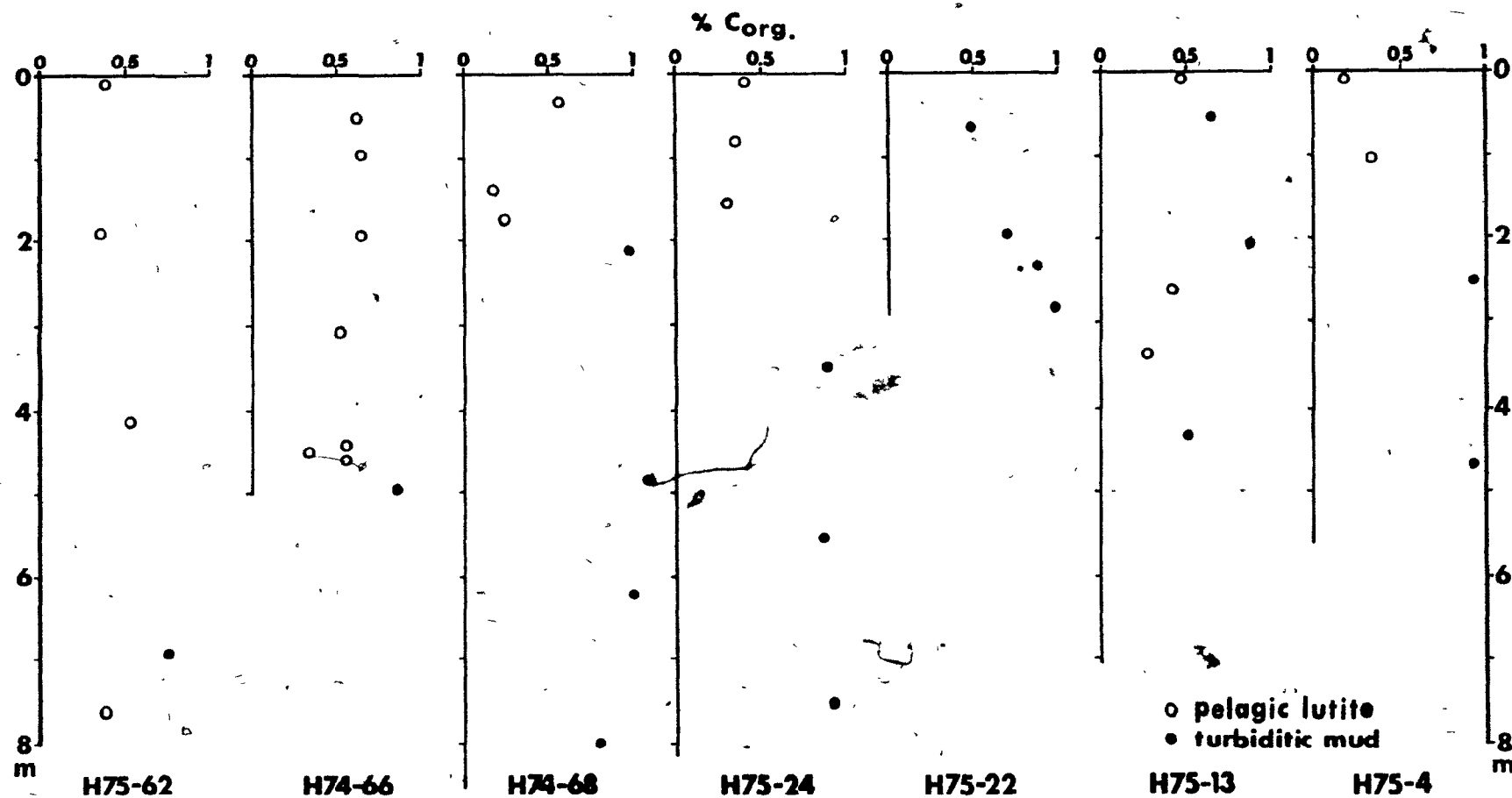


Figure 23. Organic carbon content plotted against core depth; all cores are from the levees except cores H74-66 and H75-62 which are from the upper reaches of the channel-floor (for core locations see Figure 3).

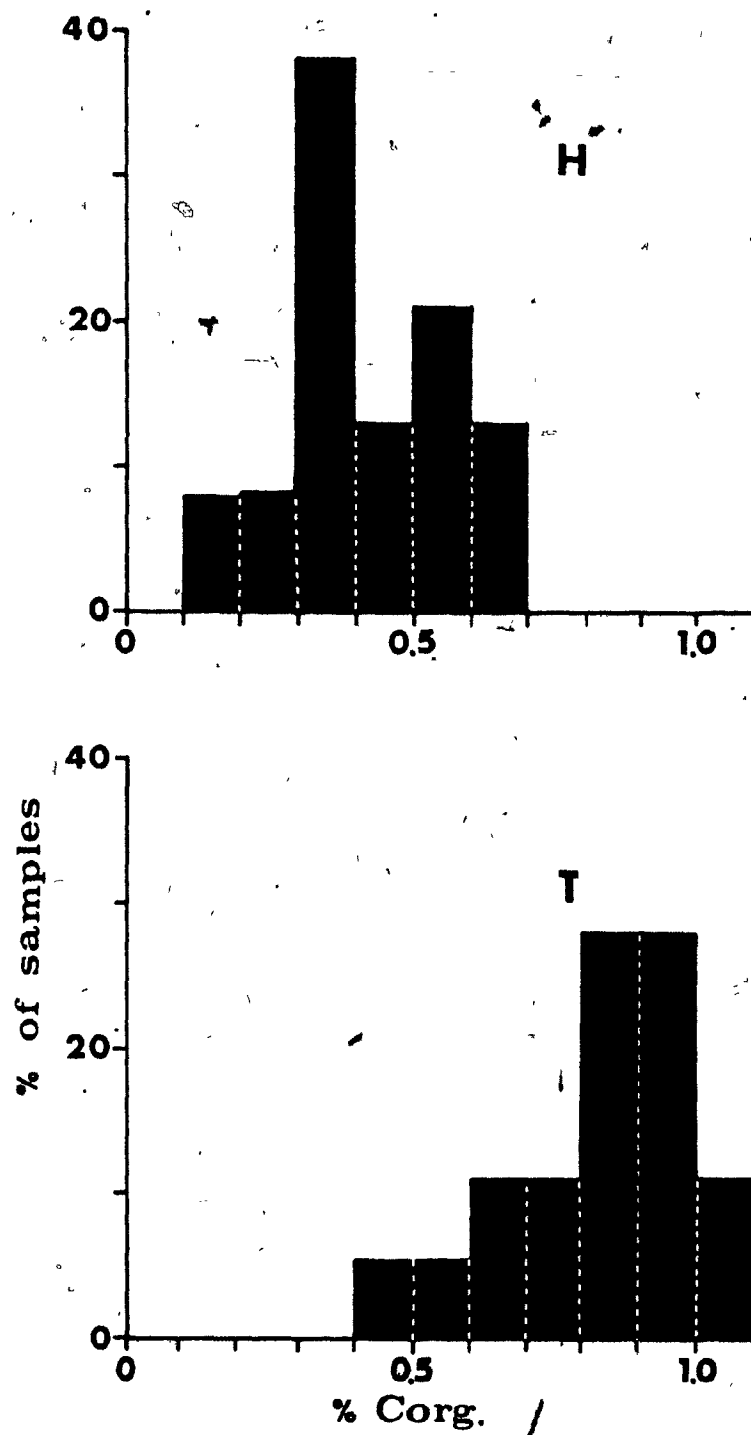


Figure 24. Frequency histogram of organic carbon content, comparing the abundance of organic carbon in pelagic oozes (P) and turbiditic muds (T). Total number of samples: 40 (pelagic: 22; turbiditic: 18).

the pelagic oozes probably results from pre-burial oxidizing conditions on the sea-floor (Froelich et al., 1971) and from consumption by organisms.

CHAPTER V - CORRELATION AND STRATIGRAPHY

Correlation of Individual Cores

Distinct differences between the channel-fill and levee facies have been pointed out in previous chapters. The difference is particularly evident with the correlation of cores from the channel-fill and the levee facies. The gravel and sand layers of the channel-fill facies do not correlate, even between cores that are only a few kilometers apart, (Figure 11). This may be attributed to lenticular and discontinuous development of sand and gravel bodies that build point bar sequences in meander bends or from lag deposits in the talweg.

On the other hand, a layer-by-layer matching is, in fact, possible between some layers in the spill-over facies. This can be demonstrated in two cores from the right levee which are 70 km. apart in the downchannel direction (stations 24 and 22, Figure 25; see Figure 3 for detailed core location). The correlation is self-evident from corresponding core sections on Plates 18 to 20. It is obvious from a sequence of marker units, i.e. the crudely laminated "A"-divisions of some of the layers. Divisions of parallel laminated mud between the marker layers also match. The type and intensity of bioturbation and the amount of coarser ice-rafted debris in pelagic layers are comparable as well. A downcurrent decrease in layer thickness is not apparent.

Four stratigraphic units can be distinguished in most of the levee cores on the basis of lithofacies (pelagic versus turbiditic), tephra correlation and radiocarbon dates. They include from top to bottom: a) an

CORRELATION OF LEVEE CORES.

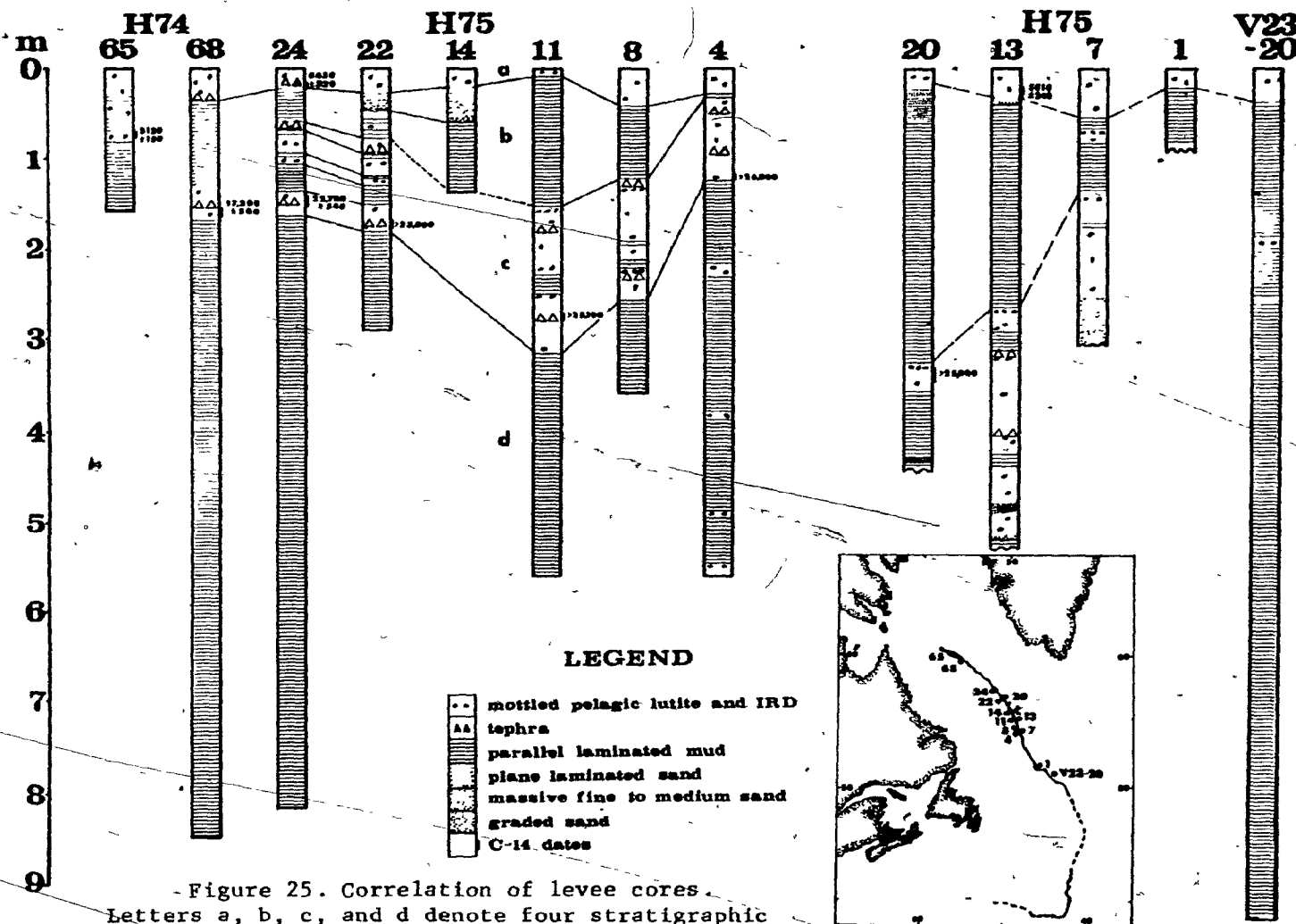


Figure 25. Correlation of levee cores. Letters a, b, c, and d denote four stratigraphic units, i.e. upper pelagic, upper turbiditic, lower pelagic, and lower turbiditic units, respectively.

upper pelagic, b) an upper turbiditic, c) a lower pelagic and d) a lower turbiditic sequence. The thickness of the upper pelagic sequence is more or less uniform (30 cm on the average). The upper turbiditic sequence overlies the lower pelagic sequence, often with an erosional contact at the base. The lower turbiditic sequence is of undetermined thickness. In core H75-4, however, four more pelagic layers are intercalated within the lower turbiditic sequence.

Longitudinal and Lateral Variations

Thickness variations of the four stratigraphic horizons in the spill-over facies along the channel axis are shown in Figure 25. Being present in most cores the top pelagic layer is of more or less uniform thickness on both levees and also in the channel. Minor thickness variation may have been caused by current winnowing and local differences in the rate of ice-rafting. Anomalous low or high thickness of the top layer in some of the cores may be partly attributed to sediment loss or stretching during coring operations, as shown by a comparison of trigger weight cores with piston cores from the same station.

The upper turbidite horizon has a lenticular distribution in the middle channel segment. This horizon is thicker on the left levee than on the right levee. At the top of the upper turbidite horizon a layer of medium to coarse sand occurs in four cores which are as far as 200 km apart from one to the other (i.e. cores 22 and 14 on the right levee and cores 20 and 13 on the left levee; see Figure 25). Although it is not known whether the coarser layer is age-equivalent and forms a continuous blanket on both levees, the stratigraphic position of the layer, i.e. just below the boundary between the upper pelagic and the upper turbiditic horizon, suggests

that it represents an extensive overflow from a single turbidity current.

The lower pelagic horizon contains some turbidite layers. On the right levee the thickness is relatively uniform parallel to the channel axis. On the left levee it is relatively irregular.

Stratigraphy

The time framework of the stratigraphic horizons has been established from a) a number of radiocarbon dates (Table 2), b) correlation of disseminated tephra horizons and c) biostratigraphic evidence. Most of the radiocarbon dates were obtained from the tephra-bearing foraminiferal ooze layers near the bases of the upper and lower pelagic horizons. Because of abundant detrital carbonates in pelagic layers foraminifera used for dating were hand-picked.

Three radiocarbon ages were obtained from the base of the upper pelagic layer: $6,930 \pm 200$ y B.P. for the interval between 17 and 26 cm in core H75-25; $8,630 \pm 320$ y B.P. for the interval between 13 and 19 cm in core H75-24; $5,810 \pm 240$ y B.P. for the interval between 15 and 27 cm in core H75-13. The interval 32-36 cm in core H74-68 also contains ice-rafted tephra particles which by extrapolation of the 8,600 y date were deposited at about $8,000 \pm$ y B.P. This age for brownish tephra deposits in the central Labrador Sea is slightly younger than that of the North Atlantic clear bubble-wall shard layer I (9,300 y B.P.) determined by Ruddiman and McIntyre (1973) and Ruddiman and Glover (1975). According to these determinations the boundary between the upper pelagic and the upper turbiditic horizon in the NAMOC cores is slightly older than 7,100 y B.P. This boundary occurs at an average subsurface depth of 30 cm in most of the cores from the axis of the Labrador Basin.

The lower pelagic horizon contains two disseminated tephra layers

TABLE 2. CARBON-14 DATES

Core No.	Core Depth (cm)	Location	Laboratory	Lab. No.	C-14 Dates (B.P.)	Material
H75-25	17-26	Channel Floor	Geol. Surv. Canada	GSC-2451	6,930±200	Foraminifera
H74-65	70-76	Right Levee	Geol. Surv. Canada	GSC-2205	5,160±150	Foraminifera
H74-68	157-179	Right Levee	Geol. Surv. Canada	GSC-2208	17,200±600	Foraminifera
H75-24	13-19	Right Levee	Geol. Surv. Canada	GSC-2444	8,630±320	Foraminifera
H75-24	140-155	Right Levee	Geol. Surv. Canada	GSC-2430	22,700±540	Foraminifera
H75-22	175-180	Right Levee	Geol. Surv. Canada	GSC-2332	> 23,000	Foraminifera
H75-11	270-280	Right Levee	Teledyne	I-9870	> 25,100	Foraminifera
H75-4	115-122	Right Levee	Teledyne	I-9814	> 26,000	Foraminifera
H75-20	330-345	Left Levee	Geol. Surv. Canada	GSC-2356	> 25,000	Foraminifera
H75-13	15-27	Left Levee	Teledyne	I-10,079	5,810±240	Foraminifera
H75-6	29-35	Channel Floor	Teledyne	I-10,078	4,775±110	Foraminifera

(Figure 25): one occurs near the top and the other near the base. Figure 22 shows a correlation of both layers in most levee cores. An age of $22,700 \pm 540$ (and $>23,000$) was obtained for the lower tephra layer in two cores (H75-24 and 22), in which a layer-by-layer matching is established as described in the section on correlation of individual cores. The same layer dated in core H74-68 from a slightly higher latitude gives a $17,200 \pm 500$ y B.P. age. If the minimum ages obtained from the base of the same layer in the lower latitudes (i.e. $>25,000$, $>25,000$ and $>26,000$ y B.P. in cores H75-20, 11 and 4, respectively; Figure 25) are used, the boundary between the lower pelagic and the lower turbiditic horizon would appear time-transgressive from southeast to northwest.

In addition to the radiocarbon dates a relative time stratigraphy of core H75-4 was established by means of foraminiferal abundances. Planktonic foraminifera are well established as paleoecologic indicators because the temperature of the water mass has a direct influence on the abundance of different foraminiferal species and coiling directions of Globigerina pachyderma. According to Bé and co-workers (Bé, 1959, 1960; Bé and Hamlin, 1967) polar water is represented by the sinistral-coiling G. pachyderma; subpolar species include dextral-coiling G. pachyderma, Globigerina bulloides and others; Globorotalia inflata characterizes the transitional water mass. Using these criteria and coccolith abundance McIntyre et al. (1972) have identified fluctuations of the polar front in the eastern North Atlantic during the last 225,000 years.

In order to determine the age of sediments in core H75-4 the abundance of planktonic foraminifera and the relative frequency of sinistral-coiling G. pachyderma versus G. bulloides and Gt. inflata were determined (Figure 26) by Dr. R.H. Fillon, Bedford Institute of Oceanography. Both the cold-water

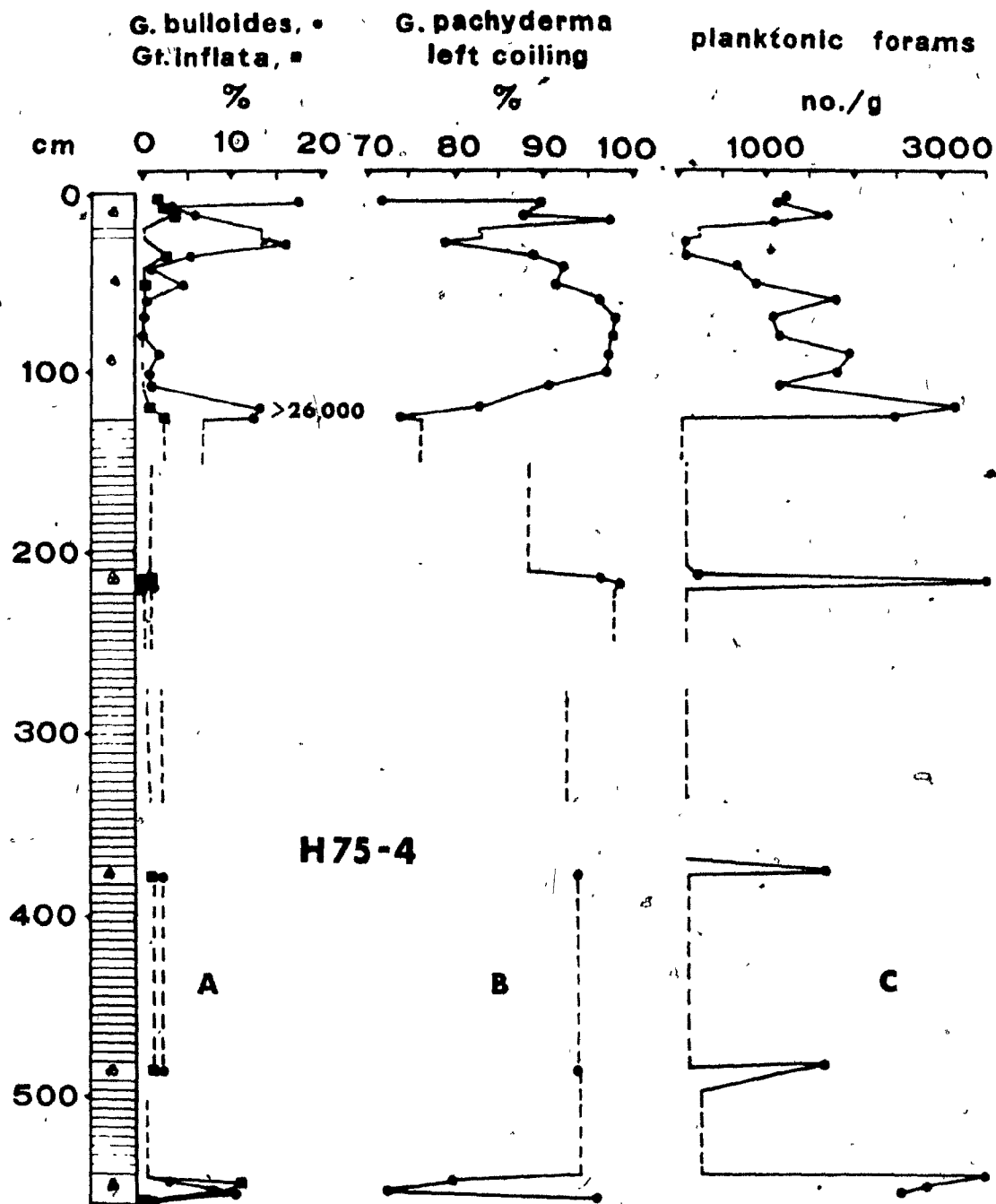


Figure 26. Variations of the foraminiferal fauna in core H75-4, right levee (R.H. Fillon, pers. comm., unpublished data). Each vertical broken line denotes the data obtained from the specified interval of laminated turbidites. Closely spaced horizontal lines represent parallel laminated turbidite mud; the rest for foraminifera rich pelagic lutite.

species (G. pachyderma - left coiling) and warm-water species (G. bulloides, Gt. inflata and G. pachyderma - right coiling) make up essentially 100 percent of the foraminiferal fauna (Figure 26A, B).

Less than 80 percent sinistral-coiling G. pachyderma occur in four stratigraphic horizons (Figure 26B) and the third horizon from the top has been dated as >26,000 y B.P. (Figure 26A, B). If the turbidite sequence is assigned relatively short periods of time for deposition, the generalized curve of left-coiling G. pachyderma is seen to resemble the polar water fluctuation curves of McIntyre et al. (1972) for the North Atlantic. This may suggest a last interglacial age of 110-125,000 y B.P. for the bottom-most Gt. inflata rich pelagic layer at about 550 cm in core H75-4. It is rather difficult to give time brackets for the subsequently younger pelagic layers because of superposed turbidite deposition and the prevailing polar water conditions recorded in the core. Nevertheless, "faunal termination I", corresponding to the Pleistocene-Holocene transition, can be placed at the youngest change from the minimum to the maximum of the planktonic foraminifera abundance at about 20 cm in the core. The termination approximately corresponds to a level just above the boundary between the upper pelagic and the thin upper turbiditic horizon which has been dated in other cores (Figure 25) at about 7,100 y B.P. This agrees with the faunal termination I of less than 8,000 y B.P. suggested by Ruddiman and McIntyre (1973) for the southern Labrador Sea. The abundance curve of sinistral-coiling G. pachyderma in Figure 26B closely matches that of core V23-23 (Ruddiman and McIntyre, 1973, Figure 3, p. 120).

Assuming constant and rapid sedimentation rates for the intervening turbidites, midpoints of the 3 pelagic layers between the base of the lower pelagic horizon and the last interglacial stage (110-125,000 y B.P.) may be

placed at about 70,000, 90,000 and 100,000 y B.P., respectively (R.H. Fillon, pers. comm.).

CHAPTER VI - SEDIMENTARY PROCESSES

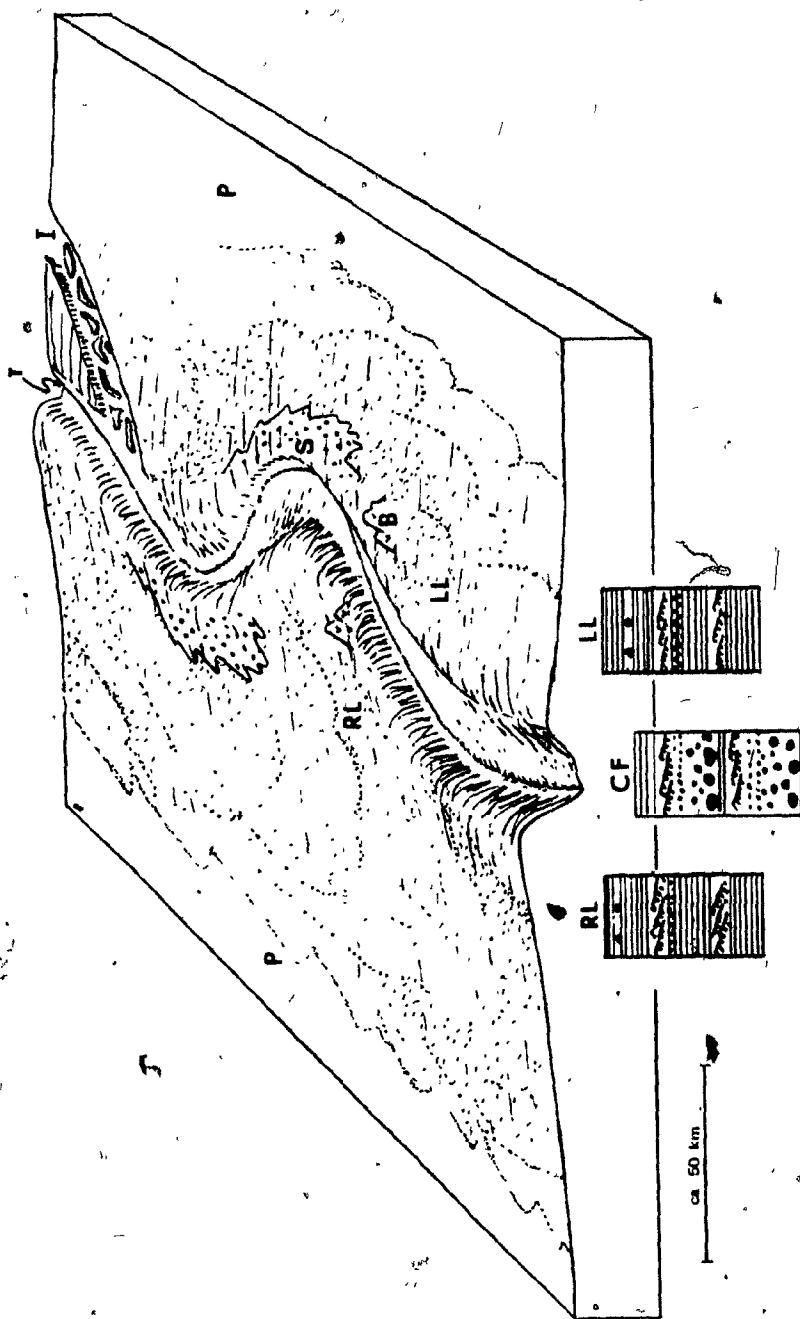
In this chapter an attempt is made to interpret the data that have been presented in the foregoing chapters in terms of the processes of sediment transport and deposition in the NAMOC system. A facies model for the mid-ocean channel (Figure 27) is developed based on the detailed observations of channel morphology and sedimentary facies relations. The model comprises four distinct sedimentary facies, i.e. a) channel-fill facies, b) spill-over facies, c) pelagic facies and d) contourite facies, each of which is attributed to specified inferred depositional processes.

Channel Processes

Sedimentary processes in deep-sea channels have been inferred from circumstantial evidence. Most workers concerned with the study of deep-sea channels seem to agree that turbidity currents play a major role in the formation of these channels (Komar, 1969; Griggs and Kulm, 1970; Ness and Kulm, 1973; Damuth and Gorini, 1976 and others). The evidence comes largely from findings of layers of terrigenous sand and gravel and shallow water biogenic carbonate particles such as algal fragments or shallow water benthonic foraminifera in deep-sea channels many hundred kilometers away from land. Although the phenomena of sand falls and creep have been observed in submarine canyons (Shepard, 1963a) and sediment gravity movements such as slumps and debris flows are possible mechanisms to transport terrigenous materials into deep basins (Hampton, 1972; Middleton and Hampton, 1973) in most cases channel processes appear to be dominated by turbidity currents. Turbidity currents seem to be the only reasonable transport mechanism to build natural levees that occur along the channels for hundreds of kilometers. Nevertheless, bottom currents

Figure 27. Facies model for the NAMOC.

CF = channel-fill facies; spill-over (RL = right levee, LL = left levee); P = pelagic facies; S = spill-over sand; T = meandering talweg; B = basement ridge (mid-Labrador Sea ridge); I = Imarssusk Mid-Ocean Channel (braided). Refer to Figures 11 and 25 for the symbols of the sedimentary structures.



are also assumed to play an important role in certain deep-sea channels (i.e. Falkland and Vema Channels in the South Atlantic, Le Pichon et al.; 1971a, b).

Certain characteristics of subaerial river channels and their deposits have been used to describe deep-sea channels such as the differentiation between coarse-grained channel deposits and fine-grained, thin bedded levee deposits (Nelson and Kulm, 1973). Also, meandering or braided channel patterns have been found in submarine channels (Shepard, 1966; Haner, 1971; Cherkis et al., 1973; Egloff and Johnson, 1975). Unlike meandering river channels in which point bars develop, individual turbidite layers in the Cascadia Channel were interpreted to blanket a flat channel floor for long distances (Griggs et al., 1969).

Comparison Between the NAMOC and Subaerial Meandering Channels

As to the morphological similarities between subaerial meandering river channels and the NAMOC perhaps the most important finding is the discovery of a meandering talweg in the NAMOC (Chough and Hesse, 1976). Talwegs may be seen on many published bathymetric and seismic profiles of deep-sea channels (e.g. Cherkis et al., 1973, Griggs and Kulm, 1973) but their occurrence has been generally disregarded. Apart from this study the presence of a meandering talweg has only briefly been described from La Jolla Submarine Canyon by Palmer (1976) and from the Monterey Deep-Sea Fan valleys by Normark (1970) and Hess and Normark (1976).

Associated with the meandering talweg in the channel are morphological features that may be interpreted as submarine point bars (Figure 9). The presence of submarine point bars is also indicated on high-resolution echo-sounding profiles that show inclined subbottom reflectors probably

representing point-bar stratification. Due to the limited depth of penetration of the coarse-grained channel sediments by conventional piston corers the core material presently available from the channel floor is insufficient to verify the presence of submarine point-bar deposits that might be compared with fluvial sequences. The cores obtained from the channel floor are generally too short to reveal complete vertical sequences suitable for a comparison with subaerial channels. Nevertheless, most channel cores consist of sandy or coarser-grained terrigenous sediment and are long enough to display primary sedimentary structures such as graded bedding, parallel lamination, cross-bedding, cross-lamination and climbing ripples that are at least difficult to distinguish from and may in fact be identical to those found in subaerial point-bars. The submarine point-bars inferred for the NAMOC are envisaged to form in a similar fashion to those of meandering river channels, i.e. by lateral accretion on the inner bends of meanders.

The third major feature of the NAMOC that bears an analogy to certain large meandering river channels is the development of natural levees. The natural levees of the NAMOC which are up to 100 km wide accompany the channel for its entire length, and merge with flood plain-like areas on either side of the channel. The natural levees are on the average 60 m higher than the adjacent plains. Due to the effect of Coriolis force the right (west) levee is consistently higher (up to 90 m) than the left (east) levee.

The marked differentiation between the coarse-grained and probably thick bedded channel-fill facies and the fine-grained, thin bedded spill-over facies occurs because only the dilute top portions of turbidity currents which are laden with fine-grained materials will overtop channel

banks with a relief as high as that of the NAMOC (i.e. up to 200 m).

In subaerial river channels catastrophic events such as floods are more important in the development of channel morphology than the normal processes (cf. Leopold and Maddock, 1953; Stewart and LaMarche, 1967 and others). Deposition of sediments on the bed occurs usually at the waning stage of floods or bankful stages due to the mutual adjustment among discharge and bed load (suspended load), velocity, width, and depth of the channel. If large-scale turbidity currents in the NAMOC were also in equilibrium with channel morphology as floods are with river morphology submarine point bars will most likely form during the waning stages of turbidity currents. Due to lack or weakness of permanent bottom currents in the NAMOC, however, the channel morphology most likely changes very little during the times between successive turbidity currents. Channel-wall undercutting as a cause of lateral shift of meander bends probably plays a minor role in the NAMOC. Significant adjustment between channel morphology and discharge by point-bar accretion is, therefore, probably not required. Consequently, point-bar accretion in the NAMOC is probably much slower than in subaerial river channels of comparable size.

This also explains the relatively low sinuosity of the NAMOC which is one of the differences compared with meandering subaerial channels. Sinuosity of subaerial river channels varies from a value of unity to a value of 4 or more and is usually highest in alluvial valleys with very low slope gradients (Leopold et al., 1964). Despite the very low slope gradient the sinuosity of the NAMOC ranges only from 1.05 to 1.10. Associated with this low sinuosity of the channel is the apparent stability of the channel position. On many seismic reflection profiles (Plate 1) evidence for extensive lateral channel migration with time is lacking. The

channel course has shifted only slightly, less than about 10 km, and mostly toward the left (northeast) levee (see profiles 9, NNE-SSW, IIC; Plate 1).

Turbidity Current Processes in the NAMOC

In the light of the discovery of, a meandering talweg and associated submarine point bars certain aspects of turbidity current processes in the NAMOC may be evaluated from analogies with processes in relatively stable meandering river channels. Numerical values for the flow parameters and the hydrodynamics of large-scale turbidity currents can, however, only be inferred. Inferences can be made from: a) small-scale experiments on density currents, b) theoretical considerations using certain boundary conditions, based on the theory of open channel flows, c) direct velocity measurements of some slow-moving turbidity currents in submarine canyons and lakes and d) indirect velocity determinations derived from the timing of submarine cable breaks on the sea floor.

Experiments on density and turbidity currents have shown that three morphologically distinct regions exist within these flows; head, body and tail. According to Middleton's (1966b, c, 1967) experimental results different velocity equations apply to the head and body of turbidity currents. For the head velocity v , Keulegan's (1957, 1958) formula

$$v = C_1 (\Delta\rho/\rho_t g h_1)^{1/2} \quad (1)$$

may be used, where $\Delta\rho = \rho_t - \rho$,

ρ_t = density of turbidity currents,

ρ = density of ambient water,

C_1 = Keulegan's coefficient (dimensionless),

g = acceleration due to gravity,

h_1 = flow thickness of the head.

Assuming steady state conditions for the body a Chezy-type equation

$$u = [\Delta\rho/\rho_t g h_2 \sin \beta / (1+\alpha) C_f]^{1/2} \quad (2)$$

is applicable, where h_2 = flow thickness of the body,

β = slope angle,

α = the ratio of the drag on the upper surface of the flow to the drag on the bottom and

C_f = drag coefficient.

Comparison of equations (1) and (2) shows that among other factors v depends on the height of the head, h_1 , but not on the slope gradient ($\sin \beta$) whereas u depends on both body height, h_2 , and $\sin \beta$. Since h_1 depends on the amount of suspension advancing from the body into the head, it depends indirectly on u and thus on $\sin \beta$. The velocity of the head (v) will thus adjust to the body velocity (u), accelerating or decelerating with varying slope gradients ($\sin \beta$). At increasing slope gradients, acceleration of the body and consequently an increase in h_1 will occur whereas at decreasing slope gradients the body slows down, and thus less material will be supplied to the head. The critical slope gradients ($\sin \beta$) for which h_1 surpasses h_2 have been estimated by Middleton (1966b) to range from 0.005 to 0.01. Kersey and Hsü (1976) give an average value of 0.009, whereas Komar (1972) assumed a value of 0.002.

To evaluate velocities of channelized turbidity currents from Keulegan's formula (1) or the Chezy-type equation (2) certain flow parameters such as the flow depth (h_1 or h_2) may reasonably be assessed assuming channel-full flow as boundary condition. Slope gradient $\sin \beta$ may also be determined with reasonable accuracy from bathymetric profiles. Other parameters in the

equations are, however, difficult to assess, i.e. a) the dimensionless coefficient C_1 , b) the effective density of turbidity currents ($\rho_t - \rho$), c) the drag coefficient C_f and the drag ratio α .

The difference in thickness between the head and body height ($h_1 - h_2$) is principally controlled by the slope gradient of the channel and determines whether spill-over of channelized turbidity currents will be from the head or the body. As will be discussed in detail in the section on spill-over processes in the upper segment of the NAMOC the channel depth H may be assumed to represent the head height h_1 , because the channel slope gradients are greater than critical (i.e. greater than 0.002, Komar, 1972). Here, the head height will be greater than the body height because the body advances faster than the head. In this case, the head velocity reflects the velocity with which the turbidity current advances and, therefore, Keulegan's formula (1) may be applicable to calculate turbidity current velocities in the upper channel.

To solve for v in the equation (1) the density of turbidity currents (ρ_t) must be known. As to the maximum density of turbidity currents Bagnold (1962) has shown that an upper limit of 1.18 g/cm^3 or sediment concentration of 9 percent exists, above which the average distance between particles becomes so small that particle-to-particle collisions generate considerable intergrain friction. The value of 1.18 g/cm^3 is therefore often used as an upper limit for the density of turbidity currents. The lower limit, on the other hand, may be obtained from dilute turbidity currents in lakes which is in the order of 1.03 to 1.06 g/cm^3 (Gould, 1951; Normark and Dickson, 1976). These densities are slightly higher than the density of sea water ($\rho = 1.028 \text{ g/cm}^3$) and are required for turbidity currents to break through the density stratification of sea water in ocean basins (e.g. Hesse, 1975).

For Keulegan's coefficient C_1 Middleton (1966b) experimentally obtained numerical values ranging from 0.65 - 0.92 for Reynolds numbers greater than 10^3 . Kersey and Hsü (1976) in their density current experiments in a horizontal flume also found that the coefficient is not constant but decreases with increasing travel distance due to energy dissipation by friction. An average value of 0.71 for C_1 , obtained by Kersey and Hsü (1976) for experimental turbidity currents on a nearly horizontal slope, may be applicable for turbidity currents in the NAMOC because of its extremely low slope gradients.

Based on the foregoing discussions it seems reasonable to use the following numerical values for the parameters in equation (1): $\rho = 1.028 \text{ g/cm}^3$, $\rho_t = 1.08\text{-}1.15 \text{ g/cm}^3$ and $C_1 = 0.71$. Equation (1) yields average velocities v ranging from 490 to 720 cm/s for turbidity currents in the upper channel where h_1 averages 100 m.

The Chezy-type equation (2) may be applicable to the middle and lower segments of the NAMOC where the height of the body (h_2) is more likely to be equal or thicker than that of the head (h_1). Here, the channel depth H which is, on the average, 150 m in the middle channel, most probably reflects body height (h_2) of turbidity currents. In the lower channel h_2 is on the average about 100 m. Values of α and C_f in equation (2) may be taken from experimental and theoretical results, i.e. $\alpha = 0.40\text{-}0.50$ and $C_f = 3 \times 10^{-3}$, respectively (Komar, 1969, 1970, 1975; Kersey and Hsü, 1976). Using $\rho = 1.028 \text{ g/cm}^3$, $\rho_t = 1.08\text{-}1.15 \text{ g/cm}^3$ equation (2) gives average velocities ranging from 400 to 600 cm/s for the middle channel ($\sin\theta = 0.001$) and of 240 to 350 cm/s for the lower channel ($\sin\theta = 0.0005$).

Equations (1) and (2) provide first order approximations for the head and body velocities of turbidity currents. Bagnold (1962, 1963) has developed a model whereby fine-grained sediments maintained in the flow by

auto-suspension provide the force to drive the flow. Turbidity currents will maintain a state of auto-suspension as long as the difference between $u \sin \beta$ (i.e. the vertical component of the body velocity) and the settling velocity of the sedimentary particles w is greater than a certain constant A (Bagnold's auto-suspension criterion): $u \sin \beta - w > A$. This provides another possibility to calculate the flow velocity of turbidity currents:

$$\frac{\Delta \rho}{\rho_t} g h_2 (u \sin \beta - w) = (1 + \alpha) C_f u^3 \quad (3)$$

where w = settling velocity and the other notations are the same as in equation (2). What the numerical value of A should be is debatable (Middleton, 1966a), but as may readily be seen, equation (3) reduces to the Chezy-type equation (2), if w equals zero, i.e. if the force necessary to maintain the sediment in suspension is omitted.

Using the same numerical figures as in (2) and assuming a settling velocity of 0.01-0.06 cm/s for particles of 10 to 35 microns in diameter (Bagnold, 1963) equation (3) may be solved for u , yielding velocities from 600 to 250 cm/s for channelized turbidity currents in the NAMOC.

The velocities obtained from equations (1), (2) and (3) for the NAMOC are of the same order of magnitude as those inferred from the timing of submarine cable breaks for large-scale turbidity currents on abyssal plains (i.e. 600-980 cm/s on the Sohm Abyssal Plain over 400 km from the source, Heezen and Ewing, 1952; Heezen, 1963; Menard, 1964). Calculations for turbidity currents from ancient channel gravels in Doheny Channel (Komar, 1970) gave similar velocities, i.e. 690 cm/s.

The foregoing equations (1), (2) and (3) apply to straight channels. Additional parameters may be obtained for flows in meandering channels. Turbidity currents in meandering channels are characterized by a surface

slope resulting from the combined effects of centrifugal and Coriolis forces. Under the condition of channel-full flow it may be assumed that the difference in levee height on both sides of the channel reflects the surface slope of the flows. Komar (1969, p. 4546) used the following equation to calculate the body velocity u from the surface slope:

$$\frac{u^2}{R} + 2\Omega u \sin \phi = g \frac{\Delta \rho}{\rho_t} \frac{\Delta H}{W} \quad (4)$$

where u = flow velocity
 R = radius of meander
 Ω = angular velocity of earth rotation
 ϕ = latitude
 ΔH = difference in height of the levees
 W = width of the channel.

In equation (4) the centrifugal force and the Coriolis force balance the horizontal pressure gradient force that results from the cross-sectional surface slope of the current.

Equation (4) may be solved for ΔH by feeding into it the velocity values obtained from equations (1), (2) and (3). The calculated values of ΔH may then be compared to the observed ones. As stated above the difference in levee height (ΔH) in meanders reflects the cross-sectional surface slope of channelized turbidity currents and primarily results from the combination of the centrifugal and Coriolis forces. In southwesterly (i.e. right) meanders the Coriolis and centrifugal forces will support one another, whereas in northeasterly (left) meander bends the two forces will counter-act each other. Consistently higher right levees along the entire length of the NAMOC are in good agreement with the fact that the Coriolis force is always larger than the centrifugal force by about 20 percent for velocities between 700 and 300 cm/s. The relatively small magnitude of the centrifugal force in the NAMOC is due to the low sinuosity, or the very large meander radius

which ranges from 60 to 70 km. The effect of the centrifugal force can be seen in the fact that the difference in levee height in northeasterly (i.e. left) meander bends is less than in southwesterly (i.e. right) meander bends by an average 5 m (see Appendix 2). This accordance between channel morphology and the forces causing the surface of channelized turbidity currents in the NAMOC meanders to slope conversely suggests that the calculated velocities are in the right order of magnitude.

Spill-over Processes

An important aspect of the channelized flow of turbidity currents is the overspilling of the channel banks and the development of natural levees. As has been pointed out, pronounced natural levees occur along the entire length of the NAMOC attesting to the frequent occurrence of currents overtopping the channel banks. Because overflows will be fed from the dilute top of the channelized flows the extent of the facies differentiation between the generally fine-grained, thin bedded levee facies and the generally coarse-grained channel-fill facies will enable us to estimate at least qualitatively the degree of vertical and possibly horizontal gradation in the flow. The contrast between the channel-fill and the levee facies will, of course, be the greater the higher the relief, i.e. the greater the depth of the channel. Theoretically, it should also increase with increasing flow distance, that is, increasing maturity (i.e. vertical and horizontal grain size gradation) of the flow.

Overflow conditions may vary in the downchannel direction due to the change in slope gradient of the channel. In addition, the thickness of individual overflows will be influenced by local channel relief and other factors such as the variation in momentum resulting from the superposition

of the Coriolis and centrifugal forces which, as discussed above, add up or counteract at right or left meander bends, respectively.

Komar (1972, 1973) theoretically analyzed overflow conditions of channelized turbidity currents. He recognized that the thickness of individual overflows was dependent upon channel gradient. Thicker overflows result from a decrease in gradients because the corresponding velocity decrease will cause the flow to thicken in order to maintain continuity of discharge. Komar also pointed out that overflow will occur either from the head or the body of a turbidity current depending on channel slope gradients. According to Komar's assumption head spillover dominates if the channel gradient is greater than 0.002 because the head will be thicker than the body, whereas body overflow occurs at lower gradients. Dividing equation (1) by equation (2) and using the relationship

$$Fr = C_1 (\sin \beta)^{\frac{1}{2}} \quad (5)$$

Komar (1972, p. 1153) showed that the ratio of the head velocity to the body velocity (v/u) is inversely proportional to the Froude number (Fr) but directly proportional to the ratio of the head height to the body height (h_1/h_2):

$$v/u = C_1 (h_1/h_2)^{\frac{1}{2}} \frac{1}{Fr} \quad (6)$$

The inverse relationship between the ratio of v to u and the Froude number (Fr) is also evident from experimental results summarized by Middleton (1966b). For low Fr the ratio v/u approaches unity and may even be smaller, although this condition cannot be maintained for any length of time. If the body velocity is about the same as the head velocity the head thickness (h_1) may be expected to be close to the body thickness (h_2). To satisfy equations (5) and (6) this condition will occur at a Froude number of 0.71

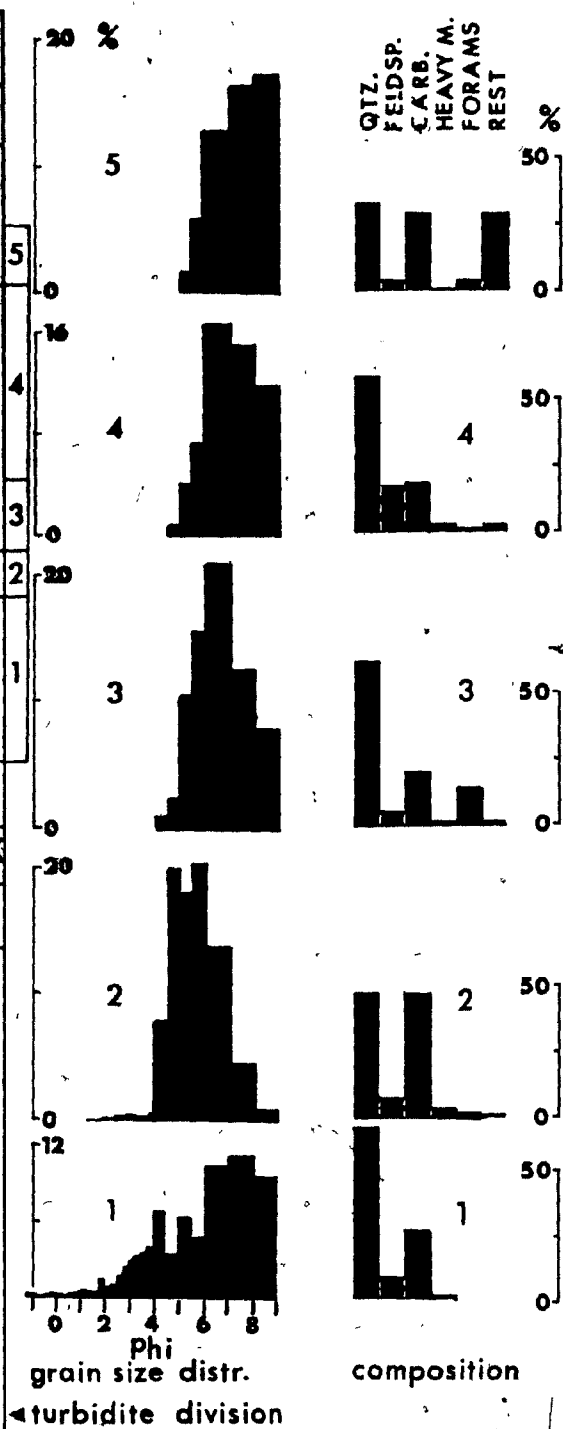
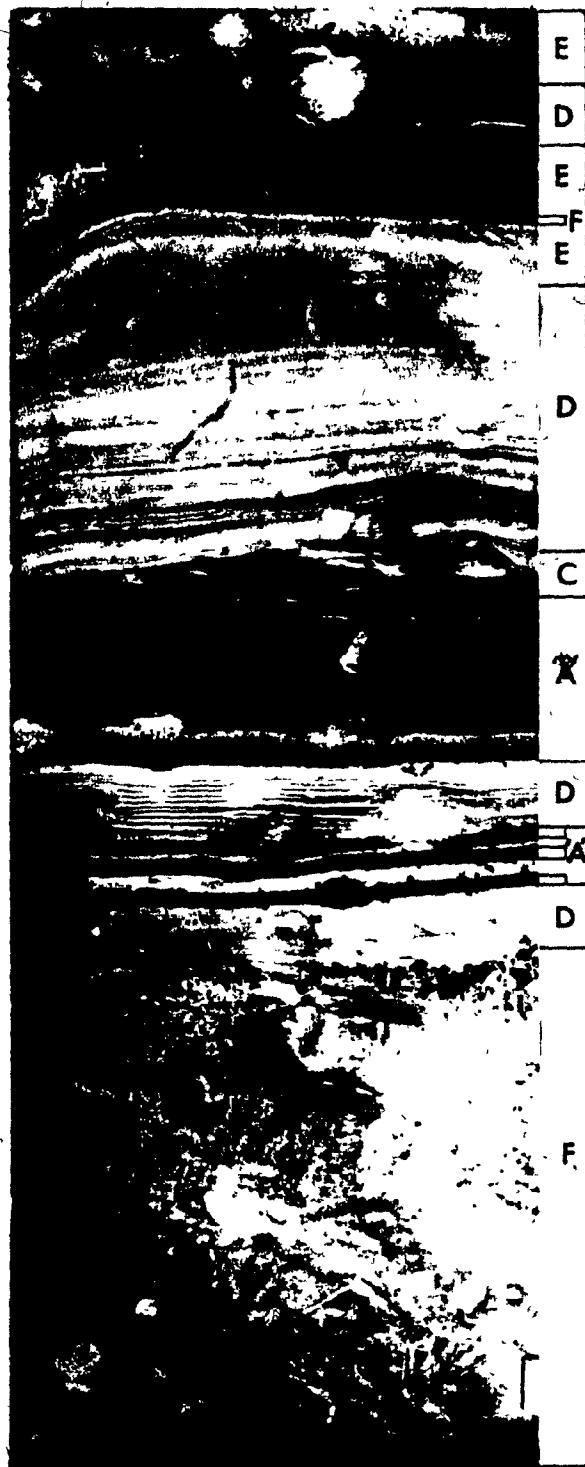
(or 0.75, Komar, 1972) or a bottom slope gradient of about 0.002.

As Komar (1972, p. 1154) pointed out the above values for the critical condition $h_1 = h_2$ should be taken with some reservation because a) u may still be slightly higher than v for $h_1 = h_2$ resulting in a slightly larger Froude number, b) of the uncertainty concerning the coefficient (C_1) which might be less than 0.71 resulting in a smaller Froude number, and c) the general uncertainty concerning the applicability of Keulegan's or Chezy-type equations respectively, to large-scale turbidity currents. Both equations assume steady state conditions that are certainly not fulfilled over very long distances.

To my knowledge different kinds of turbidites on natural levees have not yet been identified in the literature as either head spillover or body spillover deposits. From the study of the levee facies of the NAMOC it appears that this distinction is possible. The crudely laminated "A"-structure divisions observed in cores from the right levee in the upper channel reach (Figure 28, see also section on crudely laminated "A"-division) are considered to represent head spill-over deposits. This structural unit is extremely poorly sorted. The vague laminations are formed by an incomplete separation of coarser and finer grains, with some pebbles scattered throughout the "A" unit. The upper contact of the unit with the overlying cross-laminated (T_c) or parallel laminated (T_d) unit is sharp. The contrast in the degree of sorting and textural maturity across this boundary is striking.

The "A"-structure division is interpreted as head overflow deposit for the following reasons. It is known from experiments (e.g. Middleton, 1966a, b, 1970) that the head is characterized by the turbulent upward movement of suspension from which individual larger grains rapidly settle and fall back

Figure 28. Head spill-over versus body spill-over turbidites. Bar = 1 cm. A graded sequence of turbiditic structure divisions (numbers 1-5: crudely laminated, poorly sorted T_{1a} unit, cross-laminated (T_c), parallel laminated (T_p) and homogeneous (T_h) divisions) is interpreted as having resulted from head spill-over (T_{1a}) and subsequent body spill-over (T_{c-p}) of the same turbidity current. See text for discussion. Numbers (1-5) in the middle and right-hand columns correspond to those numbers for the turbiditic structure divisions in the left-hand column. Pelagic lutites (F) with ice-rafted debris intercalate between turbidite sequences; note intense bioturbation in the bottommost layer (F).



into the body of the current. Considering the high relief of the channel the head of the current is the only likely portion where particles of granule size may be thrown up high enough by turbulent motion to leave the channel. The sharp break in grain size and sorting at the upper boundary of the "A"-division suggests that the overlying C-division may have resulted from subsequent body spill-over as the turbidity current continued its passage at the spill-over region. Thus a highly differentiated overflow resulted with coarse suspended particles in the frontal portions and much finer material comprising the bulk of the overflow. Interestingly, the T_{a} -divisions occur most frequently on the levees of the upper channel where the channel gradient is steep (0.002). On the other hand, in the middle and lower reaches of the studied channel segment where the gradient is less than 0.002 (0.001 and 0.0005, respectively), the "A"-division occurs in less than 5 percent of the levee deposits. This is in accordance with Komar's (1972) choice of the critical slope gradient of 0.0022.

The common occurrence of basal turbidite divisions on the levees of the upper channel supports the idea that initially overflows may have been in the upper flow regime. On the other hand, extremely rare occurrence of basal turbidite divisions (A and B) in the middle channel levees suggests that the flow conditions of overflows were largely subcritical. Although instantaneous overflows could result in a kind of shooting flow due to a sudden decrease in flow depth, subsequent decrease in velocity will, however, lower the Froude number below the critical value.

In the middle and lower channel segments parallel laminated and homogeneous muds that are often underlain by micro-cross-laminated (micro-climbing ripple lamination) fine sand and silt prevail in the spill-over facies. Evidently, the layers of climbing ripples and micro-cross-laminated

fine sand and silt result from bed-load transport under lower flow regime conditions. Furthermore, the preservation of stoss sides in these climbing ripples indicates that the rate of sediment fall-out was relatively high. The overlying parallel laminated muds formed under similar conditions but at a slightly later stage when the flow velocity had decreased further whereas the depth of flow probably remained relatively constant.

Deposition of Laminated Turbidite Muds

It is known from the works of hydraulic engineers, and others studying coastal and estuarine environments, that deposition of fine-grained sediment (less than about 50 microns) differs from that of fine sand in that cohesive forces between the particles as well as between the bed surface and the particles play a role (Einstein and Krone, 1961, 1962; Partheniades, 1965). Flocculation of particles results from collisions by Brownian movement, internal shear of fluid and differential settling velocity (Einstein and Krone, 1961, 1962). Flocs formed by internal shear are denser and stronger than those formed by Brownian movement or differential settling (Krone, 1976). Fine-grained materials in turbidity currents are important because they facilitate auto-suspension (Bagnold, 1962) which is effective in maintaining the currents to flow for long distances.

The deposition of fine-grained particles as flocs is largely controlled by shear stress on the bed (Partheniades, 1965, 1972), flow turbulence, settling velocity (Einstein and Krone, 1961) and other factors such as physico-chemical properties of the clay-water system (Partheniades, 1972). Deposition of flocs will occur if flocs overcome the limiting shear stress (τ_l) of flow on the bed. Experimental values of τ_l range from 0.41 to 0.81 dynes/cm² (Einstein and Krone, 1962; Partheniades et al., 1969).

McCave and Swift (1976) proposed a viscous sublayer model for the deposition of fine-grained sediment. The viscous sublayer is a viscosity-dominated flow region, immediately adjacent to the boundary of the flow. The viscous sublayer is not entirely laminar but displays instability involving periodic turbulence. The sublayer has a structure of high- and low-velocity streaks which have been detected by dye injection, a hydrogen bubble technique and high-speed motion picture photography (Kline et al., 1967; Corino and Brodkey, 1969; Grass, 1971; Kim et al., 1971; Offen and Kline, 1974, 1975). Periodic high velocity eddies or fluid intrusions trigger the instability of the sublayer and interact with streaks of low-velocity, resulting in ejection of low-momentum fluid from the sublayer toward the main flow away from the boundary. The periodic fluid intrusion and ejection events, which are known as "bursts" also occur in marine boundary layers (Gordon, 1974; Heathershaw, 1974). It may be assumed that fine-grained suspended particles in the viscous sublayer of dilute turbidity currents are concentrated in the low-velocity streaks.

The thickness of the viscous sublayer δ is expressed as

$$\delta = 10\nu/(\rho/\tau_o)^{1/2} \quad (7)$$

where ν is kinematic viscosity, τ_o is shear stress at the bed, ρ is fluid density. McCave and Swift (1976) assume that the rate of deposition (R_d) from the sublayer is given by the difference between the net ejection rate (E) and the settling input per unit of time to it (S):

$$R_d = S - E \quad (8)$$

The settling flux input (S) is given by $C_b w$ under depositional condition and the ejection flux (E) may be expressed as $C_b w (\tau_o/\tau_l)$ (McCave and Swift, 1976), where C_b is particle concentration just outside of the

sublayer, w is settling velocity and τ_l is limiting shear stress above which no deposition takes place. The relationship (8) then becomes

$$R_d = C_b w (1 - \tau_o/\tau_l). \quad (9)$$

The term $(1 - \tau_o/\tau_l)$ is the probability (p) of a particle settling to the bed which is also affected by factors such as bioturbation and bed roughness. Einstein and Krone (1962) and Krone (1962, 1976) express an empirical formula for the rate of particle settling (and thus concentration of particles in suspension):

$$\ln C_t/C_o = - \frac{w}{D} (1 - \tau_o/\tau_l)t \quad (10)$$

where C_t is mean concentration at time t , C_o is initial concentration with flow depth (D). McCave and Swift (1976) pointed out that equations (9) and (10) are similar to each other. Equation (10) is identical to (11),

$$\ln C_o - \ln C_t = \frac{w}{D} (1 - \tau_o/\tau_l)t. \quad (11)$$

The left side of equation (11) gives the amount (or concentration) of particles that have settled after time t . The logarithmic decrease of concentration in suspension with time is also shown by Krone (1976, Figures 3 and 4) for diluted suspended sediments at varying mean flow velocities. Using White's (1970) data McCave and Swift (1976, p. 543, Figure 1) show the variation of limiting shear stress (τ_l) with settling velocity (w). Particles of higher settling velocity may be deposited at higher bed shear stress (τ_o). Although this relationship was initially derived for non-cohesive fine particles it may be applicable to fine cohesive particles (McCave and Swift, 1976). The term $(1 - \tau_o/\tau_l)$ will then vary with w . From equation (11), therefore, the settling of fine-grained particles from a viscous sublayer may be stated in terms of the settling velocity (w).

Kuenen (1966) produced thin parallel laminations in a circular flume and suggested that the laminations were formed from uniform flow by a sorting process which he called a "kind-seeks-kind" mechanism. Current pulsation was not envisaged to play a role because pulses were too numerous to match the relatively small number of laminae in each depositional unit. Based on a number of studies of thin parallel laminated turbidite muds Piper (1972, 1973, in press) suggested that; a) the laminations reflect velocity fluctuations of the turbidity currents; and b) the mode of transport is different for the silts and for the clays; fine silt is carried as bed load at higher velocities and deposited when the velocity decreases, the clay is carried in suspension and deposited when velocity decreases even further. For thinly laminated turbidites from the Nova Scotian outer continental margin Stow (1977) suggested a mechanism of depositional shear sorting through the viscous sublayer: silt grains settle through the viscous sublayer, while increased shear in the boundary layer causes flocs to break up; as mud concentration builds up on the top of the boundary layer, reflocculation occurs and at some critical concentration floc aggregates overcome shear break-up and deposit rapidly through the laminar sublayer as a mud blanket. In this model current pulsation was not envisaged as necessary to produce the segregation of silt and clay particles.

The occurrence of micro-ripple cross-laminations in the NAMOC spill-over sediments suggests that the coarse silt to very fine sand at the base of some laminated layers is dominantly deposited from bed load transport (cf. Figure 14). However, some of this material may have been carried in suspension as suggested by the preservation of stoss-side laminae (Plates 4 and 5) indicative of a relatively high ratio of fall-out. At the transition from the ripple laminated division to the parallel laminated division

the mean grain-size decreases below 50 to 40 microns. The lowermost silt laminae of the D-division, therefore, consists of material fine enough to be carried in suspension (cf. auto-suspension limit of Bagnold, 1962). It is, therefore, suggested here that essentially all material deposited in the parallel laminated division was transported in suspension.

In the light of recent observations of bursting phenomena in the viscous sublayer of experimental flows and of natural marine boundary layers, a suggestion is here put forward for the mechanics of formation of thin parallel laminations from dilute turbidity currents.

The similarity of equations (9) and (11) indicates that fine-grained particles in turbulent suspension of dilute turbidity currents settle via the viscous sublayer. It is also apparent from equation (11) that the settling velocity, i.e. the difference between granular silty and flocculated clayey particles assumes an important role for the segregation during deposition. The segregation is envisaged to occur via the viscous sublayer enhanced by a series of "bursts": during the sweep (or strong velocity pulse) incorporation of granular particles into the sublayer may be accelerated, whereas finer-grained clayey particles are ejected from the sublayer toward the main flow. During or just after a period of a sweep granular particles in the sublayer most likely settle first to the bed at relatively high bed shear stress. The overall concentration of granular particles in the suspension and the viscous sublayer are, therefore, depleted first logarithmically with time (cf. Krone, 1976, Figures 3 and 4).

In the meantime, flocs of clayey particles are progressively enriched in the low-velocity streaks of the viscous sublayer. Settling of flocs from the low-velocity streaks will occur when aggregates reach sufficient specific weight (equivalent to that of individual silt particles) and floc

bonding overcomes critical shear stress (τ_c). This process will be accelerated as turbidity currents decay with time because current velocity as well as both critical and bed shear stress decrease.

There are, of course, some flocs in granular laminae and granular materials in flocculated laminae. As Stow (1977) suggested, the discrete boundary between the granular and flocculated laminae can only be formed by rapid settling of flocs. This may be related to the instability of low-velocity streaks or other factors such as rate of velocity decrease, and of shear stress in the viscous sublayer.

Frequencies of velocity fluctuations observed in small-scale turbidity currents (Shepard et al., 1975, 1977; Normark and Dickson, 1976; Lambert et al., 1976) are in the same order of magnitude to those of "bursts" observed in marine boundary layers (Gordon, 1974; Heathershaw, 1974). In fact, it is most likely that individual laminae result from a number of bursts.

Upward logarithmic variation in alternating laminae thickness of granular and flocculated particles may be related to the bursting phenomena in the viscous sublayer. It is, however, beyond the scope of this study to further speculate on the relationship. An explanation must be approached from careful experiments.

Levee Turbidites vs. Contourites

For the past decade there has been discussion concerning the relative importance of turbidity currents and deep oceanic bottom currents in transporting fine-grained deep-sea sediments. It started with the finding of bottom current activity off the southeastern Greenland Continental Rise (Heezen and Hollister, 1963). The study of contour-following geostrophic bottom currents on the continental rise of the western North Atlantic was initiated by Heezen et al. (1966). These studies suggested that fine sand

and finer-grained sediments along the continental rise (and the margins of the deep-ocean basins in general) are mainly transported by contour-following bottom currents (therefore named "contourites" e.g. Hollister and Heezen, 1972), which previously had been taken for granted by most workers as being turbidites.

On PDR records, sedimentary ridges composed of contourites are characterized by a wavy and hyperbolic surface morphology; on seismic reflection profiles sedimentary ridges are transparent and distinguished from internally layered turbidite sequences (i.e. Davies and Laughton, 1972; Bouma and Hollister, 1973). On bottom photographs the surface of ridges reveals current lineations, ripples and other features that are indicative of bottom currents (Heezen and Hollister, 1971).

In general, ocean bottom currents and turbidity currents operate in different parts of ocean basins in transporting deep-sea sediments: bottom currents tend to dominate the margins of basins due to the Coriolis force, whereas turbidity current activity concentrates in the base-of-slope environment and the basin centres (Bouma and Hollister, 1973). Bottom currents produce sufficient turbulence near the bottom to keep fine-grained material in suspension, causing nepheloid layers (Ewing et al., 1971; Eittreim et al., 1976). Nepheloid layers are also caused by slow-moving, low-concentration turbidity currents in the vicinity of submarine canyons (Beer and Gorsline, 1971; Baker, 1976).

A number of criteria have been proposed to distinguish contourites from turbidites of sand- and silt-sized materials (Bouma, 1972b; Hollister and Heezen, 1972; Bouma and Hollister, 1973). Also, criteria for the distinction of fine-grained, parallel laminated turbidites from contourites have been

proposed by Piper (1972, 1973, in press). Piper and Brisco (1975) observed the lenticular and discontinuous nature of laminations of probable contourite origin on the continental rise off Antarctica (DSDP site 268). In contrast to some of the criteria proposed by Bouma and Hollister (1973) for the identification of contourites Piper and Brisco pointed out that heavy mineral placers were absent in their examples; that grain orientation was lacking; and that low matrix content was not characteristic. Stow (1977, in prep.) used various lines of evidence to distinguish between turbidites and interbedded contourites on the continental margin off Nova Scotia. He indicated that abundant parallel laminae are more indicative for turbidites than for contourites. For coarser layers this was also suggested by Fritz and Pilkey (1975).

In the following paragraphs further distinctive criteria for the differentiation of turbidites and contourites are derived from a comparison of the NAMOC spill-over facies and the contourites of Eirik Ridge.

On X-radiographs the most obvious difference between the levee turbidites and the contourites is the intensity of bioturbation: more than 95 percent of the turbidites retain their primary sedimentary structures, whereas more than 98 percent of the contourites are bioturbated and mottled. The mottled contourites are, in fact, so similar to normal (hemi-)pelagic lutites in sedimentary structures and texture that they may be referred to as "reworked" pelagic lutites with some terrigenous material. Although it may be possible that the analyzed core samples are not entirely representative of the typical deposits on Eirik Ridge, less than 1 percent of the contourites shows more or less undisturbed parallel laminations (Plate 17).

Apart from the abundance of parallel laminae in the turbidites, also

the characteristics of the laminations in the l  v   turbidites are different from those of the contourites. The laminae in contourites consist of simple alternations of coarser-grained and finer-grained laminae, both of which are largely composed of biogenic debris and some terrigenous materials (Plate 17). No systematic upward thickness variations of the laminae were observed. Both the laminated turbidites and the contourites are poorly sorted (Appendix 5).

Whereas primary sedimentary structures in contourites are seldom preserved due to bioturbation during slow-settling of pelagic particles, bioturbational disturbance of primary structures in the turbidites is insignificant because of rapid deposition. Bioturbation in the contourites is probably enhanced by the bottom currents that supply oxygen for the burrowing benthonic animals.

Source of Sediment

The source of the NAMOC sediment can be traced using the position of the channel head and tributaries, the composition of channel gravels, and heavy mineral assemblages.

North of 60° 30' N the NAMOC becomes morphologically indistinct. The confluence of two branches of the upper channel, however, trends northwest toward the shelf area off Hudson Strait with one other indistinct tributary trending north toward Cumberland Sound (Figures 1 and 3).

In the middle channel segment near 56° N the channel is joined by a major tributary - the Imarss  ak Mid-Ocean Channel, which originates in the West Reykjanes Basin on the southeast side of Greenland. Another eastern tributary near 57° N heads for the southwestern Greenland slope.

Pebble composition of the gravel layers (Appendix 6) is indicative

of a Canadian source for the sediment. The prevalence of Paleozoic carbonates in channel gravels may be related to abundant carbonate detritus found on the northeastern Canadian shelves and slopes (Grant, 1965; 1971; Krank, 1964; Marlowe, 1968; McMillan, 1973), but not on the Greenlandian shelves or slopes (Grant, 1965; McMillan, 1973; Johnson et al., 1975a, b, c). The carbonate pebbles on the northeastern Canadian shelves have probably been derived by ice-rafting via the prevailing Baffin and Labrador Currents from the eastern Canadian Arctic archipelago where the Lower Paleozoic carbonate rocks are exposed (Thorsteinsson and Tozer, 1970). A recent discovery of Ordovician carbonate rocks underlying the Baffin shelf by MacLean et al. (1977) offers an additional source for the abundant carbonate pebbles on the shelf. The Ordovician carbonates from the shelf are similar to the channel carbonates. On the other hand, carbonate pebbles are absent along the coast of Greenland, although they were dredged from the southwestern Greenlandian continental slope (Johnson et al., 1975b).

Pebbles of anorthosites with intermediate plagioclase composition (An₂₅₋₄₅, andesine-oligoclase) also indicate a Canadian source because they are not known from occurrences in Greenland (Windley, 1969).

Heavy mineral assemblages both from the NAMOC floor and older sediments of the central Labrador Sea (DSDP site 113) support a Canadian source. The major heavy mineral assemblages from the NAMOC and Imarssuak Mid-Ocean Channel area are basically identical to each other, except for some occurrence of actinolite/tremolite in the latter (Appendix 7). Also, the relative abundance of hornblende and garnet differs. The ratio of garnet to hornblende for the NAMOC floor is 2:1, whereas it is 1:2 for the Imarssuak

Channel area (DSDP site 113). As noted by Johnson *et al.* (1973) and Laughton *et al.* (1972), the Imarssuak Channel received considerable amounts of volcanic sediments and reworked sandstones, metamorphic and igneous rocks from Greenland, in which hornblendes are more common than garnet along with actinolite/tremolite. The assemblage and abundances of heavy minerals from the NAMOC are in good agreement with those of Slatt and Lew (1973) from the Labrador shelf and slope.

History of Channel Development

At DSDP sites 111, 112 and 116 in the Labrador Sea and the northern North Atlantic a pronounced change in composition from dominantly pelagic to terrigenous sediments, together with a faunal change from warm to cold assemblages and the appearance of ice-rafted debris led Berggren (1972) and Laughton *et al.* (1972) to place the pre-glacial/glacial boundary at about 3 my B.P., i.e. in Mid-Pliocene time. At DSDP site 113 in the central Labrador Basin this boundary occurs at a subsurface depth of about 550 m (Laughton *et al.*, 1972). The interpretation of seismic reflection profiles across the NAMOC (Plate 1) suggests that much of the approximately 500 m thick sequence of layered sediments in the central Labrador Sea represents terrigenous turbidites derived from the NAMOC or its predecessors. Where penetration is sufficient on the seismic profiles, sediments below the subsurface depth of 500 m are acoustically transparent. This then suggests that the base of the turbidites is also about 3 my old.

In the NAMOC cores 4 litho-stratigraphic units were recognized (p. 67), i.e., a) an upper pelagic, b) an upper turbiditic, c) a lower pelagic, and d) a lower turbiditic unit.

The base of the upper pelagic unit in the NAMOC cores occurs at an average depth of 30 cm. Its age has been extrapolated to be slightly older

than 7,100 y B.P. averaged from three radiocarbon dates (i.e. $6,930 \pm 200$ y B.P., $8,630 \pm 320$ y B.P., and $5,810 \pm 240$ y B.P., Table 2) obtained from a mean depth of 25 cm, i.e. 5 cm above the boundary between the upper pelagic and the upper turbiditic units. It yields an average sedimentation rate of 3.5 cm/1,000 y for the upper pelagic unit. An average age of 23,000 y was determined for the base of the lower pelagic unit (refer to Table 2 and Figure 25). This unit is about 40 cm thick in core H74-68, but tends to thicken in more southerly cores (H75-24, 22, 11, 8, and 4; refer to Figure 25). The age for the upper boundary of this unit is tentative because radiocarbon dates for its top are not yet available. If the sedimentation rate of 3.5 cm/1,000 y of the upper pelagic unit is applicable for the lower pelagic unit as well, its top may be expected to be about 11,000 y old. The upper turbiditic unit would then have been deposited in a time span of only 4,000 y. This would yield an approximate sedimentation rate of 13 cm/1,000 y for the upper turbiditic unit which is 50 cm thick on the average (for stratigraphic correlation see Figure 25). In core H74-68, the base of the lower pelagic unit is younger than in more southerly cores (i.e. $17,200 \pm 500$ compared with 23,000 y). Therefore, the sedimentation rate of the upper turbiditic unit in core H74-68 which is about 100 cm thick is about 10 cm/1,000 y. The estimated age limit for the upper boundary of the lower pelagic unit and sedimentation rate for the turbidites of the upper turbiditic unit are only approximate because: a) the lower pelagic unit appears to be time-transgressive from southeast to northwest and b) a number of turbidite layers are intercalated in the lower pelagic unit in cores H75-24, 22, 14 and 8, respectively.

Nevertheless, the rates of turbidite sedimentation are comparable with the average sedimentation rate of 10 cm/1,000 y for the upper 200 m of the

Pleistocene turbidites in the Imapssuak Mid-Ocean Channel area determined by Laughton et al. (1972) at DSDP site 113. Heezen et al. (1969) assumed an average sedimentation rate of 9 cm/1,000 y for the NAMOC levee sediments. For the lower sequence of Pliocene turbidites at site 113, which is 350 m thick, Laughton et al. (1972) estimated a higher sedimentation rate of 35 cm/1,000 y. If one further assumes that the sedimentation rate of the Pliocene turbidites at DSDP site 113 is similar to that of older NAMOC turbidites, then the initiation of turbidity current activity in the NAMOC is probably related to the onset of Quaternary glaciation in the Labrador Sea about 3 my B.P.

The termination of large-scale turbidity currents in the NAMOC occurred 7,100 y B.P., although smaller turbidity currents that were confined to the channel appear to have occurred as late as 4,800 y B.P. (refer to channel core No. 6 in Table 2). The age of 7,100 y approximately corresponds to the last glacial/post-glacial transition in the Labrador Sea. Glacial conditions in the southern Labrador Sea ended slightly before 8,000 y B.P. based on faunal evidence (Ruddiman and McIntyre, 1973). On the Labrador shelf off Hudson Strait the Laurentide Ice Sheet, which reached as far as the shelf edge during the last glacial maximum (Ives et al., 1975) had also retreated considerably by this time. The retreat resulted in the rapid incursion of the sea into Hudson Strait (Andrews et al., 1974; Ives et al., 1975, Figure 3; Sugden, 1977, Figure 7). A warming of ocean water in the eastern Arctic region beginning slightly earlier than 8,000 y B.P. is indicated by faunal evidence and radiometric chronology of deglaciation (Andrews, 1972; Andrews et al., 1972). The margin of the Laurentide Ice Sheet in eastern Baffin Island and northern Labrador was stable before this until 9,000 y B.P. (Andrews, 1975). Thus it seems likely that the

termination of turbidity current activity in the NAMOC resulted from events causing the deglaciation of the Labrador shelf, especially off Hudson Strait.

No evidence has yet been found concerning triggering mechanisms and the precise timing of turbidity currents in relation to the advance and retreat of glaciers. Turbidity currents could have been initiated during glacial advance by slumping of unstable glacial sediments that were progressively accumulated at the shelf edge. It may have also been possible that while glaciers advanced turbidity currents were initiated as discharges of sediment-laden subglacial melt water. Although the question of triggering mechanism is beyond the scope of this study, the short period of turbidity current activity in the NAMOC near the end of the last glaciation (corresponding to the upper turbidite unit) suggests that special conditions existed which permitted the triggering of turbidity currents and these conditions ceased shortly after deglaciation progressed farther. If the episodes of large-scale turbidity currents that overflowed the channel banks occurred more or less regularly during glacial advance the estimated sedimentation rate of 13 cm/1,000 y gives an average recurrence time of 230 years for turbidity currents that have deposited spill-over mud with an average thickness of 3 cm. On the other hand, it could be significantly shorter if turbidity current activity was concentrated toward the end of glacial periods.

Earlier studies of the NAMOC based on fragmentary channel crossings (Shepard, 1963b; Drake et al., 1963; Rvachev, 1967) have suggested possible tectonic control in the formation of the channel. Heezen et al. (1969) and Egloff and Johnson (1975) have, however, shown that the channel is a depositional-erosional feature formed by sedimentary processes, unrelated to

the direct tectonic control.

In Plate 1, it can be seen that a sequence of primarily terrigenous sediments derived from the NAMOC (approximately 500 m thick) overlies the buried mid-Labrador Sea ridge or partially fills the topographically depressed areas. The initiation of turbidity current activity postdates the last event of the ridge formation by more than 40 my (e.g. Laughton *et al.*, 1972). During this time pelagic sediments have partially filled the "rift valley" and the ridge flank. The channel was thereafter formed by turbidity currents that followed the maximum depth of the basin. In a sense, therefore, the channel has an expression of the topography partly created by mid-Labrador Sea ridge. Nevertheless, the configuration was controlled solely by the sedimentary processes of channelized turbidity currents.

Paleoceanography

The following brief discussion of the paleoceanography is made based on some tentative observations of ice-rafted sediments in pelagic layers from NAMOC levee cores. A detailed faunal study and its significance on the paleoceanography will be assessed elsewhere by Fillon (in prep.).

Sedimentological Effects of Ice Cover

The ocean's response to climatic fluctuations has a significant effect on the type and amount of pelagic particles and ice-rafted debris that are settling through the water column. Since turbidity currents in the NAMOC most likely occurred intermittently pelagic sediments and ice-rafted debris would be expected to occur between successive turbidites. If ice-rafted debris had been deposited between the influxes of turbidity currents this material should be detectable in the spill-over facies of the NAMOC because

the velocities (or shear stresses) of turbid overflows are most probably too low to winnow away the ice-rafted particles. The absence of ice-rafted debris in the laminated turbidite sequences then suggests the existence of an ice cover which limited the influx of icebergs.

Paleoceanographic information on the western and central parts of the Labrador Sea is lacking in the literature. The western continental shelf is presently influenced by the cold Labrador Current and covered with sea ice for half of the year (Dunbar, 1951). During this time ice persists in the central regions of the sea. To the east ice free conditions are maintained due to the inflow of warmer North Atlantic water via the Irminger Current and the East and West Greenland Currents.

McIntyre et al. (1972) and Ruddiman and McIntyre (1973) have proposed a time-transgressive northwest-southeast migration of the polar front in the North Atlantic and Labrador Sea for the last 225,000 years. During maximum glaciation at 18,000 y B.P., for instance, much of the Labrador Sea was covered with ice (McIntyre et al., 1976). For the southwestern continental margin of Greenland, however, Fillon (in prep.) suggests that for much of the Wisconsinian the eastern Labrador Sea was virtually free of long-lived shelf ice and received a continuous supply of ice-rafted volcanic ash of probable Icelandic origin. The counterclockwise East and West Greenland Currents in the eastern Labrador Sea appear to have persisted both during glacial and interglacial periods. On the contrary, Ruddiman and McIntyre (1977) further emphasized that the warm North Atlantic water was only able to penetrate northwestward into the Labrador Sea during interglacial periods during the last 800,000 y.

The occurrence of a thick sequence of repetitive turbidites, barren of ice-rafted debris and lacking pelagic interlayers in most of the levee

cores from the central Labrador Sea has important paleoceanographic implications for the northwestern Labrador Sea. The complete absence of ice-rafted debris (including ice-rafted tephra) implies that there was either a very rapid input of successive turbidites or an absence of icebergs over the area at the time of deposition. The absence of ice-rafted debris between successive turbidite layers supports the sea-ice hypothesis for the formation of sea-ice may substantially reduce the mobility of icebergs. The sea-ice would also markedly lower productivity of planktonic organisms.

This agrees with the assumption by Denton et al. (1971), Fillon (1972) and Anderson (1972) that in the high latitudes episodes of glacial maxima correspond with a lack of ice-rafted debris in deep-sea sediments because ice-rafting requires an ice-free ocean surface which in these latitudes will be associated with interglacial or warmer periods. For the Southern Ocean Watkins et al. (1974) and Keany et al. (1976) stated that the distribution of ice-rafted debris corresponds to interglacial periods in the high latitudes and to glacial periods in the lower latitudes.

During glacial maxima the northwestern Labrador Sea was probably similar to the modern Arctic Ocean, where, as Hunkins et al. (1971) suggest, the present ice conditions (average thickness of 2.5 m, Swithinbank, 1971) have persisted more or less unchanged for the last 80,000 years. According to Hunkins and Kutschale (1967), turbidites on the Canada Abyssal Plain recurred every 500 years and masked pelagic sedimentation (pelagic sedimentation rate of 0.2 cm/1,000 y). There was no appreciable accumulation of pelagic ooze due to the general lack of primary productivity under the sea-ice (Mohr and Tibbs, 1963; Meguro et al., 1967; Dunbar, 1968).

The absence of ice-rafted debris and lack of planktonic foraminifera in the thick lower turbidite horizon along the central axis of the basin

suggests that the northwestern Labrador Sea was also covered with ice during the time prior to about 23,000 y B.P. The sea-ice probably extended toward the southeast to the cold front of the Labrador currents and excluded much of the area from receiving ice-rafted debris.

In the area further south (south of $54^{\circ} 30' N$) planktonic foraminifera and abundant ice-rafted debris present in a number of pelagic layers in core H75-4 (Figure 26) suggest that several ice-free episodes prevailed in the southern Labrador Sea.

CHAPTER VII - SUMMARY AND CONCLUSION

The Northwest Atlantic Mid-Ocean Channel extends for more than 3,800 km from the northwestern Labrador Sea off Hudson Strait to Sohms Abyssal Plain in the northwestern North Atlantic Ocean. For the last 3 my the channel has played a dominant role in the resedimentation of glacially derived terrigenous materials into the deep basins of the Labrador Sea and northwestern North Atlantic. In the Labrador Sea alone the channel has accumulated a sequence of layered, predominantly terrigenous sediments more than 500 m thick and 100 km wide. The present study has revealed the detailed morphology of the middle channel segment and its sedimentary facies, and attempts to interpret the sedimentary processes and the history of development of the channel.

Channel Processes

For the first time, the existence of a submarine meandering talweg and associated submarine point bars has been documented in this study for a deep-sea channel. The talweg meanders with about the same wavelength but with slightly higher amplitude than the channel (wavelength, 50 km; amplitude, 10 km). The channel floor is inclined toward the talweg with an angle of 0.2° - 1.5° in opposite directions in successive meander bends.

Subbottom reflectors on the channel floor reveal oblique internal stratification, which appear to be caused by layers of sandy gravel and turbidites recovered in piston cores from the channel floor. These deposits (channel-fill facies) occur along the entire length of the channel and are envisaged as forming discrete and discontinuous deposits of submarine point bars.

The formation of the meandering talweg and submarine point bars in the deep-sea channel is attributed to the combined effect of the centrifugal force and the Coriolis force on channelized turbidity currents. The process of submarine point bar formation would appear to be similar in some respects to those of subaerial river channels. The marked differentiation between coarse-grained and thick bedded channel-fill facies and fine-grained, thin bedded spill-over facies is ascribed to spill-over processes analogous to those in certain large subaerial meandering channels.

Submarine point bars in the NAMOC appear, however, morphologically less pronounced than those in rivers and the meanders of the channel and the talweg show a comparatively low sinuosity. Associated with the low sinuosity of the channel is the apparent stability of the channel position which in the past has shifted only slightly. The low sinuosity is probably due to the relatively weak centrifugal force of turbidity currents (low meander-curvature, average radius = 60-70 km) and partly due to the absence of strong currents that undercut the channel banks during times between turbidity currents. Turbidity currents may have attained maximum velocities of up to 720 cm/s.

Spill-over Facies

The natural levees of the NAMOC that result from overflows of channelized turbidity currents over the channel banks accompany the channel on both sides for its entire length, merging with broad flood plain-like areas up to 100 km wide. The spill-over facies marginally interfingers with pelagic and contourite facies.

The spill-over facies consists of thin bedded and fine-grained layers of predominantly terrigenous and subordinate pelagic sediments. The pelagic sediments are intensely bioturbated and include abundant ice-rafted debris. The most distinctive feature of the spill-over facies is a monotonous repetition of thin parallel laminated units of terrigenous fine sand and mud, which are often accompanied by climbing micro-ripple cross-laminated units at the base and by homogeneous mud at the top. The upper turbidite units occur most frequently on the levees of the middle and lower channel segments where the channel slope gradient is less than about 0.002. These are attributed to body overflows of channelized turbidity currents over the channel banks under lower flow regime conditions.

Overflows from the head of turbidity currents are believed to have frequently occurred on the levees of the upper and upper middle channel segments, where the channel slope gradient is greater than about 0.002. The head overflow deposits are crudely laminated and poorly sorted turbidite "A"-division ($T_{a,n}$), that consist of about equal proportions of sand, silt and clay.

A layer-by-layer matching of a sequence of layers is possible between levee cores, H75-24 and 22, which are 70 km apart (in the downchannel direction). The correlation shows laterally persistent layers of the spill-over facies. For deep-sea channels it is more appropriate to use the term "spill-over facies" to describe thin bedded, fine-grained turbidites rather than the term "distal facies" (cf. Nelson *et al.*, 1977; Walker, 1977).

Individual units of parallel laminated turbidite mud of the spill-over facies display systematic upward thickness variations of granular silty and

flocculated clayey laminae; the thickness of granular laminae decrease logarithmically upward, whereas that of flocculated laminae increase logarithmically. The upward logarithmic variation of pairs of granular and flocculated laminae appears to result largely from a difference in settling velocity through the viscous sublayer of dilute turbidity currents.

Mineralogically, the turbidite mud is different from pelagic lutite: detrital carbonates are more common in turbidites than in pelagic sediments; the former are rich in illite (70%) whereas the latter are rich in montmorillonite (25-40%). The organic carbon content of turbidite mud (av. 0.8%) is on the average twice as high as that of the pelagic sediments.

The parallel laminated turbidite mud of the NAMOC is also distinctly different from parallel laminated contourites from Eirik Sedimentary Ridge in that no systematic upward variation of laminae thickness occurs in the latter. Furthermore, the parallel laminated units are quantitatively unimportant in contourites (less than 1%); most Eirik Ridge contourites are intensely bioturbated and mottled.

Source of Sediment

The dominant source of sediment for the NAMOC, judging from the prevalence of carbonate pebbles and a high ratio of hornblende to garnet, in the heavy mineral analyses, was on the northeastern Canadian continental margin, especially in the region off Hudson Strait. This region was supplied with large volumes of glacially derived terrigenous sediments.

History of Channel Development

The history of the NAMOC is closely related to the Quaternary glaciations. With the onset of Quaternary glaciation as early as 3 my B.P.

(Mid-Pliocene) the channel probably developed as the most important transport system for glacially derived materials from the outer shelf to the deep basins of the Labrador Sea and northwestern North Atlantic Ocean. The source material for submarine mass flows in the NAMOC originated from the outer continental margins off Hudson Strait to which glacial debris were carried directly across the shelf. The sea level was, of course, lower and probably near the shelf edge and much of the northwestern Labrador Sea was covered with ice. Submarine mass flows were presumably intermittently triggered probably at beginning and end of glacial cycles, either by earthquakes or due to the instability of glacial piles which could have been incorporated with subglacial melt water flows. During Late Quaternary period episodes of large-scale turbidity currents that overflowed channel banks occurred probably as frequent as 230 years. An average sedimentation rate of levee turbidite during this time was about 13 cm/1000 years.

In response to the retreat of glaciers from the shelf and synchronous sea-level rise slightly before 7,100 y B.P. (Pleistocene-Holocene transition) source materials for submarine mass flows no longer reached the shelf edge and thereafter submarine mass flows ceased. Since then the channel became inactive. Fine-grained pelagic materials in the NAMOC have been redistributed by weak to moderate bottom currents, filling depressed channel floor such as the talweg.

Suggestions for Further Research

The results of the present study lead to the following suggestions for further research:

- a) A study of vertical and lateral facies changes within submarine point

bars; this requires systematic transverse sampling across a number of submarine point bars using a deep-sea vibro corer and precise control of core locations. Deep-sea Side Scan Sonar (GLORIA-system) may be employed for a detailed study of the morphology of submarine point bars.

- b) A study of lateral facies variations of the spill-over facies with a number of systematic transverse core samples across the levees flood plain-like areas.
- c) A more accurate estimation of the sedimentation rate of the lower turbiditic unit and a detailed faunal study of a core (H75-4) and other northerly cores for precise timing of submarine mass flows with respect to the glacial/interglacial events, and paleoceanographic and paleoclimatic changes in the Labrador Sea.
- d) An experimental study of channelized turbidity currents for the mode of talweg and point-bar formation.
- e) An experimental study of fine-grained turbidity currents concerning the formation of thinly parallel laminated turbidite mud; and for the mechanics of the logarithmic variations in thickness between granular and flocculated laminae.

Acknowledgements

The research was supported through grants to Dr. R. Hesse by the National Research Council of Canada; the Dept. of Energy, Mines and Resources, Ottawa; and Imperial Oil Ltd., Toronto.

I am indebted to my thesis advisor, Dr. R. Hesse, for his able advise and encouragement during the research and for his methodical and critical reading of the manuscript.

Thanks are due to officers and crew of C.S.S. Hudson (cruise 74-026, Phase IV and cruise 75-009, Phase IV). Drs. S.P. Srivastava and R.H. Fillon of the Bedford Institute of Oceanography, chief scientists on these cruises, are thanked for their kind cooperation. Dr. Srivastava kindly provided copies of the original seismic reflection profiles obtained aboard M/V Minna. Dr. Fillon provided results of his faunal study on core H75-4 and also critically read an earlier version of the thesis.

Drs. B.F. d'Anglejan and E.W. Mountjoy shared valuable discussions during the study and made helpful comments on the earlier draft of the thesis. Thanks are also extended to Drs. J.A. Elson and J. Lajoie who read parts of the manuscript and offered suggestions for its improvement.

Special thanks are extended to Dr. W. Blake, Jr., Geological Survey of Canada for his particular interest in this study and providing radio-carbon dates.

Vema core samples were made available by Lamont-Doherty Geological Observatory of Columbia University (through grants of the Office of Naval Research N00014-67-A-0108-0004 and NSF-GA-35454).

Dr. J. Egloff of U.S. Naval Oceanographic Research and Development Activity, Bay St. Louis, Mississippi provided copies of original bathymetric and seismic reflection profiles of USNS Lynch.

Dr. J. Müller of Technische Universität, Munich kindly provided helpful assistance during the 1974 cruise and made a detailed mineralogical analyses of two cores.

Dr. F. Kalsbeek, Greenland Geological Survey, Copenhagen, Denmark kindly provided sand samples and mineral specimens from West Greenland for heavy mineral studies.

Many people assisted in data acquisition: N.E. Fenerty, A. Sherin, C.F. Stevens and R. Sparks of the Bedford Institute of Oceanography, and M. Koziol and C. Valentin of McGill University. R. Yates did some of the drafting. Colleagues M. Bouchard, O.G. Burrowes, I.G. Hunter, M.W. Milner, G. Ogunyomi, H. Veldhuyzen and R.A. Walls shared animated discussions throughout the study. Dr. D.E. Sheeran of the Soil Physics Laboratory, McGill University introduced me to the method of impregnating unconsolidated sediments. Dr. M.J. Dunbar helped me in identifying organisms on bottom photographs. Dr. C.W. Stearn assisted in identifying fossils in carbonate pebbles. N. Tassé assisted in translating the Abstract into Résumé. Miss E. Forrest did the final typing. All help mentioned is gratefully acknowledged.

I thank my wife, my family at home, and my mother who passed away during this study for their constant encouragement.

REFERENCES

- Allen, J.R.L., 1973, A classification of climbing-ripple cross-lamination: Jour. Geol. Soc. London, v. 129, p. 537-541.
- Anderson, J.B., 1972, Nearshore glacial-marine deposition from modern sediments of the Weddell Sea: Nature Phys. Sci., v. 240, p. 189-192.
- Andrews, J.T., 1972, Recent and fossil growth rates of marine bivalves, Canadian Arctic, and late Quaternary arctic marine environments: Paleogeography, Paleoclimatology, Paleoecology, v. 11, p. 157-176.
- Andrews, J.T., 1975, Support for a stable late Wisconsin ice margin (14,000 to 9,000 B.P.): A test based on glacial rebound: Geology, v. 3, p. 617-620.
- Andrews, J.T., Funder, S., Hjort, C., and Imbrie, J., 1974, Comparison of the glacial chronology of eastern Baffin Island, East Greenland, and the Camp Century accumulation record: Geology, v. 2, p. 355-358.
- Andrews, J.T., Mears, A., Miller, G.H., and Pheasant, D.R., 1972, Holocene late glacial maximum and marine transgression in the eastern Canadian Arctic: Nature, v. 239, p. 147-149.
- Anonymous, 1965, Newfoundland and Labrador Pilot, v. II, The Hydrographer of the Navy, London, 9th ed.
- Bagnold, R.A., 1962, Auto-suspension of transported sediment; turbidity currents: Proc. Royal Soc. London A, v. 265, p. 315-319.
- Bagnold, R.A., 1963, Mechanics of marine sedimentation: in: Hill, M.N., ed., The Sea, v. 3, p. 507-528.
- Bailey, E.H., and Stevens, R.E., 1960, Selective staining of K-feldspar and plagioclase on rock slabs and thin sections: Am. Mineralogist, v. 45, p. 1020-1025.
- Baker, E.T., 1976, Distribution, composition and transport of suspended particulate matter in the vicinity of Willapa Submarine Canyon, Washington: Geol. Soc. Am. Bull., v. 87, p. 625-632.
- Bé, A.W.H., 1959, Ecology of Recent planktonic Foraminifera. Part I. Areal distribution in the Western North Atlantic: Micropaleontology, v. 5(1), p. 77-100.
- Bé, A.W.H., 1960, Ecology of Recent planktonic Foraminifera. Part II. Bathymetric and seasonal distributions in the Sargasso Sea off Bermuda: Micropaleontology, v. 6(4), p. 373-392.
- Bé, A.W.H., and Hamlin, W.H., 1967, Ecology of Recent planktonic Foraminifera. Part III. Distribution in the North Atlantic during the summer of 1962: Micropaleontology, v. 13(1), p. 87-106.

- Beer, R.M., and Gorsline, D.S., 1971, Distribution, composition and transport of suspended sediment in Redondo Submarine Canyon and vicinity (California): *Mar. Geol.*, v. 10, p. 153-175.
- Berger, W., and Heath, G.R., 1968, Vertical mixing in pelagic sediments: *Jour. Mar. Res.*, v. 26, p. 135-143.
- Berggren, W.A., 1972, Late Pliocene-Pleistocene glaciation: in: Initial Reports of the Deep-Sea Drilling Projects, XII, Laughton, A.S., Berggren, W.A. et al., eds., p. 953-963.
- Biscaye, P.E., 1965, Mineralogy and sedimentation of Recent deep sea clays in the Atlantic Ocean and adjacent seas and oceans: *Geol. Soc. Am. Bull.*, v. 76, p. 803-832.
- Blatt, H., Middleton, G.V., and Murray, R., 1972, Origin of Sedimentary Rocks: Prentice-Hall, Englewood Cliffs, New Jersey, 634 p.
- Bouma, A.H., 1962, Sedimentology of Some Flysch Deposits: A Graphic Approach to Facies Interpretation: Elsevier Publ. Co., Amsterdam, 168 p.
- Bouma, A.H., 1972a, Distribution of sediments and sedimentary structures in the Gulf of Mexico: in: Rezak, R. and Henry, V.J., eds., Contributions on the Geological and Geophysical Oceanography of the Gulf of Mexico, Texas A & M Oceanographic Studies, Gulf Publ. Co., Houston, v. 3, p. 35-65.
- Bouma, A.H., 1972b, Recent and ancient turbidites and contourites: *Trans. Gulf Coast Asso. Geol. Soc.*, v. 22, p. 205-221.
- Bouma, A.H., and Hollister, C.D., 1973, Deep ocean basin sedimentation: in: Turbidites and Deep Water Sedimentation, Middleton, G.V. and Bouma, A.H., eds., p. 79-118.
- Bramlette, M.N., and Bradley, W.H., 1941, Geology and biology of North Atlantic deep-sea cores between Newfoundland and Ireland: 1. Lithology and geologic interpretation: *U.S. Geol. Surv. Prof. Paper*, 196-A, p. 1-34.
- Carroll, D., 1970, Clay minerals: A guide to their X-ray identification: *Geol. Soc. Am. Special paper*, 126, 80 p.
- Carver, R.E., 1971, Heavy mineral separation: in: Procedures in Sedimentary Petrology, Carver, R.E., ed., Wiley-Interscience, New York, p. 427-452.
- Cherkis, N.Z., Fleming, H.S., and Feden, R.H., 1973, Morphology and structure of Maury Channel, northeast Atlantic Ocean: *Geol. Soc. Am. Bull.*, v. 84, p. 1601-1606.
- Chough, S.K., and Hesse, R., 1976, Submarine meandering talweg and turbidity currents flowing for 4,000 km in the Northwest Atlantic Mid-Ocean Channel, Labrador Sea: *Geology*, v. 4, p. 529-533.

- Corino, E.R., and Brodkey, R.S., 1969, A visual investigation of the wall region in turbulent flow: Jour. Fluid Mech., v. 37, p. 1-30.
- Crease, J., 1965, The flow of Norwegian Sea water through the Faroe Bank Channel: Deep-Sea Res., v. 12, p. 143-150.
- Crömmelin, R.D., 1937, A sedimentary petrological investigation of a number of sand samples from the south coast of Greenland between Ivigtut and Frederiksdal: Medd. Grønland, v. 113(1), 32 p.
- Curray, J.R., and Moore, D.G., 1971, Growth of the Bengal Deep-Sea Fan and denundation of the Himalayas: Geol. Soc. Am. Bull., v. 84, p. 1601-1606.
- Damuth, J.E., and Gorini, M.A., 1976, The Equatorial Mid-Ocean Canyon: A relict deep-sea channel on the Brazilian continental margin: Geol. Soc. Am. Bull., v. 87, p. 340-346.
- Davies, T.A., and Laughton, A.S., 1972, Sedimentary processes in the north Atlantic: in: Initial Reports of the Deep-Sea Drilling Project, XII, Government Printing Office, Washington, D.C., p. 905-934.
- Denton, G.H., Armstrong, R.L., and Stuiver, M., 1971, The late Cenozoic glacial history of Antarctica: in: Late Cenozoic glacial ages, Turekian, K.K., ed., New Haven and London, Yale Univ. Press, p. 267-306.
- Dietz, R.S., 1953, Possible deep-sea turbidity current channels in the Indian Ocean: Geol. Soc. Am. Bull., v. 64, p. 375-378.
- Dill, R.F., Dietz, R.S., and Stewart, H.B., 1954, Deep-sea channels and delta of the Monterey Submarine Canyon: Geol. Soc. Am. Bull., v. 65, p. 191-194.
- Drake, C.L., Campbell, N.J., Sander, G., and Nafe, J.E., 1963, A mid-Labrador Sea ridge: Nature, v. 200, p. 1085-1086.
- Dunbar, M.J., 1951, Eastern Arctic Waters: Fish. Res. Board Bull., No. 88, 131 p.
- Dunbar, M.J., 1968, Ecological Development in Polar Regions: A Study in Evolution, Prentice-Hall Inc., Englewood Cliffs, N.J., 119 p.
- Egloff, J., and Johnson, G.L., 1975, Morphology and structure of the southern Labrador Sea: Can. Jour. Earth Sci., v. 12, p. 2111-2133.
- Egloff, J., Johnson, G.L., Campsie, J., Dittmer, F., and Rasmussen, M., 1972, A new mid-ocean channel south of Cape Farewell, Greenland: Trans. Am. Geophys. Union, v. 53, p. 424.
- Einstein, H.A., and Krone, R.B., 1961, Estuarial sediment transport patterns: Jour. of the Hydraulics Division, ASCE, proc. v. 87, No. HY2, p. 51-59.

- Einstein, H.A., and Krone, R.B., 1962, Experiments to determine modes of cohesive sediment transport in salt water: *Jour. Geophys. Res.*, v. 67, p. 1451-1461.
- Eittreim, S.L., Thorndike, E.M., and Sullivan, L., 1976, Turbidity distribution in the Atlantic Ocean: *Deep-Sea Res.*, v. 23, p. 1115-1128.
- Embley, R.W., Ewing, J.I., and Ewing, M., 1970, The Vidal Deep-Sea Channel and its relationship to the Demerara and Barracuda Abyssal Plains: *Deep-Sea Res.*, v. 17, p. 539-552.
- Ewing, M., Eittreim, S.L., Ewing, J.I., and Le Pichon, X., 1971, Sediment transport and distribution in the Argentine Basin: Part 3. Nepheloid layers and processes of sedimentation: *in: Physics and Chemistry of the Earth*, Runcorn, S.K., ed., p. 51-77.
- Ewing, M., Heezen, B.C., Ericson, D.B., Northrup, J., and Dorman, J., 1953, Exploration of the Northwest Atlantic Mid-Ocean Canyon: *Geol. Soc. Am. Bull.*, v. 64, p. 865-868.
- Fillon, R.H., 1972, Evidence from the Ross Sea for widespread submarine erosion: *Nature Phys. Sci.*, v. 238, p. 40-42.
- Fillon, R.H., 1975, Deglaciation of the Labrador Continental Shelf: *Nature*, v. 253(5491), p. 429-431.
- Fillon, R.H., in prep., Labrador Sea surface circulation and ice cover during the last 200,000 years:
- Fisher, R.V., 1964, Maximum size, median diameter, and sorting of tephra: *Jour. Geophys. Res.*, v. 69, p. 341-355.
- Folk, R.L., 1968, Petrology of sedimentary rocks: Hemphill's, Austin, Texas.
- Foster, R.H., and De, P.K., 1971, Optical and electron microscopic investigation of shear induced structures in lightly consolidated (soft) and heavily consolidated (hard) kaolinite: *Clays and Clay Minerals*, v. 19, p. 31-47.
- Fritz, S.J., and Pilkey, O.H., 1975, Distinguishing bottom and turbidity current coarse layers on the continental rise: *Jour. Sed. Pet.*, v. 45, p. 57-62.
- Froelich, P., Golden, B., and Pilkey, O.H., 1971, Organic carbon in sediments of the North Carolina continental rise: *Southeastern Geol.*, v. 13(2), p. 91-97.
- Garner, D.M., 1972, Flow through the Charlie-Gibbs Fracture Zone, Mid-Atlantic Ridge: *Can. Jour. Earth Sci.*, v. 9, p. 116-121.
- Gibbs, R.J., 1971, X-ray diffraction mounts: *in: Carver, R.E., ed., Procedures in Sedimentary Petrology: Wiley-Interscience, New York*, p. 531-539.

- Gordon, C.M., 1974, Intermittent momentum transport in a geophysical boundary layer: *Nature*, v. 248, p. 392-394.
- Gould, H.R., 1951, Some quantitative aspects of Lake Mead turbidity currents: *Soc. Econ. Paleontologists and Mineralogists Spec. Paper* 2, p. 34-52.
- Grant, A.C., 1965, Distributional trends in the Recent marine sediments of northern Baffin Bay: *Bedford Institute of Oceanography, Dartmouth, N.S., Report B.I.O. 65-9*, 74 p. Unpublished Manuscript.
- Grant, A.C., 1971, Distributional trends in the Recent marine sediments of northern Baffin Bay: *Maritime Sediments*, v. 7, p. 41-63.
- Grass, A.J., 1971, Structural features of turbulent flow over smooth and rough boundaries: *Jour. Fluid Mech.*, v. 50, p. 233-255.
- Griffin, J.J., Windom, H., and Goldberg, E.D., 1968, The distribution of clay minerals in the world ocean: *Deep-Sea Res.*, v. 15, p. 433-459.
- Griggs, G.B., Carey, A.G., Jr., and Kulm, L.D., 1969, Deep-sea sedimentation and sediment-fauna interaction in Cascadia Channel and Cascadia Abyssal Plain: *Deep-Sea Res.*, v. 16, p. 157-160.
- Griggs, G.B., and Kulm, L.D., 1970, Sedimentation in Cascadia Channel: *Jour. Geol.*, v. 78, p. 611-619.
- Griggs, G.B., and Kulm, L.D., 1973, Origin and development of Cascadia Channel: *Jour. Geophys. Res.*, v. 78(27), p. 6325-6339.
- Grim, P.J., and Naugler, F.P., 1969, Fossil deep-sea channel on the Aleutian Abyssal Plain: *Science*, v. 163, no. 3865, p. 383-386.
- Hampton, M.A., 1972, The role of subaqueous debris flow in generating turbidity currents: *Jour. Sed. Pet.*, v. 42, p. 775-793.
- Haner, B.E., 1971, Morphology and sediments of Redondo Submarine Fan, southern California: *Geol. Soc. Am. Bull.*, v. 82, p. 2413-2432.
- Heathershaw, A.D., 1974, "Bursting" phenomena in the sea: *Nature*, v. 248, p. 394-395.
- Heezen, B.C., 1963, Turbidity currents: in: Hill, M.N., ed., *The Sea*: Wiley-Interscience, New York, N.Y., v. 3, p. 742-775.
- Heezen, B.C., Coughlin, R., and Beckman, W.C., 1960, Equatorial Atlantic Mid-Ocean Canyon: *Geol. Soc. Am. Bull.*, v. 71, p. 1886.
- Heezen, B.C., and Ewing, M., 1952, Turbidity currents and submarine slumps, and the 1929 Grand Banks earthquakes: *Am. Jour. Sci.*, v. 250, p. 849-873.
- Heezen, B.C., Ewing, M., and Menzies, R.J., 1955, The influence of submarine turbidity currents on abyssal productivity: *Oikos*, v. 6, p. 170-182.

- Heezen, B.C., and Hollister, C.D., 1963, Evidence of deep-sea bottom currents from abyssal sediments (abs.), Abstracts of papers, Internat. Assoc. of Phys. Oceanog., 13th General Assembly, Internat. Union Geodesy and Geophys., v. 6, p. 111.
- Heezen, B.C., and Hollister, C.D., 1971, The Face of the Deep: Oxford Univ. Press, New York, 659 p.
- Heezen, B.C., Hollister, C.D., and Ruddiman, W.F., 1966, Shaping of the continental rise by deep geostrophic contour currents: Science, v. 152, p. 502-508.
- Heezen, B.C., Johnson, G.L., and Hollister, C.D., 1969, The Northwest Atlantic Mid-Ocean Canyon: Can. Jour. Earth Sci., v. 6, p. 1441-1453.
- Heezen, B.C., Menzies, R.J., Schneider, E.D., Ewing, W.M., and Granelli, N.C.L., 1964, Congo Submarine Canyon: Am. Assoc. Petrol. Geol. Bull., v. 48, p. 1126-1149.
- Hess, G.R., and Normark, W.R., 1976, Holocene sedimentation history of the major fan valleys of Monterey Fan: Mar. Geol., v. 22, p. 233-251.
- Hesse, R., 1973, Flysch-Gault und Falknis-Tasna-Gault (Unterkreide): Kontinuierlicher Übergang von der distalen zur proximalen Flyschfazies auf einer penninischen Trogebene der Alpen: Geologica Palaeont. SB2, 55 p.
- Hesse, R., 1975, Turbiditic and non-turbiditic mudstone of Cretaceous flysch sections of the East Alps and other basins: Sedimentology, v. 22, p. 387-416.
- Hesse, R., von Rad, U., and Fabricius, F.H., 1971, Holocene sedimentation in the Strait of Otranto between the Adriatic and Ionian Seas (Mediterranean): Mar. Geol., v. 10, p. 293-355.
- Hollister, C.D., and Heezen, B.C., 1972, Geologic effects of ocean bottom currents: western North Atlantic: in: Studies in Physical Oceanography, Gordon, A.L., ed., v. 2, p. 37-66.
- Horn, D.R., Ewing, M., Horn, B.M., and Delach, M.M., 1971, Turbidites of the Hatteras and Sohm Abyssal Plains, western North Atlantic: Mar. Geol., v. 11, p. 287-323.
- Hunkins, K., Bé, A.W.H., Opdyke, N.D., and Mathieu, G., 1971, The late Cenozoic history of the Arctic Ocean: in: Turekian, K.K., ed., Late Cenozoic Glacial Ages, p. 215-305.
- Hunkins, K., and Kutschale, H., 1967, Quaternary sedimentation in the Arctic Ocean: Prog. in Ocean., v. 4, p. 89-93.
- Hurley, R.J., 1960, The geomorphology of abyssal plains in the northeast Pacific Ocean, San Diego, California: Scripps Institute of Oceanography, Marine Physical Laboratory, SIO Reference 60-7, 105 p.

- Ives, J.D., Andrews, J.T., and Barry, R.G., 1975, Growth and decay of the Laurentide ice sheet and comparisons with Fenno-Scandinavia: *Naturwissenschaften*, v. 62, p. 118-125.
- Johnson, G.L., Egloff, J., Campsie, J., Rasmussen, M., Dittmer, F., and Freitag, J., 1973, Sediment distribution and crustal structure of the southern Labrador Sea: *Bull. Geol. Soc. Denmark*, v. 22, p. 7-24.
- Johnson, G.L., McMillan, N.J., and Egloff, J., 1975a, East Greenland continental margin: *in*: Canada's Continental Margins, Yorath, C.J., Parker, E.R., and Glass, D.J., eds., *Can. Soc. Pet. Geol., Mem. 4*, p. 205-224.
- Johnson, G.L., McMillan, N.J., Rasmussen, M., Campsie, J., and Dittmer, F., 1975b, Sedimentary rocks dredged from the southwest Greenland continental margin: *in*: Canada's Continental Margins, Yorath, C.J., Parker, E.R., and Glass, D.J., eds., *Can. Soc. Pet. Geol., Mem. 4*, p. 391-409.
- Johnson, G.L., and Schneider, E.D., 1969, Depositional ridges in the North Atlantic: *Earth Planet. Sci. Lett.*, v. 6, p. 416-422.
- Johnson, G.L., Sommerhoff, G., and Egloff, J., 1975c, Structure and morphology of the West Reykjanes Basin and the southeast Greenland continental margin: *Mar. Geol.*, v. 18, p. 175-196.
- Johnson, G.L., Vogt, P.R., and Schneider, E.D., 1971, Morphology of the Northeastern Atlantic and Labrador Sea: *Deutschen Hydrographischen Zeitschrift, Band 24, Heft 2*, p. 49-73.
- Jones, E.J.W., Ewing, M., Ewing, J.I., and Eittreim, S.L., 1970, Influences of Norwegian Sea overflow water on sedimentation in the northern North Atlantic and Labrador Sea: *Jour. Geophys. Res.*, v. 75, p. 1655-1680.
- Jopling, A.V., and Walker, R.G., 1968, Morphology and origin of ripple-drift cross lamination, with examples from the Pleistocene of Massachusetts: *Jour. Sed. Pet.*, v. 38, p. 971-984.
- Keany, J., Ledbetter, M., Watkins, N.D., and Huang, T-C., 1976, Diachronous deposition of ice-rafted debris in sub-Antarctic deep-sea sediments: *Geol. Soc. Am. Bull.*, v. 87, p. 873-882.
- Kennett, J.P., and Brunner, C.A., 1973, Antarctic Late Cenozoic glaciation: evidence for initiation of ice rafting and inferred increased bottom-water activity: *Geol. Soc. Am. Bull.*, v. 84, p. 2043-2052.
- Kersey, D.G., and Hall, K., 1976, Energy relations of density-current flows: an experimental investigation: *Sedimentology*, v. 23, p. 761-789.
- Keulegan, G.H., 1957, Thirteenth progress report on model laws for density currents. An experimental study of the motion of saline water from locks into fresh water channel: Washington, D.C., U.S. Natl. Bur. Standard Rept. 5168.

- Keulegan, G.H., 1958, Twelfth progress report on model laws for density currents. The motion of saline fronts in still water: Washington, D.C., U.S. Natl. Bur. Standard Rept. 5831.
- Kim, H.T., Kline, S.J., and Reynolds, W.C., 1971, The production of turbulence near a smooth wall in a turbulent boundary layer: Jour. Fluid Mech., v. 50, p. 133-160.
- Kline, S.J., Reynolds, W.C., Schraub, F.A., and Rundstadler, P.W., 1967, The structure of turbulent boundary layers: Jour. Fluid Mech., v. 30, p. 741-773.
- Komar, P.D., 1969, The channelized flow of turbidity currents with application to Monterey deep-sea fan channel: Jour. Geophys. Res., v. 74, p. 4544-4557.
- Komar, P.D., 1970, The competence of turbidity current flow: Geol. Soc. Am. Bull., v. 81, p. 1555-1562.
- Komar, P.D., 1972, Relative significance of head and body spill from a channelized turbidity current: Geol. Soc. Am. Bull., v. 83, p. 1151-1156.
- Komar, P.D., 1973, Continuity of turbidity current flow and systematic variations in deep-sea channel morphology: Geol. Soc. Am. Bull., v. 84, p. 3329-3338.
- Komar, P.D., 1975, Supercritical flow in density currents: A discussion: Jour. Sed. Pet., v. 45(3), p. 747-749.
- Krank, K., 1964, Sediments of Exeter Bay, District of Franklin: Bedford Institute of Oceanography, Dartmouth, N.S., Reports B.I.O. 64-15, 60 p., Unpublished Manuscript.
- Krone, R.B., 1962, Flume studies of the transport of sediment in estuarial shoaling processes: Hydraulic Engineering Laboratory and Sanitary Engineering Research Laboratory, University of California, Berkeley, 110 p.
- Krone, R.B., 1976, Engineering interest in the benthic boundary layer: in: The Benthic Boundary Layer, McCave, I.N., ed., Plenum Pub. Co., New York, p. 143-156.
- Kuenen, Ph. H., 1966, Experimental turbidite lamination in a circular flume: Jour. Geol., v. 74, p. 523-545.
- Lambert, A., Kelts, K., and Marshall, N.F., 1976, Measurements of density underflows from Walensee, Switzerland: Sedimentology, v. 23, p. 87-105.
- Laughton, A.S., 1960, An interplain deep-sea channel system: Deep-Sea Res., v. 7, p. 75-88.
- Laughton, A.S., 1968, New evidence of erosion on the deep ocean floor:

Deep-Sea Res., v. 15, p. 21-30.

- Laughton, A.S., Berggren, W.A., Benson, R.N., Davies, T.A., Franz, U., Musich, L.F., Perch-Nielsen, K., Ruffman, A.S., van Hinte, J.E., and Whitmarsh, R.B., 1972, The Southern Labrador Sea - a key to the Mesozoic and Tertiary evolution of the North Atlantic: in: Initial Reports of the Deep-Sea Drilling Project, XII, Government Printing Office, Washington, D.C., p. 1155-1169.
- Leopold, L.B., and Maddock, T., Jr., 1953, The hydraulic geometry of stream channels and some physiographic implications: U.S. Geol. Surv. Prof. Paper, 252, p. 1-57.
- Leopold, L.B., and Wolman, M.G., 1960, River meanders; Geol. Soc. Am. Bull., v. 71, p. 769-794.
- Leopold, L.B., Wolman, M.G., and Miller, J.P., 1964, Fluvial processes in geomorphology: San Francisco, W.H. Freeman and Co., 522 p.
- Le Pichon, S., Hreim, S.L.E., and Ludwig, W.J., 1971a, Sediment transport and distribution in the Argentine Basin - 1. Antarctic bottom current passage through the Falkland Fracture Zone: in: Ehrens, L.H., et al., eds., Physics and Chemistry of the Earth, Pergamon Press, v. 8, p. 1-28.
- Le Pichon, X., Ewing, M., and Truchan, M., 1971b, Sediment transport and distribution in the Argentine Basin - 2. Antarctic bottom current passage into the Brazil Basin: in: Ehrens, L.H., et al., eds., Physics and Chemistry of the Earth: Pergamon Press, v. 8, p. 29-48.
- MacLean, B., Jansa, L.F., Falconer, R.K.H., and Srivastava, S.P., 1977, Ordovician strata on the southeastern Baffin Island shelf revealed by shallow drilling: Can. Jour. Earth Sci., v. 14, p. 1925-1939.
- Macnab, R.F., and Srivastava, S.P., 1975, A regional geophysical survey of the Labrador Sea: Geol. Surv. Can., Paper 75-1, Part A, p. 177-179.
- Margolis, S.V., and Kennett, J.P., 1971, Cenozoic paleoglacial history of Antarctica recorded in subantarctic deep-sea cores: Am. Jour. Sci., v. 271, p. 1-36.
- Marlowe, J.I., 1968, Unconsolidated marine sediments in Baffin Bay: Jour. Sed. Pet., v. 38, p. 1065-1078.
- McCave, I.N., and Swift, S.A., 1976, A physical model for the rate of deposition of fine-grained sediments in the deep-sea: Geol. Soc. Am. Bull., v. 87, p. 541-546.
- McIntyre, A., Ruddiman, W.F., and Jantzen, R., 1972, Southward penetrations of the North Atlantic Polar Front: faunal and floral evidence of large-scale surface water mass movements over the last 225,000 years: Deep-Sea Res., v. 19, p. 61-77.

- McIntyre, A., Kipp, N.G., BÉ, A.W.H., Crowley, T., Kellogg, T., Gardner, J.V., Prell, W., and Ruddiman, W.F., 1976, Glacial North Atlantic 18,000 years ago: CLIMAP reconstruction: in: Investigation of Late Quaternary Paleoceanography and Paleoclimatology, Cline, R.M., and Hays, J.D., eds., Geol. Soc. Am. Mem., 145, p. 43-56.
- McMillan, N.J., 1973, Shelves of Labrador Sea and Baffin Bay, Canada: in: The Future Petroleum Provinces of Canada, McCrossan, R.G., ed., Can. Soc. Petrol. Geol. Mem. 1, p. 473-517.
- Meguro, H., Ito, K., and Fukushima, H., 1967, Ice flora (bottom type): A mechanism of primary production in polar seas and the growth of diatoms in sea ice: Arctic, v. 20(2), p. 114-133.
- Menard, H.W., 1964, Marine Geology of the Pacific: New York, McGraw-Hill Book Co., 271 p.
- Middleton, G.V., 1966a, Small scale models of turbidity currents and the criterion for auto-suspension: Jour. Sed. Pet., v. 36, p. 202-208.
- Middleton, G.V., 1966b, Experiments on density and turbidity currents. I. Motion of the head: Can. Jour. Earth Sci., v. 3, p. 523-546.
- Middleton, G.V., 1966c, Experiments on density and turbidity currents. II. Uniform flow of density currents: Can. Jour. Earth Sci., v. 3, p. 627-637.
- Middleton, G.V., 1967, Experiments on density and turbidity currents. III. Deposition of sediments: Can. Jour. Earth Sci., v. 4, p. 475-505.
- Middleton, G.V., 1970, Experimental studies related to problems of flysch sedimentation: in: Lajoie, J., ed., Flysch Sedimentology in North America: Geol. Assoc. Canada Spec. Paper 7, p. 253-272.
- Middleton, G.V., and Hampton, M.A., 1973, Sediment gravity flows: mechanics of flow and deposition: in: Soc. Econ. Paleon. Min. Pacific Sect., Short Course, Turbidites and deep water sedimentation, p. 1-38.
- Mohr, J.L., and Tibbs, J., 1963, Ecology of ice substrates: Proceedings of the Arctic Basin Symposium, Arctic Institute of North America, p. 245-252.
- Nelson, C.H., and Kulm, L.D., 1973, Submarine fans and channels: in: Turbidites and deep water sedimentation: Soc. Econ. Paleon. Min. Pacific Sect., Short Course lecture notes, p. 39-78.
- Nelson, H., Mutti, E., and Ricci Lucchi, F., 1977, Upper Cretaceous resedimented conglomerates at Wheeler Gorge, California: description and field guide - a discussion: Jour. Sed. Pet., v. 47(2), p. 926-928.
- Ness, G.E., 1972, The structure and sediments of Surveyor Deep-Sea Channel: M.S. thesis, Corvallis, Oregon State University, 77 p.
- Ness, G.E., and Kulm, L.D., 1973, Origin and development of Surveyor Deep-Sea Channel: Geol. Soc. Am. Bull., v. 84, p. 3339-3354.

- Normark, W.R., 1970, Channel piracy on Monterey Deep-Sea Fan: *Deep-Sea Res.* v. 17, p. 837-846.
- Normark, W.R., and Dickson, F.H., 1976, Man-made turbidity currents in Lake Superior: *Sedimentology*, v. 23, p. 815-831.
- Offen, G.R., and Kline, S.J., 1974, Combined dye-streak and hydrogen-bubble visual observations of a turbulent boundary layer: *Jour. Fluid Mech.*, v. 62, p. 223-239.
- Offen, G.R., and Kline, S.J., 1975, A proposed model of the bursting process in turbulent boundary layers: *Jour. Fluid Mech.*, v. 70, p. 209-228.
- Palmer, H.D., 1976, Erosion of submarine canyons: La Jolla Submarine Canyon, California: *Geol. Soc. Am. Bull.*, v. 87, p. 427-432.
- Partheniades, E., 1965, Erosion and deposition of cohesive soils: *Jour. of the Hydraulics Division, ASCE*, v. 91, No. HY1, Proc. Paper 4204, p. 105-138.
- Partheniades, E., 1972, Results of recent investigations on erosion and deposition of cohesive sediments: in: *Sedimentation*, Shen, H.W., ed., Fort Collins, 20-1-20-39.
- Partheniades, E., Cross, R.H., and Ayora, A., 1969, Further results on the deposition of cohesive sediments: *Proc. 11th Conf. Coastal Engineering*, London, 1968, p. 723-742.
- Piper, D.J.W., 1972, Turbidite origin of some laminated mudstones: *Geol. Mag.*, v. 126, p. 109-115.
- Piper, D.J.W., 1973, The sedimentology of silt turbidites from the Gulf of Alaska: in: Kulm, L.D., von Huene, R., et al., Initial Report of Deep-Sea Drilling Project, v. 18, p. 847-867.
- Piper, D.J.W., in press, Turbidite muds and silts on deep-sea fans and abyssal plains: in: *Submarine Canyon and fan sedimentation*, Stanley, D.J., and Kelling, G., eds., Dowden, Hutchinson and Ross.
- Piper, D.J.W., and Brisco, C.D., 1975, Deep water continental margin sedimentation: in: Initial Reports of the Deep-Sea Drilling Project, XXVIII, Antarctica, Hayes, D.E., and Frakes, L.A., eds., p. 727-755.
- Piper, D.J.W., and Marshall, N.F., 1969, Bioturbation of Holocene sediments on La Jolla Deep-Sea Fan, California: *Jour. Sed. Pet.*, v. 39(2), p. 601-606.
- Piper, D.J.W., and Schrader, H.J., 1973, Bioturbation of sediments: in: Kulm, L.D., et al., eds., Initial Reports of the Deep-Sea Drilling Project, XVIII, Government Printing Office, Washington, D.C., p. 869-875.
- Piper, D.J.W., von Huene, R., and Duncan, J.R., 1973, Late Quaternary Sedimentation in the active eastern Aleutian Trench: *Geology*, v. 1, p. 19-22.
- Piper, D.J.W., and Slatt, R.M., 1977, Late Quaternary clay-mineral distribution on the eastern continental margin of Canada: *Geol. Soc. Am. Bull.*, v. 88, p. 267-272.

Pratt, R.M., 1967, The seaward extension of submarine canyons of the north-east coast of the United States: *Deep-Sea Res.*, v. 14, p. 409-420.

Rabinowitz, P.D., and Eittreim, S.L., 1974, Bottom current measurements in the Labrador Sea: *Jour. Geophys. Res.*, v. 79, p. 4085-4090.

Reineck, H.E., and Singh, I.B., 1973, *Depositional Sedimentary Environments*: Springer-Verlag, Berlin, Heidelberg, New York, 439 p.

Rocheleau, M., and Lajoie, J., 1974, Sedimentary structures in resedimented conglomerate of the Cambrian flysch, L'Islet, Quebec Appalachians: *Jour. Sed. Pet.*, v. 44, p. 826-836.

Ruddiman, W.F., and Glover, L.K., 1972, Vertical mixing of ice-rafted volcanic ash in North Atlantic sediments: *Geol. Soc. Am. Bull.*, v. 83, p. 2817-2836.

Ruddiman, W.F., and Glover, L.K., 1975, Subpolar North Atlantic circulation at 9,300 yr BP: Faunal evidence: *Quat. Res.*, v. 5, p. 361-389.

Ruddiman, W.F., and McIntyre, A., 1973, Time-transgressive deglacial retreat of polar water from the North Atlantic: *Quat. Res.*, v. 3, p. 117-130.

Ruddiman, W.F., and McIntyre, A., 1977, Late Quaternary surface ocean kinematics and climatic change in the high-latitude North Atlantic: *Jour. Geophys. Res.*, v. 82(27), p. 3877-3887.

Rupke, N.A., and Stanley, D.J., 1974, Distinctive properties of turbidite and hemipelagic mudlayers in the Algero-Balearic Basin, Western Mediterranean Sea: *Smithson. Contrib. Ear. Sci.*, 13, 40 p.

Rvachev, V.D., 1967, Origin of the North Atlantic Mid-Oceanic Submarine Canyon: *Oceanology*, v. 7(3), p. 372-376.

Sellacher, A., 1964, Sedimentological classification and nomenclature of trace fossils: *Sedimentology*, v. 3, p. 253-256.

Shepard, F.P., 1954, Nomenclature based on sand-silt-clay ratios: *Jour. Sed. Pet.*, v. 24, p. 151-158.

Shepard, F.P., 1963a, Submarine Canyons: in: Hill, M.N., ed., *The Sea*, v. 3, p. 480-504.

Shepard, F.P., 1963b, *Submarine Geology*: Harper and Row, New York, 557 p.

Shepard, F.P., 1966, Meander in valley crossing a deep-sea ocean fan: *Science*, v. 154, p. 385-386.

Shepard, F.P., Marshall, N.F., and McLoughlin, P.A., 1975, Pulsating turbidity currents with relationship to high swell and high tides: *Nature*, v. 258, p. 704-706.

- Shepard, F.P., McLoughlin, P.A., Marshall, N.F., and Sullivan, G.G., 1977, Current-meter recording of low-speed turbidity currents: *Geology*, v. 5, p. 297-301.
- Slatt, R.M., 1973, Frosted beach-sand grains on the Newfoundland continental shelf: *Geol. Soc. Am. Bull.*, v. 84, p. 1807-1812.
- Slatt, R.M., and Lew, A.B., 1973, Provenance of Quaternary sediments on the Labrador continental shelf and slope: *Jour. Sed. Pet.*, v. 43(4), p. 1054-1060.
- Stewart, J.H., and LaMarche, V.C., 1967, Erosion and deposition produced by the flood of December, 1964, on Coffee Creek, Trinity County, California: *U.S. Geol. Surv. Prof. Paper*, 422-K, 22 p.
- Stow, D.A.V., in prep., The turbidite/contourite controversy: Distinguishing between fine-grained turbidites and contourites on the Nova Scotia deep water margin.
- Stow, D.A.V., 1977, Late Quaternary stratigraphy and sedimentation on the Nova Scotia outer continental margin: Ph.D. thesis, Dalhousie Univ., 360 p.
- Sugden, D.E., 1977, Reconstruction of the morphology, dynamics, and thermal characteristics of the Laurentide Ice Sheet at its maximum: *Arctic and Alpine Res.*, v. 9(1), p. 21-47.
- Swithinbank, C., 1971, Arctic pack ice from below: in: *Sea Ice, Proceedings of an international conference*, Reykjavik, Iceland, p. 246-253.
- Thorsteinsson, R., and Tozer, E.T., 1970, Geology of the Arctic Archipelago: in: Douglas, R.J.W., ed., *Geology and Economic Minerals of Canada*, *Geol. Surv. Can.*
- van der Linden, W.J., Fillon, R.H., and Monahan, D., 1976, Hamilton Bank, Labrador Margin: *Geol. Surv. Can. Paper* 75-40, 31 p.
- van der Lingen, G.J., 1969, The turbidite problem: *N.Z. Jour. Geol. Geophys.*, v. 12, p. 7-50.
- van der Lingen, G.J., 1973, Ichnofossils in deep-sea cores from the Southwest Pacific: in: Andrews, et al., *Initial Reports of the Deep-Sea Drilling Project, XXI*, Government Printing Office, Washington, D.C., p. 693-700.
- Walker, R.G., 1977, Upper Cretaceous resedimented conglomerates at Wheeler Gorge, California: description and field guide - a reply: *Jour. Sed. Pet.*, v. 47(2), p. 928-930.
- Watkins, N.D., Keany, J., Ledbetter, M.T., and Huang, T-C., 1974, Antarctic glacial history from analyses of ice-rafted deposits in marine sediments: New model and initial tests: *Science*, v. 186, p. 533-536.

White, S.J., 1970, Plane bed thresholds of fine-grained sediments: *Nature*, v. 228, p. 152-153.

Windley, B.F., 1969, Anorthosites of southern West Greenland: in: Kay, M., ed., *North Atlantic-Geology and Continental Drift*: Am. Assoc. Petrol. Geol. Mem. 12, p. 899-915.

Worthington, L.V., and Volkmann, G.H., 1965, The volume transport of the Norwegian Sea overflow water in the North Atlantic: *Deep-Sea Res.*, v. 12, p. 667-676.

Addendum

Sung Kwun Chough

Ph.D. Thesis

Additional References

Heezen, B.C., Ewing, M., and Tharp, M., 1959, The floors of the oceans, I: Geol. Soc. Am. Spec. Paper, 65, 122 p.

Jezek, P.A., 1972, Physiography of the North Labrador Sea, Davis Strait and Southern Baffin Bay: Maritime Sediments, v. 8(1), p. 20-24,

Johnson, G.L., Closuit, A.W., and Pew, J.A., 1969, Geological and geophysical investigations in the Northern Labrador Sea: Arctic 22, v. 22, p. 56-68.

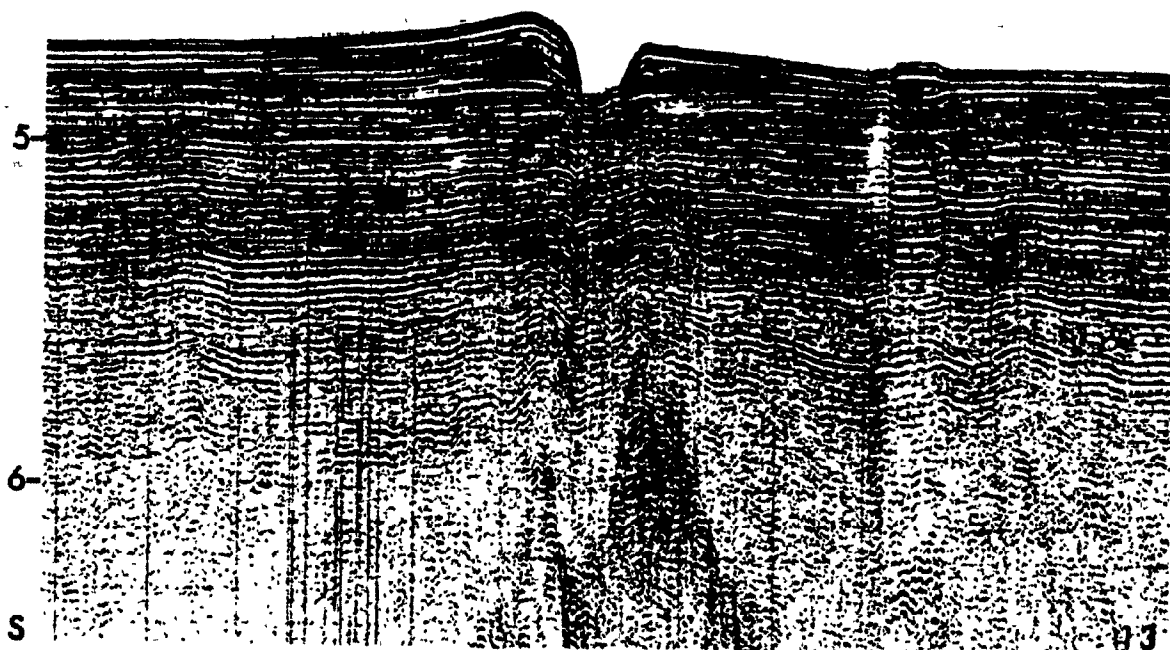
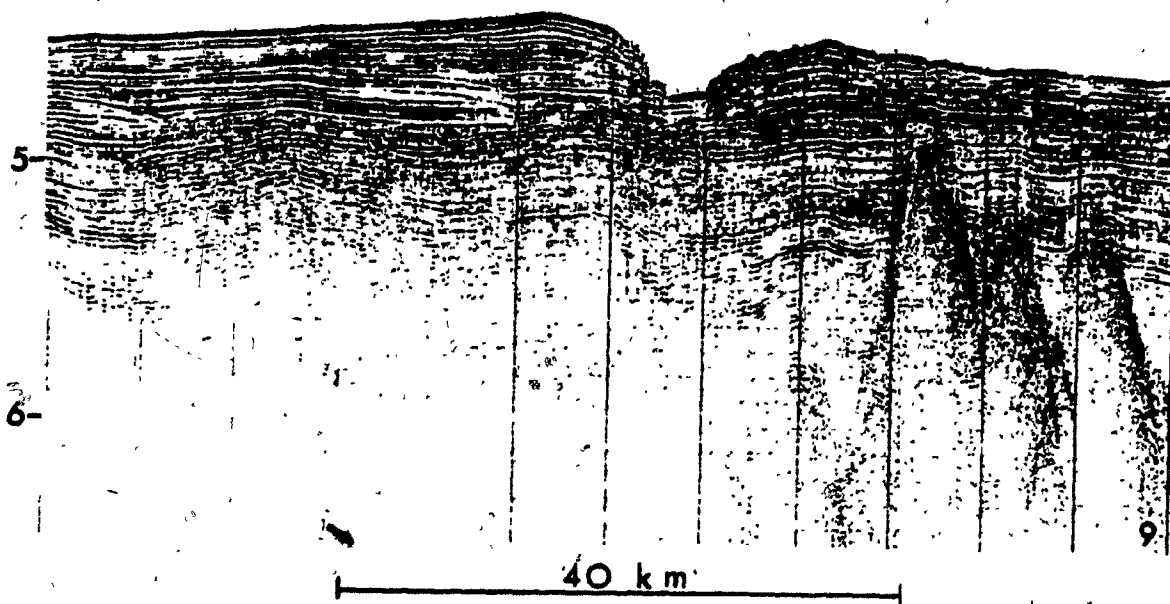
van der Linden, W.J.M., and Srivastava, S.P., 1974, The crustal structure of the continental margin off central Labrador: Geol. Surv. Can., paper 74-30, v. 2, p. 233-245.

Plate 1

Seismic reflection profiles across the NAMOC showing location of the channel above or in the vicinity of the mid-Labrador Sea ridge of the central Labrador Sea (for positions see Figure 3). Vertical scale: two way travel time in seconds; in the upper sedimentary column 1 second corresponds to approximately 1,100 m sediment thickness. Deposition of the upper, layered approximately 500 m thick sequence of sediment appears to have been dominated by channel processes. Northeasterly shift of the channel of about 10 km with time is indicated on profile 9: the channel floor appears at one time about three times wider (i.e. between 6th and 8th vertical lines from left near 4.8 sec horizon) than at present; minor tributary channels appear to have existed near 2nd and 5th vertical lines from left at 5 sec horizon. Northeasterly shift of the channel of approximately 1 km, 1.5 km or 2.5 km is also indicated on profiles 15, NNE-SSW and IIC, respectively. All profiles indicate depositional-erosional origin of the channel. Note artificial nature of the sediment draping the levee crests and channel walls on profiles 13 and NNE-SSW, respectively; fault-like feature near 7th vertical line from left on profile 13 appears to be related to the trough in the basement ridge. (Profiles 9, 13, 15 and NNE-SSW by M/V Minna; courtesy Dr. S.P. Srivastava, Bedford Institute of Oceanography, Dartmouth, N.S.; profiles IIA, IIB and IIC by USNS Lynch; courtesy Dr. J. Egloff, Naval Oceanographic Research and Development Activity of the U.S. Navy, Bay St. Louis, Miss.).

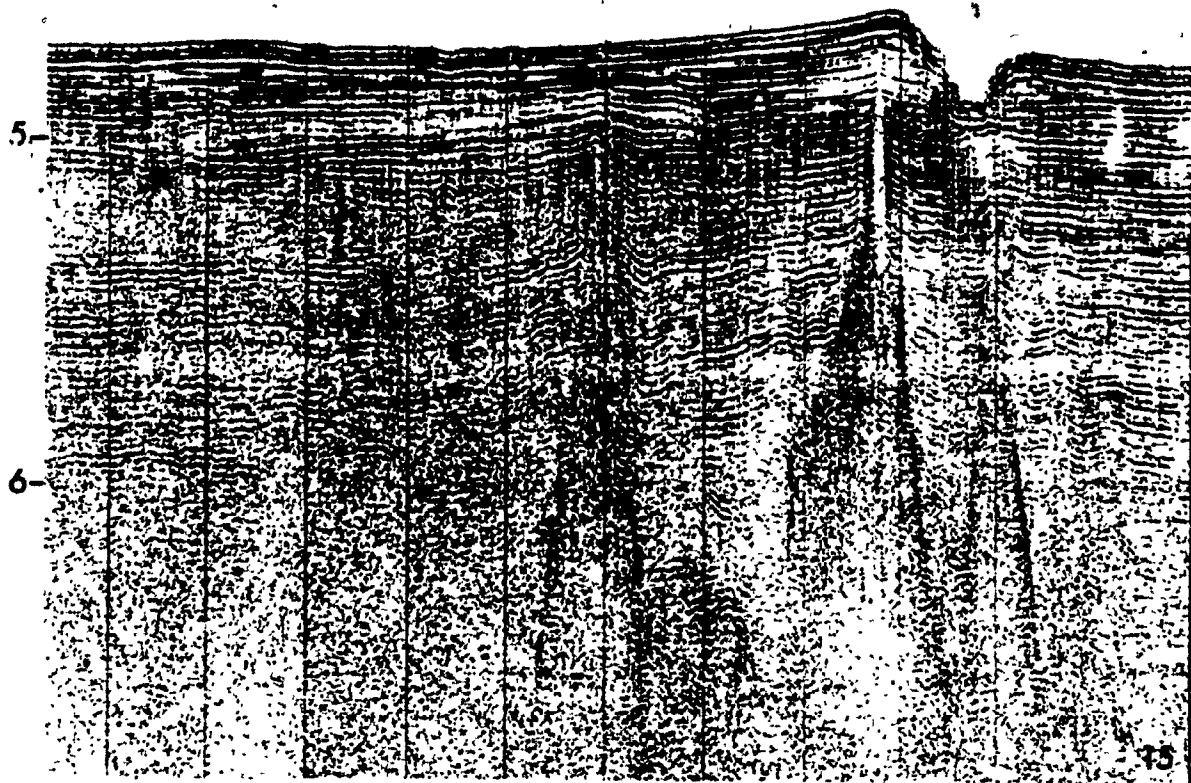
SW

NE

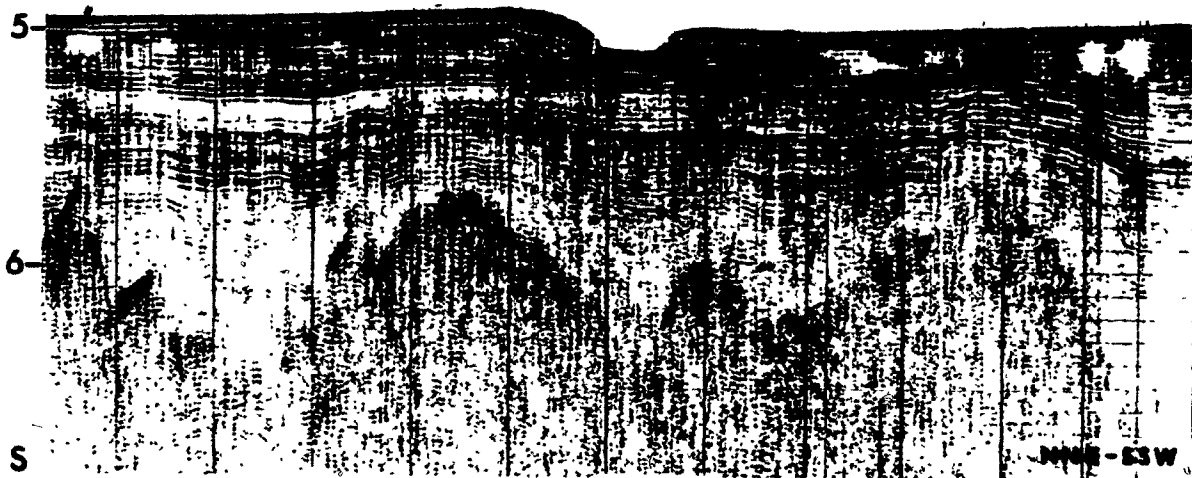


SW

NE



40 km



NNE-E3W

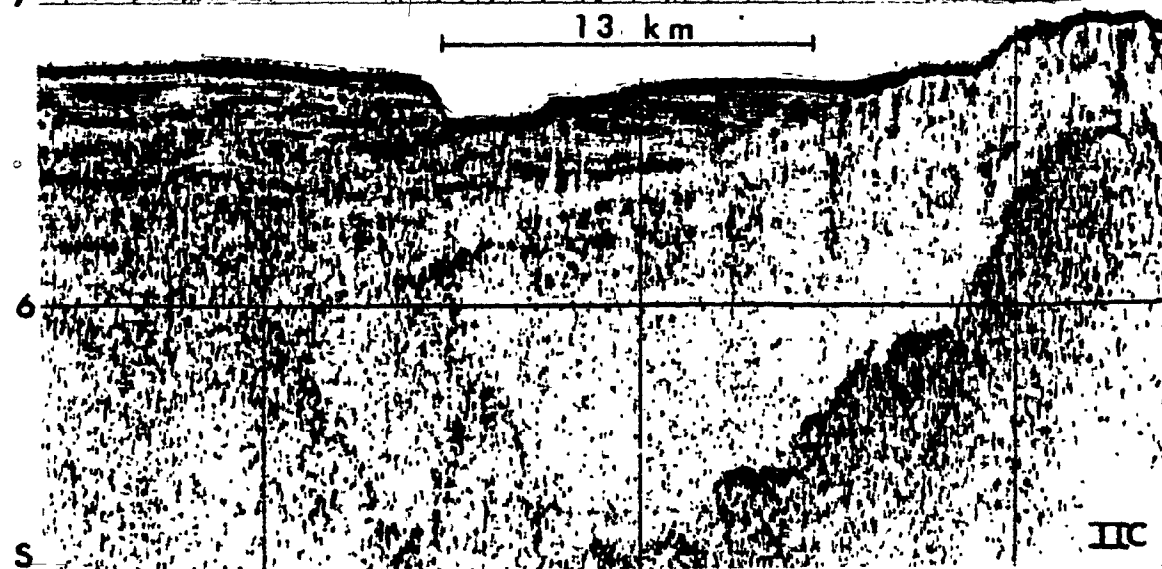
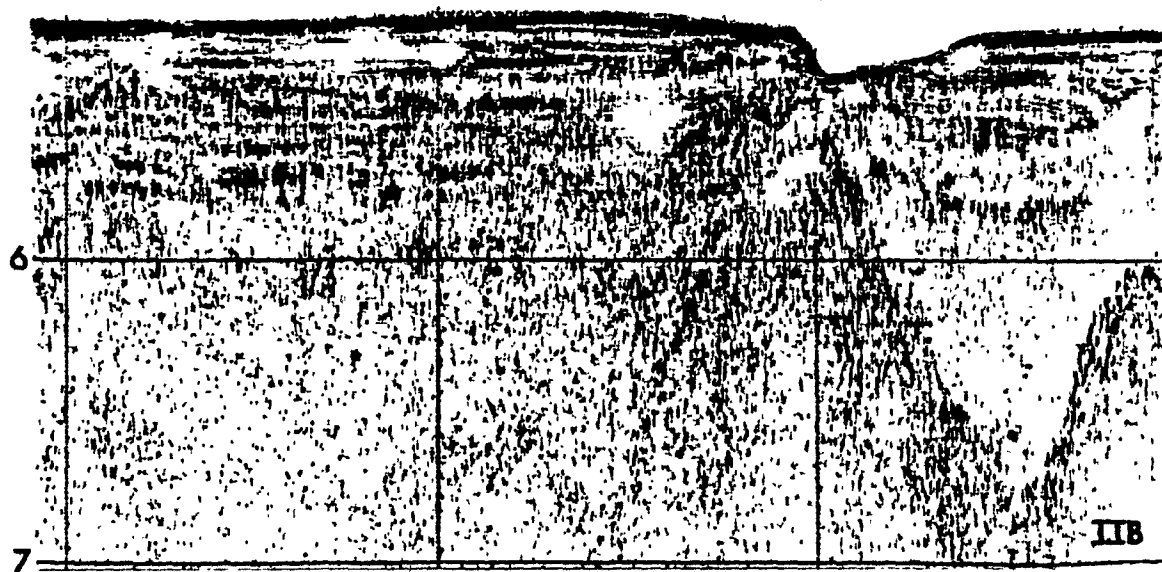
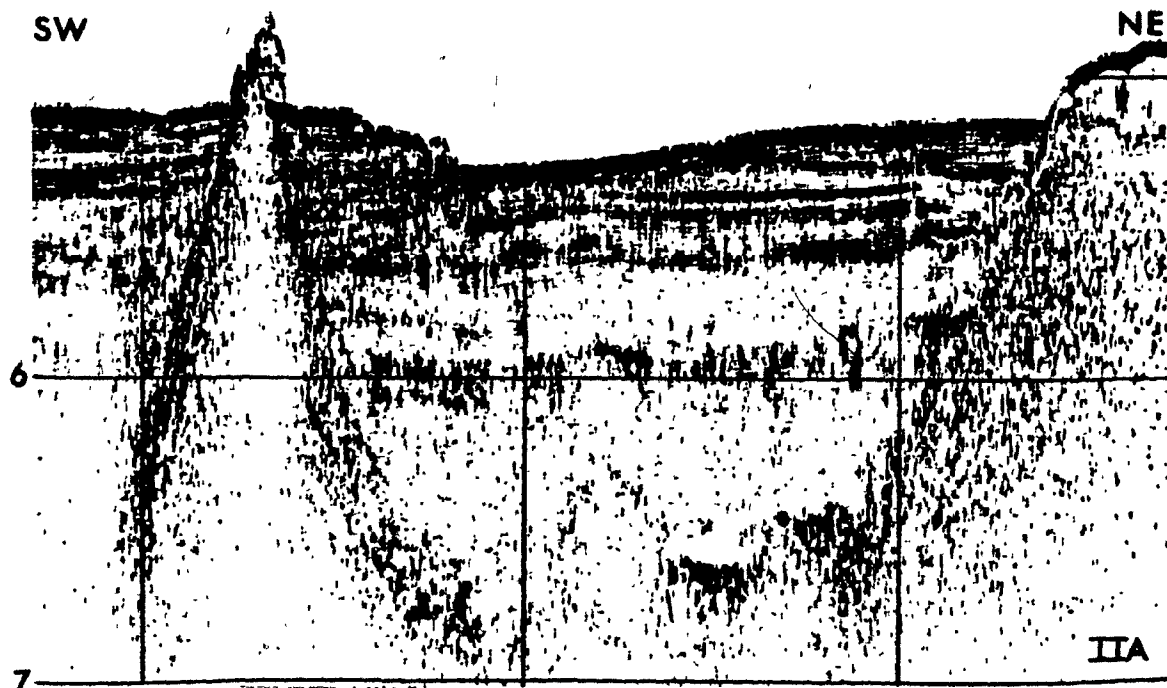


Plate 2

Gravels of channel-fill facies:

- A. Core H75-25, core depth 111-137 cm; two opposite core halves, showing a sandy gravel layer with maximum pebble size of 2 cm; the core is from the middle channel segment approximately 450 km away from the channel head region; water depth, 3,646 m (corrected).
- B. Core H75-25, core depth 152-177 cm; two opposite core halves. Maximum pebble size is about 3 cm.
- C. Core V17-196 from channel head region; water depth, 2,818 m (corrected); maximum recovered pebble size at base of 9 m thick sand and gravel layer is about 6 cm.
- D. Core V23-21 approximately 1,600 km away from the possible source off Hudson Strait; water depth, 4,232 m (corrected); maximum pebble size is about 6 cm.

The majority of gravel components examined consists of carbonates (50%), granite and granite gneisses (37%) and sandstones (7%).



1 2 3 4 5 6 7 8 9 20 1 2 3 4 5 6 7 8 9 30 1 2 3 4 5 6



1 2 3 4 5 6 7 8 9 60 1 2 3 4 5 6 7 8 9 70 1 2 3 4 5 6 7

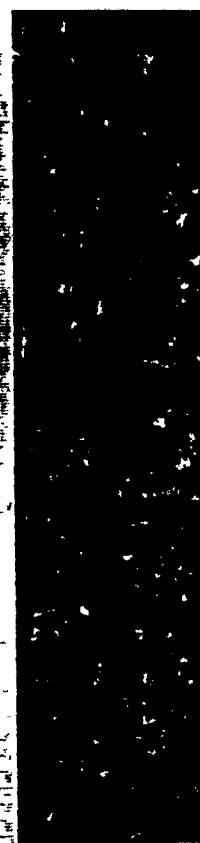


Plate 3

Radiographs of channel-fill sediments; core H75-25; natural scale (bar = .1 cm).

- A. Core depth 5-29 cm; intensely bioturbated pelagic lutite (P) with some ice-rafted debris. Note a large elliptical burrow in the lower third of photo.
- B. Core depth 34-58 cm displaying a vertical sequence of turbidite structure divisions: poorly sorted coarse-grained A-division followed by cross-laminated C-division; the thin E-division at the top is intensely bioturbated.
- C. Core depth 62-86 cm; graded A-division (T_a ; total thickness, 20 cm) followed by parallel laminated (T_d) and homogeneous mud (T_e); both T_d and T_e divisions are intensely bioturbated; (the upper portion was slightly disturbed during coring operation).



Plate 4

Radiographs of typical sediments of the spill-over facies;
natural scale (bar = 1 cm).

- A. Core H75-22, right levee, core depth 240-264 cm; individual laminated units resulted from overflow of single turbidity currents; the dark laminae consist of denser silty granular materials and the light laminae are less dense, flocculated clay-sized materials; climbing micro ripple cross-laminated silt and very fine sand at 245.5 to 247 cm and 260 to 261 cm. "Faults" near 245 and 255-260 cm due to disturbance during sample preparation for X-radiography.
- B. Core H75-4, right levee, core depth 408-432 cm. Monotonous sequence of about 15 units of thinly laminated levee spill-over turbidites.

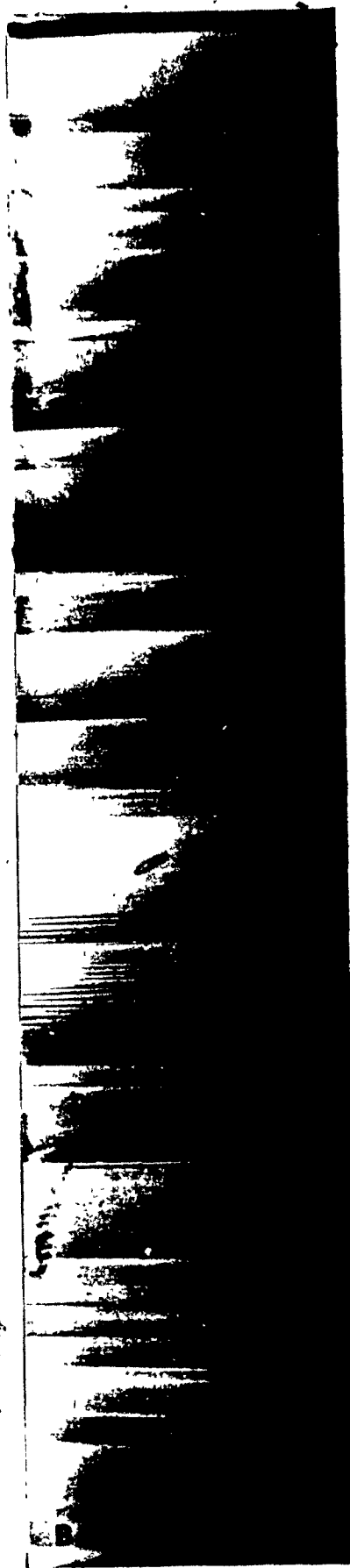
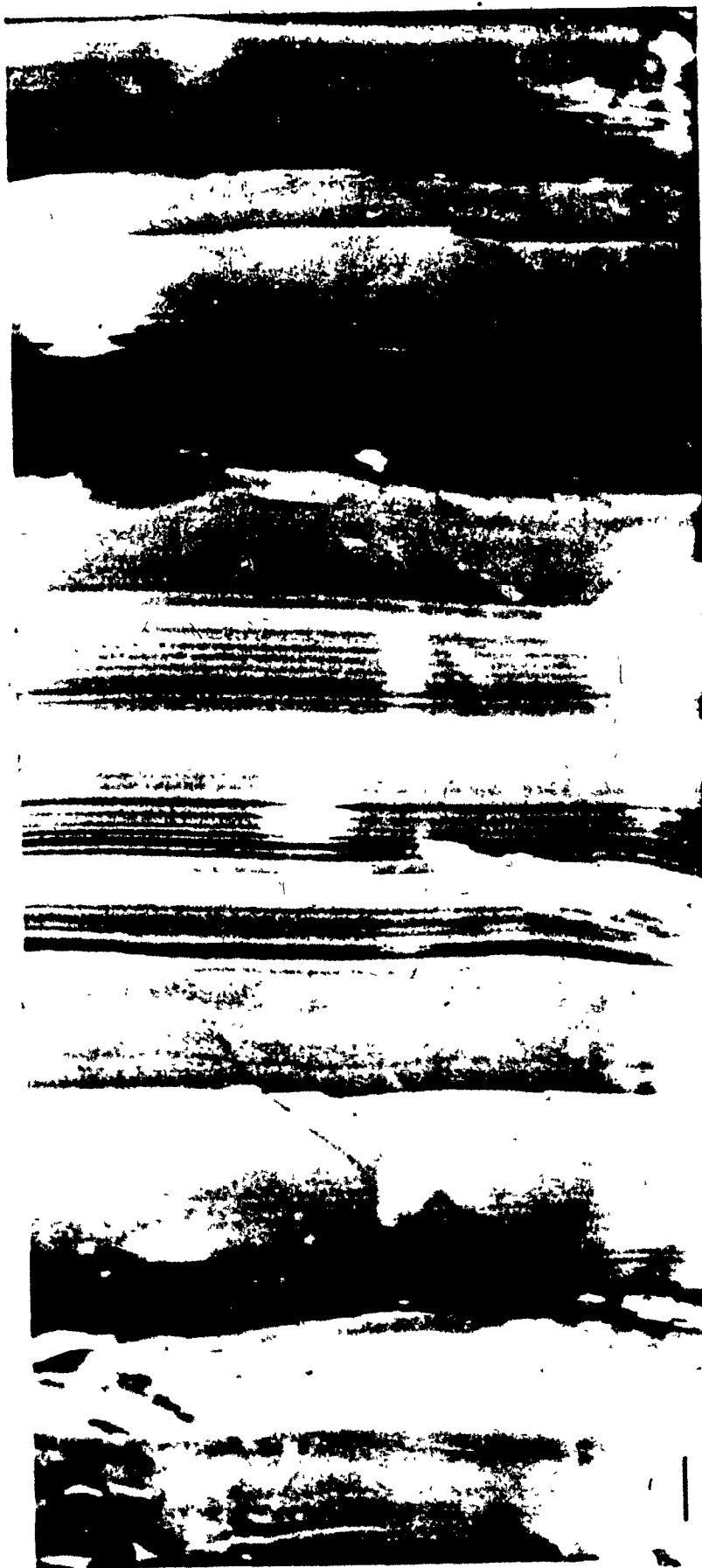


Plate 5

Radiographs of typical sediments of the spill-over facies;
natural scale (bar = 1 cm).

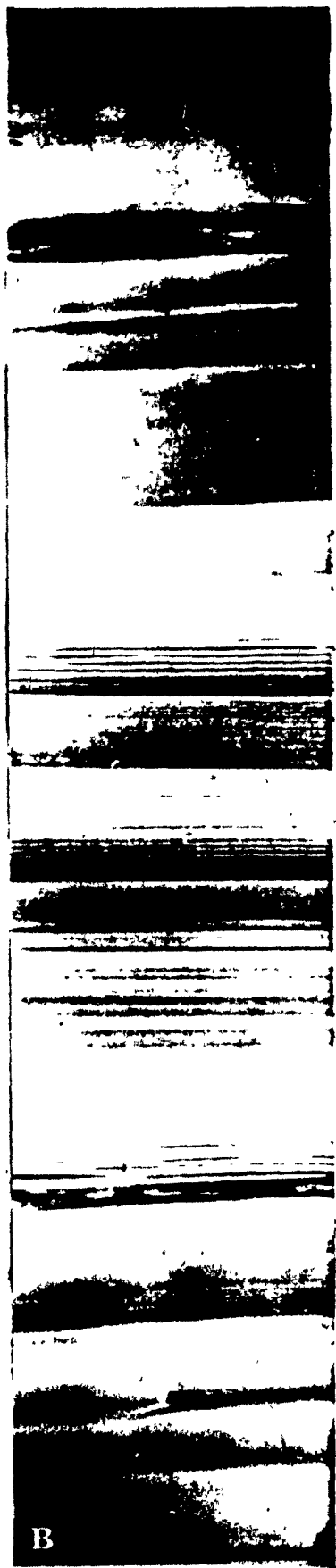
A. Core H75-8, right levee, core depth 295-319 cm;

B. Core H75-4, right levee, core depth 435-458 cm.

Monotonous sequence of about 12 (in A) and 15 (in B) units,
respectively, of thinly laminated spill-over turbidites (similar
to Plate 4); note micro ripple cross-laminated silt and very fine
sand at 300 cm in (A). Maximum thickness of individual laminated
units is about 9 cm.



A



B

Plate 6

Radiographs of spill-over sands on the natural levees; natural scale (bar = 1 cm).

- A. Core H75-13, left levee, core depth 463-487 cm; gravelly, obliquely stratified sand layer at the base whose forsets are accentuated by trains of heavy mineral concentrations grades upward into medium sand (A-division); it is followed by climbing ripple cross-laminated (T_c) and upper parallel laminated division (T_d), respectively; upper parallel laminae disturbed by bioturbation; abundant coarse-grained ice-rafted debris in the upper portion in the pelagic layer; bottom 3 cm disturbed by flow-in.
- B. Core H75-20, left levee, core depth 414-438 cm; parallel stratification of medium to fine spill-over sand on the left levee representing an incomplete Bouma-sequence of structures (i.e. T_b directly followed by T_d and T_e).
- C. Core H75-11, right levee, core depth 232-256 cm; crudely laminated basal turbidite division (T_{an}); composed of about equal mixture of sand, silt and clay; this division is interpreted as head spill-over deposit of a turbidity current (for discussion see text); bottommost 4 cm: bioturbated pelagic ooze with ice-rafted debris.

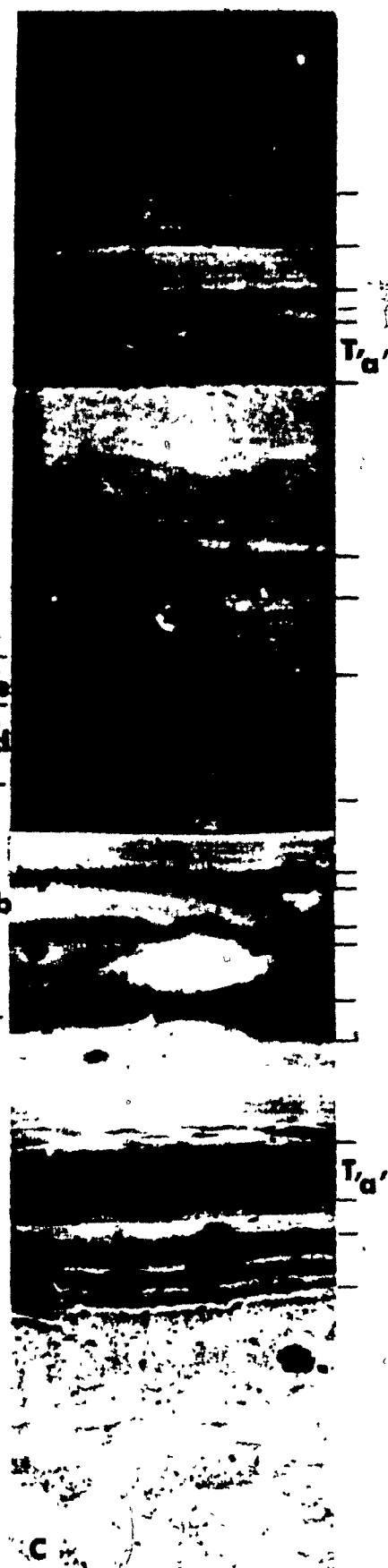
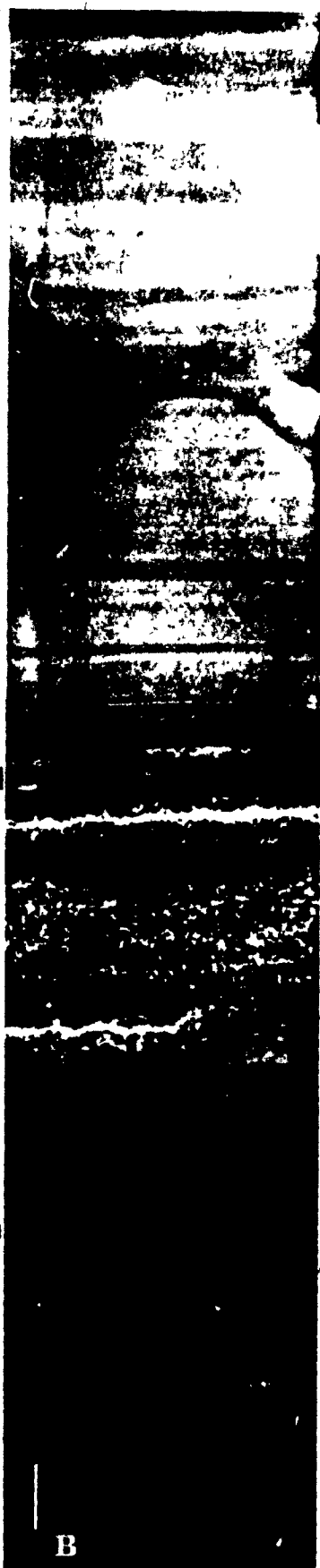
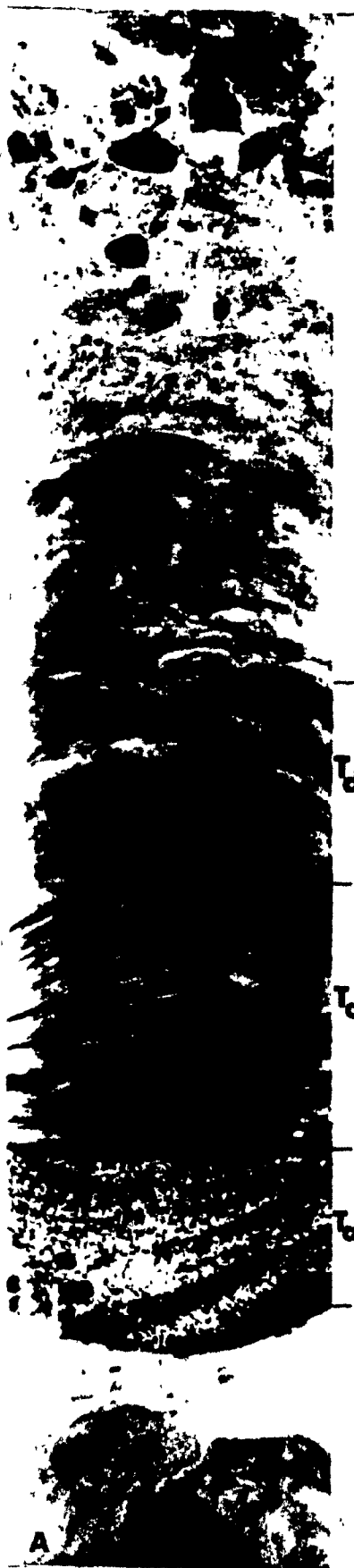


Plate 7

Radiographs of typical examples of pelagic sediments; natural scale (bar = 1 cm).

- A. Core H74-66, channel floor, core depth 414-438 cm.
- B. Core H75-13, left levee, core depth 361-385 cm.
- C. Core H75-4, right levee, pelagic layer at core depth 485-489 cm intercalated between thinly laminated spill-over turbidites.

Pelagic sediments are intensely bioturbated and mottled (for classification of the types of bioturbation see Plates 8 to 11). Note abundant ice-rafted debris in B and C; very thin curvilinear filaments in A are probably pyritized ?worm tubes or ?hyphae of marine fungi. Downward mixing of pelagic sediment into underlying laminated turbidites by burrowing organisms in C.



Plates 8 to 11 illustrate various types of burrows: natural scale (bar = 1 cm); P = pelagic ooze, T = turbidite.

Plate 8

- A. Core H75-8, right levee, core depth 197-221 cm.
(a) Type 1, tubular burrows made by polychaetes, ?crustaceans or ?pelecypods.
(b) Type 4, small dendritic burrows made by polychaetes.
(c) Type 3, oval to circular burrows, dwelling and feeding traces of polychaetes, ?holothurians or ?molluscs.
(d) Type 5, mottled and completely reworked.
- B. Core H75-61, upper channel tributary, core depth 292-316 cm; three subhorizontal burrows (type 2) with meniscus-shaped internal structure (Zoophycos). The concave side of the meniscus-shaped structures points in the same direction in all three horizontal burrows. Note that only the burrows contain coarser ice-rafted material brought down from a layer approximately 17 cm higher in the core.



Plate 9

- A. Core H75-8, right levee, core depth 176-200 cm.
(a) Large oval to circular burrows (type 3) predominate in the middle part of photo in pelagic sediment (P) and in turbidites (T); pelagic sediment in top portion mottled; note abundant ice-rafted debris in the pelagic sediment and in the material filling the large burrows (a) in turbidite.
- B. Core H75-7, left levee, core depth 45-69 cm. Numerous needle-shaped (type 4) and a few oval to circular burrows (a). Original lamination between 48 and 57 cm is significantly disturbed by these burrows. Note ice-rafted material in pelagic layer (P).

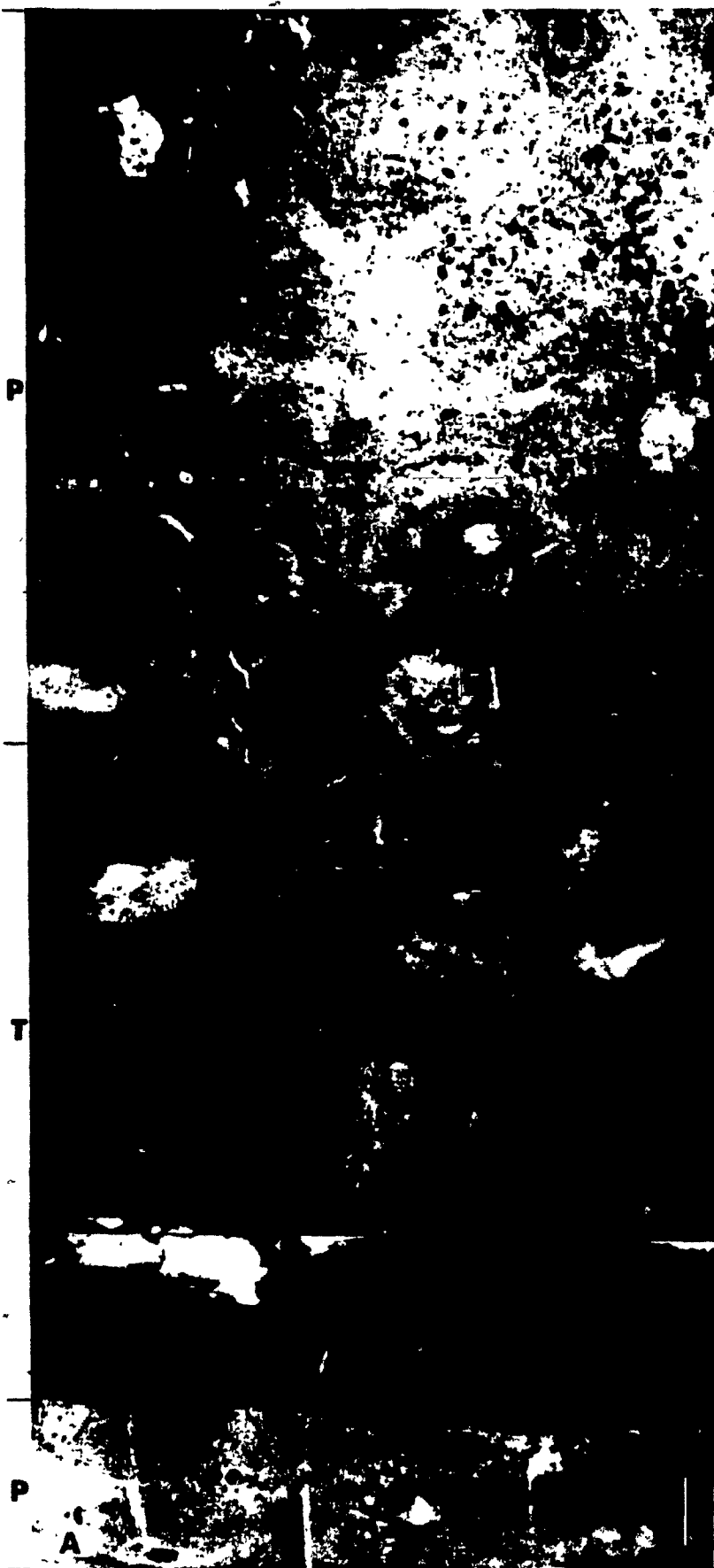


Plate 10

- A. Core H75-8, right levee, core depth 237-261 cm.
(a) Tubular burrows (type 1),
(b) oval or circular burrows (type 3).
Type 1 burrows cluster in the pelagic layers at 251 cm and between 256 and 259 cm and in the upper 7 cm of the parallel laminated turbidite mud.
- B. Core H75-7, right levee, core depth 153-177 cm.
(a) Bifurcating tubular burrows (type 1) in the lower part of turbiditic mud;
(b) needle-shaped burrows (type 4) penetrating deeper into turbidites;
(c) oval-shaped burrows (type 3) concentrated in the pelagic lutite and the part of the turbidite.



Plate 11

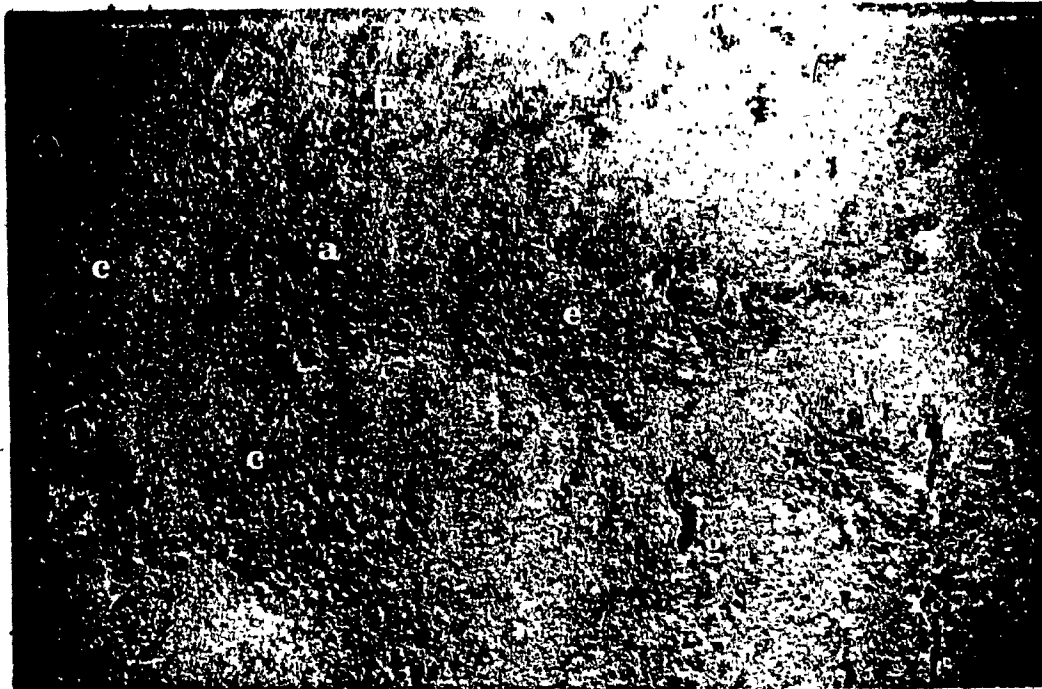
- A. Core H75-24, right levee, core depth 179-203 cm.
(a) Straight tubular burrows (type 1) penetrating deep into the parallel laminated turbidite mud; some long streaks are artificial. Note climbing micro ripple cross-laminated unit (T_c) between 186 and 187 cm.
(b) Subhorizontal Zoohycoos (type 2 burrows).
- B. Core H75-7, left levee, core depth 74-98 cm.
(a) Minute needle-shaped burrows (type 4) destroy the original parallel laminae of turbidite almost beyond recognition.



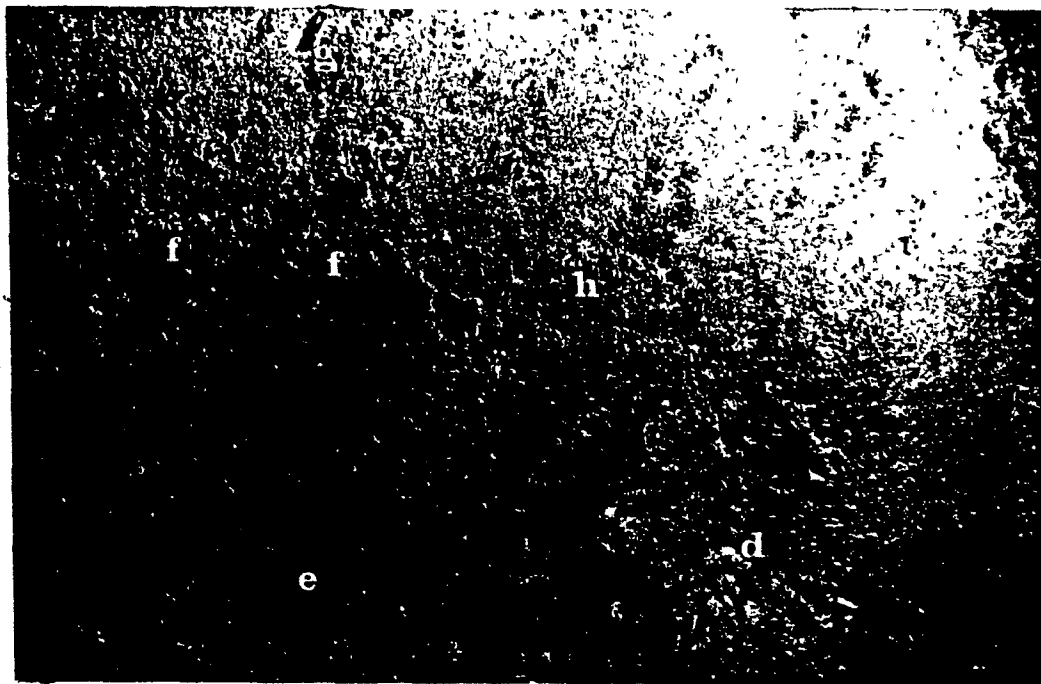
Plate 12A, B, C, D

Bottom photographs of the NAMOC floor at 56° 00' N, 49° 30' W; station H75-18; water depth 3,771 m (corrected). Current lineations (a), sediment tails (b), and deflected sediment tubes (c) indicate the existence of low to moderate bottom currents. Abundant animal tracks and trails (d) and their fecal/castings (e) as well as animals such as polychaetes (*Pectinaria* sp.) (f), holothurians (*Psolid* sp.) (g), sea anemones (h) and crustacean (i) dominate the floor. Area covered by photograph is approximately 1x1.5 m²; focal distance of 70 cm and camera angles of 38 and 51 were used (Edgerton deep-sea camera; model, 205; light model, 206 manufactured by Edgerton Bermeshausen, and Grier Inc. and supplied by Mr. N.E. Fenerty of Bedford Institute of Oceanography).

A



B



2

C



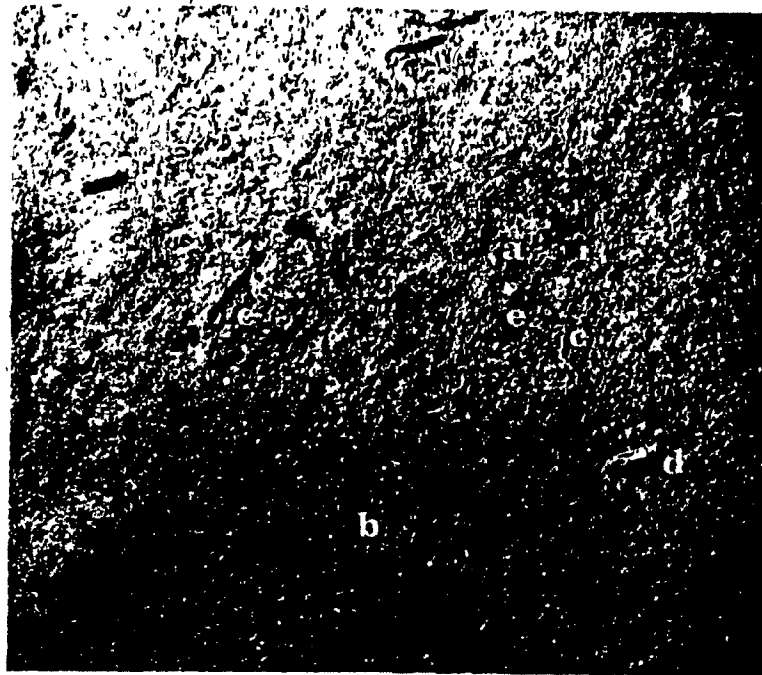
D



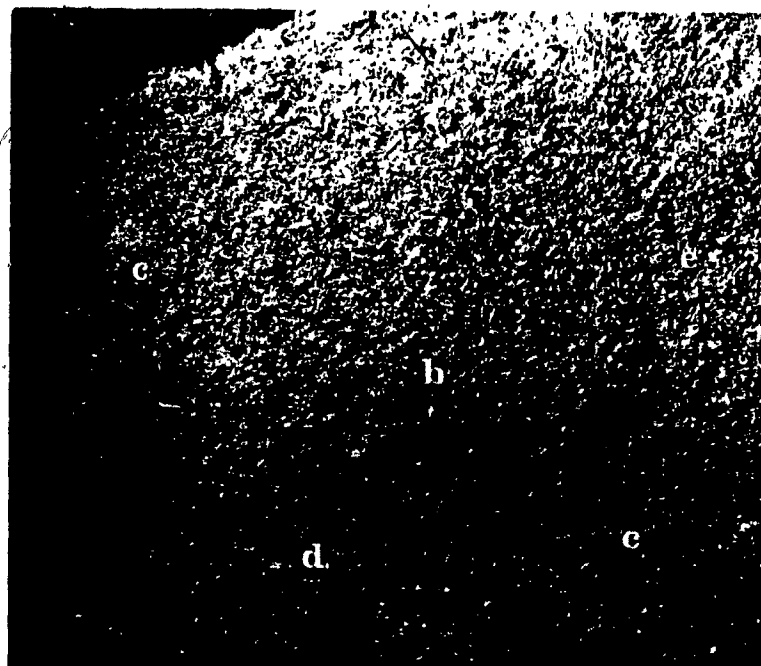
Plate 13A, B

Bottom photographs of the NAMOC channel wall at 50° 57' N, 50° 21' W; station H75-26; water depth 3,588 m (corrected). Existence of very weak bottom currents is indicated by sediment grooves; note abundant burrows (a), fecal castings (b) and animals such as polychaetes (c), holothurians (d); also scattered ice-rafted debris (e). Area covered by photograph approximately 1X1 m². Cloudy dust in the upper left corner of bottom picture is due to trigger weight. Camera settings same as for Plate 12.

A



B



Plates 14 to 16 are radiographs of contourites from Eirik Ridge; all natural scale (bar = 1 cm). Selected and arranged to demonstrate the state of preservation of original sedimentary structures: Plate 14, slightly to moderately bioturbated; Plate 15, very strongly bioturbated; Plate 16, completely bioturbated and mottled. For core locations see Figure 10.

Plate 14

Slightly to moderately bioturbated contourites (degree of bioturbation, 1-5%) showing relatively well preserved primary sedimentary structures (laminations), particularly in the topmost 5 cm in A and lower half of B and C.

- A. Core H75-29, core depth 174-198 cm.
- B. Core H75-29, core depth 34-58 cm.
- C. Core H75-30, core depth 118-142 cm.

Note the lack of distinct parallel laminations with systematic upward thickness variations which are characteristic for the laminated spill-over turbidites (cf. Plates 4 and 5); oblique fault-like features due to artificial disturbance.



Plate 15

Very strongly bioturbated contourites from Eirik Ridge (degree of bioturbation, 90-99%).

- A. Core H75-28, core depth 175-199 cm.
- B. Core H75-30, core depth 297-321 cm.
- C. Core H75-30, core depth 176-200 cm.

Note vague hummocky laminae in the middle portion of each section; the rest is intensely disturbed and mottled.



Plate 16

Completely bioturbated and mottled (degree of bioturbation, 100%).

- A. Core H75-28, core depth 85-109 cm.
- B. Core H75-30, core depth 440-464 cm.
- C. Core H75-30, core depth 469-493 cm.

No primary current-made sedimentary structures are preserved; whether they existed or not is uncertain. The degree of sediment mixing due to bioturbation is evident at the sand/lutite boundary in the middle of column B, where diffuse burrowing structures filled with pelagic lutite are visible in the top of the silt layer.

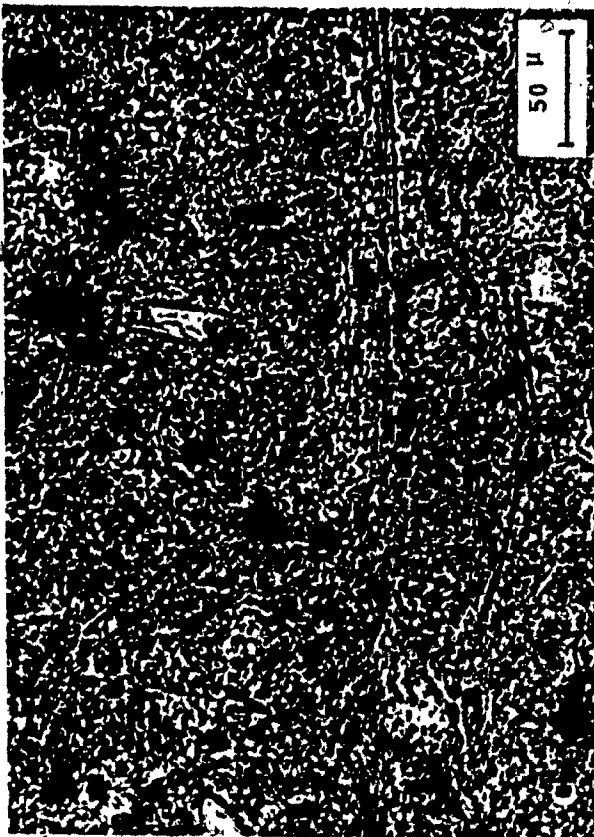


Plate 17

Photomicrographs of slightly to moderately bioturbated Eirik Ridge contourites (degree of bioturbation, 5%).

- A. Core H75-30, core depth 138-139 cm.
- B. Core H75-29, core depth 178-180 cm.
- C. Core H75-29, core depth 178-179 cm.
- D. Core H75-29, core depth 179-180 cm.

Note sharp boundary between coarse-grained band of biogenic debris and overlying fine-grained sediment in B. Imbrication or preferred orientation of biogenic debris is not evident. Note the lack of systematic variations in laminae thickness in A. C: Enlargement of the fine-grained sediment in B; fine-grained biogenic debris are randomly oriented. D: Enlargement of the coarse-grained sediment in B; note large foraminifera, abundant diatoms (a) and also terrigenous particles.



Plates 18 to 20 show a continuous layer-by-layer correlation of two adjacent right levee cores. Core H75-22 (B) is located 70 km downchannel from H75-24 (A). Length of individual section is 29 cm; bar = 1 cm. P = pelagic ooze; T_a, T_b, T_c and T_e are turbidite structure divisions of crudely laminated sand-silt-clay, lower parallel laminated sand, climbing ripple micro-cross-laminated silt, parallel laminated mud and homogeneous mud, respectively.

Plate 18

A. Core depth 88-67 cm.

B. Core depth 63-92 cm.

The one to one match of individual layers in the two columns is self-evident; for detailed analysis of B see Figure 28.

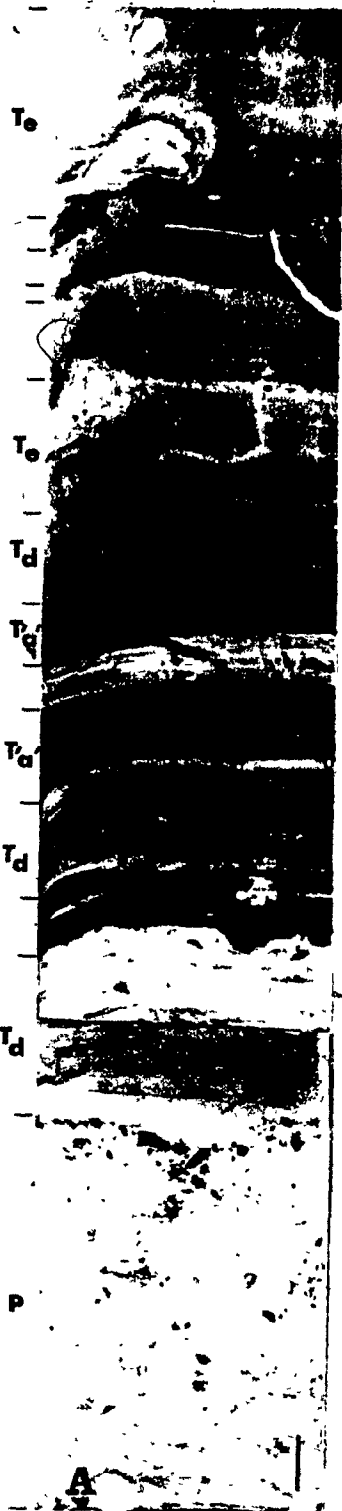


Plate 19

Correlation of cores H75-24 (A) and H75-22 (B). (Cont'd)

- A. Core depth 67-96 cm.
- B. Core depth 92-121 cm.

Parallel laminated turbidite mud bioturbated by oval and needle-shaped burrows in the uppermost 5 cm overlies completely bioturbated and mottled pelagic sediments (P) with abundant ice-rafted components; parallel laminations in the turbidite mud (T_d) in the bottom 5 cm are almost completely destroyed by the oval, tubular and needle-shaped burrows.

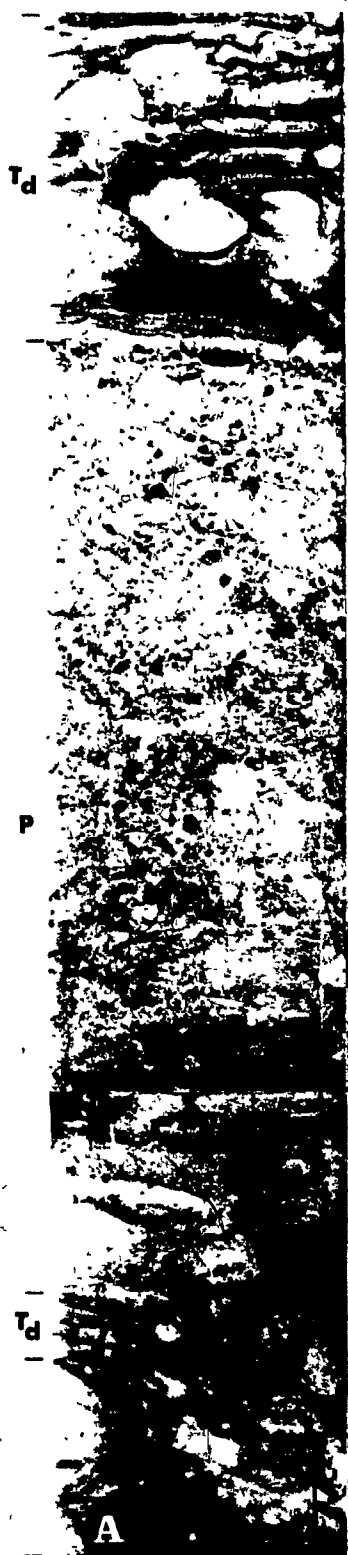


Plate 20

Correlation of cores H75-24 (A) and H75-22 (B). (Cont'd)

A. Core depth 129-158 cm.

B. Core depth 150-179 cm.

In the top 10 cm four crudely laminated "A"-divisions (T_a) match one another perfectly; also the parallel laminated mud units (laminations partly destroyed by the bioturbation) in the middle of the section match; also the types of burrows correlate from core to core as well.



Appendix 1. Deep-sea Channels of the World's Oceans

	Length (m)	Max. Width at Ledge Crest (m)	Max. Depth (m)	Cross-sectional Shape	Presence of talus	Relative Ledge Height	Relative Ledge Width	Longitudinal Gradient	Origin	Reference
ATLANTIC OCEAN										
Northeast Atlantic Mid-Ocean Channel	3,000	16	190	box-shaped, steep walls	+	right (west) levee 10-30 m higher	right levee 5-10 m wider	1:600 to 1:2500	depositional- erosional	Brink et al. (1983), Haxson et al. (1989), Johnson et al. (1977), Chapman and Moore (1976)
Equatorial Mid-Ocean Channel	21,200	76		V to U-shaped	+				erosional	Johnson et al. (1977), Egbert et al. (1972)
Northeast Atlantic Mid-Ocean Channel	3,500	10.4	140	V to U shaped	+	right levee higher			depositional- erosional	Charkis et al. (1978)
Equatorial Atlantic Mid-Ocean Channel	1,275	5-8	200	box-shaped	+	left (south) levee up to 25 m higher (S. Hemisphere)		1:1040	depositional- erosional	Haxson et al. (1989), Barnett and Gornitz (1976)
Outer Channel of Hudson Canyon	240		600	Irregular T-shaped channel		right levee (south) higher			depositional- erosional	Pratt (1967)
East and West Falkland Channel	800	30	400	U-shaped	(-)				erosional	Le Pichon et al. (1977)
Verm Channel	655	60(7)	700		(-)				erosional	Le Pichon et al. (1977)
Iberia-Biscaya Interplateau Channel	1,710	16	155	V to box-shaped	+			1:1500 to 1:2500	erosional	Laughton (1960, 1968)
Vidal Channel	2,000	5	250	V-shaped	+	either side		Av. 1:1100	erosional	Embrey et al. (1970)
Outer Cape Canyon	800	8	1,100	V to box-shaped	+		8 to 32 km wider	1:600	depositional- erosional	Haxson et al. (1984)
PACIFIC OCEAN										
Nootka Channel	270	4.5	230		+	right levee up to 27 m higher			depositional- erosional	Dill et al. (1964), Kearney (1965)
Sanroy Channel	700	5	400	V to U-shaped	+	right (north) levee 40 m higher	right levee 13 m wider	1:133 to 1:1250	depositional- erosional	Hess (1972), Hess and Riley (1972)
Relier Channel		6.5	200	V-shaped		right (west) levee higher (in order channel)				Harley (1960)
Scoones Channel	370	6	60	U-shaped		right levee higher			depositional	Griff and Mangler (1969)
Scott Channel		7.5	200	V-shaped		right (N.M.) levee higher				Harley (1960)
Hervey Channel		13	200	V-shaped		right (N.M.) levee higher				Harley (1960)
Cascadia Channel	2,200	9.3	300	U-shaped	+	right (N.M.) levee 6 to 70 m higher	right levee 7.5 m wider	Av. 1:1000	depositional- erosional	Gripps and Dula (1970)
INDIAN OCEAN										
Barrois (Eg) Channel	750	27	100	U-shaped	+				depositional- erosional	Stietz (1983), Curry and Moore (1972)

Appendix 2. Morphology of the NAMOC

Profile	Lat.	Long.	Corrected Water Depth m	Channel Depth (M) m	Difference in Levee Height (ΔH) (R-L), m	Floor (M ₁) km	Width Crest (M ₂) km	Slope Angle of Walls (degree) R L	Slope Angle of Levees (min.) R L	Talweg Width (M ₃) km	Talweg Depth (d) m	Slope Angle, Channel Floor (degree)	Crossed Course (degree)
N74-7a	60°10'N	56°11'W	3139	18	9.2	3.3	11.4				?	?	63
N74-7b	60°06'N	56°25'W	3157	93	20.5	8.1	20.0	3.0	1.5	2.1	7.3	0.4	63
N74-1a	60°04'N	56°11'W	3190	37	11	3.7	6.5	2.0	2.0	0.9	9.2	0.8	201
N74-2a	60°00'N	55°49'W	3238	37	29	(9.2)	(18.5)	1.5	1.5	2.8	3.7	0.3	90
N75-7a	59°58'N	55°40'W	3259	40	29	4.6	7.7	2.0	3.0	1.1	4.9	0.2	63
N75-7b	59°51'N	56°05'W	3196	102	13.5	3.9	12.3	3.0	2.0	1.1	2.7	0.5	63
N74-3a	59°56'N	55°21'W	3301	44	29	3.1	18.0	1.5	1.0	0.7	3.6	0.6	125
N74-4a	59°44'N	54°35'W	3364	93	14.6	(17.1)	(27.0)	1.0	1.5	7.2	18.3	0.6	119
N74-9	59°35'N	54°27'W	3393	192	73.2	3.6	19.2	3.0	1.5	1.4	6.1	0.5	63
N74-10	59°22'N	54°01'W	3420	183	91.5	4.4	16.3	4.0	4.0	1.2	9.2	0.9	243
N74-11	59°10'N	53°30'W	3449	134	73.2	4.8	10.8	5.5	5.0	1.0	9.2	1.0	63
N74-12	58°56'N	53°08'W	3503	146	64.0	2.8	8.6	2.5	2.0	0.7	9.2	1.2	63
N74-13	58°41'N	52°46'W	3530	137	64.0	3.3	8.3	6.0	3.5	1.9	9.2	1.0	243
N74-14	58°27'N	52°23'W	3555	128	73.2	3.6	10.0	3.5	5.0	0.5	16.0	2.0	64
N74-15	58°14'N	51°55'W	3579	118	82.4	2.4	8.4	3.8	3.0	0.4	0.5	0.5	245
N74-16	57°58'N	51°36'W	3594	119	64.1	3.4	7.7	11.5	6.5	?	?	?	63
N74-17	57°45'N	51°16'W	3625	101	73.2	3.5	10.1	14.0	13.0	1.0	?	2.0	243
N75-H	57°32'N	50°55'W	3652	102	73.1	2.1	5.0	3.0	9.0	0.7	7.2	0.6	230
N74-18	57°29'N	50°54'W	3658	92	82.4	2.2	11.0	3.0	2.9	0.8	9.2	2.0	65
N74-NRE-SSM	57°14'N	50°30'W	3694	96	62	3.5	12.7	2.0	2.0	1.1	3.7	0.2	217
N75-I	57°11'N	50°24'W	3709	73	96	4.5	11.0	2.0	2.0	1.3	13.0	0.2	245
N75-G	56°58'N	50°22'W	3731	110	88	2.6	7.4	7.0	3.0	0.7	2.5	0.5	252
N74-21	56°43'N	49°58'W	3740	106	99	3.5	14.3	2.9	2.0	1.0	2.5	0.4	63
N74-22	56°25'N	49°45'W	3757	118	46	4.5	14.2	3.0	3.0	1.1	4.6	0.3	245
N75-F	56°08'N	49°31'W	3776	73	46	(6.4)	(9.4)	10.0	0.7	1.0	9.2	1.5	260
N75-E	55°25'N	48°55'W	3888	128	56	2.9	10.8	3.5	3.5	0.5	9.2	0.5	260
N75-D	54°49'N	48°32'W	3909	128	28	3.0	14.8	4.5	3.0	1.1	4.6	0.4	250
LV12B-1	54°37'N	48°31'W	3928	147	46	3.7	14.8	5.1	2.5	1.4	0.9	0.4	237
N75-C	54°31'N	48°25'W	3936	146	18	3.6	13.0	6.0	7.0	0.9	0.6	0.5	250
N75-B	54°26'N	48°17'W								1.5	6.4		45
N74-6	53°51'N	48°10'W	3994	132	73	2.4	11.5	3.5	0.6	1.1	7.3	0.4	7248
LV12C-IIIB	53°32'N	47°31'W	4014	110	42	4.4	12.2	2.0	1.2	0.9	14.6	0.1	30
LV12C-IIIC	53°18'N	47°31'W	4024	102	51	4.8	18.9	5.5	4.0	0.4	1.5	0.01	223
N75-A	52°08'N	46°26'W	4047	91.5	73.2	3.4	18.7	1.5	3.0	?	?	?	68

N, W, LV: C.S.S. Hudson, R/V Minna, U.S.N.S. Lynch

() : Oblique channel crossing

R,L : Right, Left levee, respectively

a : Eastern branch of the upper channel

b : Western branch of the upper channel

Appendix 3. List of Cores

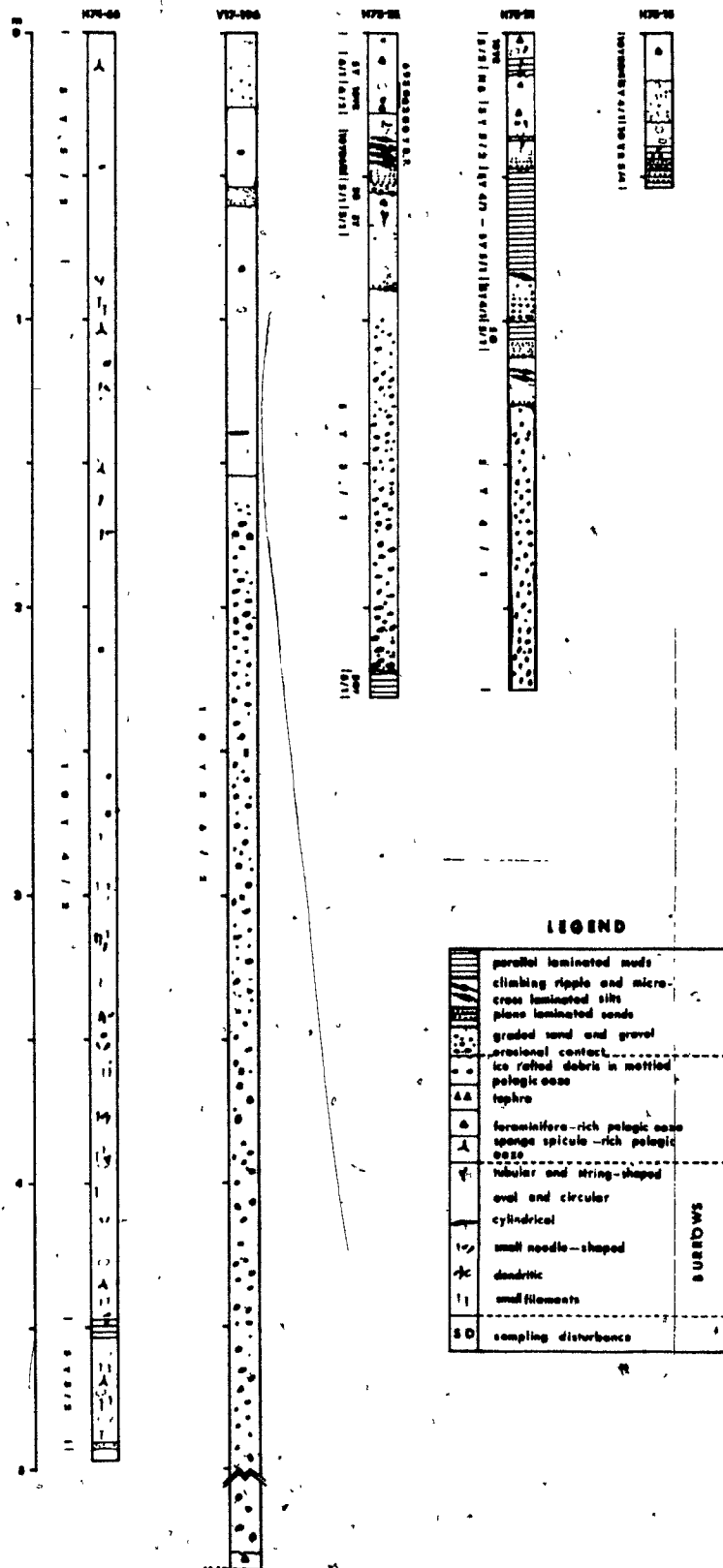
Station No.	Date Collected	Water Depth m, Corrected	Location	Latitude	Longitude	Core Length (cm)	Length of T.W. Core (cm)
H75- 1	Aug. 26, 1975	4047	LL	52°09.3'N	46°22.4'W	91	-
H75- 2	Sept. 2, 1975	3919	CF	54°23.5'N	48°17.3'W	-	23
H75- 4	Sept. 2, 1975	3783	RL	54°30.4'N	48°29.0'W	558	59
H75- 5	Sept. 2, 1975	3918	CF	54°31.7'N	48°24.8'W	26	-
H75- 6	Sept. 2, 1975	3929	CF	54°31.8'N	48°25.6'W	75	53
H75- 7	Sept. 2, 1975	3811	LL	54°32.6'N	48°20.2'W	836	17
H75- 8	Sept. 3, 1975	3756	RL	54°48.7'N	48°38.3'W	355	-
H75- 9	Sept. 3, 1975	3883	CF	54°51.2'N	48°31.7'W	300	12
H75-10	Sept. 3, 1975	3861	LL	54°50.5'N	48°26.0'W	406	8
H75-11	Sept. 3, 1975	3696	RL	55°24.0'N	48°59.7'W	575	12
H75-13	Sept. 3, 1975	3861	LL	55°25.7'N	48°49.6'W	708	68
H75-14	Sept. 4, 1975	3850	RL	56°07.1'N	49°39.6'W	135	-
H75-15	Sept. 4, 1975	3764	CF	56°07.8'N	49°30.2'W	54	-
H75-16	Sept. 4, 1975	3732	ICF	56°05.5'N	49°14.3'W	217	-
H75-17	Sept. 4, 1975	3699	ICL	56°07.5'N	49°16.8'W	365	-
H75-18	Sept. 4, 1975	3771	CF	56°08.2'N	49°31.7'W	camera station	
H75-20	Sept. 5, 1975	3635	LL	56°59.1'N	50°16.1'W	558	-
H75-21	Sept. 5, 1975	3718	CF	56°57.6'N	50°21.4'W	298	-
H75-22	Sept. 5, 1975	3553	LL	56°57.4'N	50°27.6'W	290	70
H75-23	Sept. 5, 1975	3579	RL	56°53.2'N	50°40.4'W	276	70
H75-24	Sept. 5, 1975	3507	RL	57°27.0'N	51°05.4'W	815	57
H75-25	Sept. 5, 1975	3646	CF	57°30.6'N	50°57.2'W	226	-
H75-26	Sept. 5, 1975	3588	CM	56°57.0'N	50°21.0'W	camera station	
H75-27	Sept. 6, 1975	3575	LL	57°31.2'N	50°53.6'W	478	-
H74-65	Oct. 19, 1974	3120	LL	59°58.7'N	56°15.3'W	158	-
H74-66	Oct. 19, 1974	3235	CF	60°00.1'N	55°49.5'W	499	-
H74-68	Oct. 20, 1974	3387	RL	59°32.9'N	54°29.9'W	850	-
H74-77	Oct. 28, 1974	3983	RL	53°52.0'N	48°09.2'W	grab sample	
H74-78	Oct. 28, 1974	3952	RL	53°52.9'N	48°08.7'W	grab sample	
V17-196	Sept. 6, 1961	2818	CF	60°44 'N	57°50 'W	1034	25
V17-191	Aug. 31, 1961	3768	CF	55°14 'N	48°50 'W	-	16
V16-228	Aug. 27, 1960	3407	RL	58°21 'N	52°18 'W	1170	-
V23-21	Aug. 17, 1966	4232	CF	52°06 'N	45°27 'W	100	-
V23-20	Aug. 17, 1966	4127	LL	51°24 'N	44°36 'W	930	39
A180-11	1952	5180	CF	39°07 'N	42°11 'W	370	-
H75-55	Sept. 11, 1975	2440	CM	61°30.3'N	58°38.6'W	724	-
H75-56	Sept. 11, 1975	2464	CF	61°26.9'N	58°33.4'W	386	-
H75-59	Sept. 12, 1975	1427	CF	62°39.9'N	59°29.8'W	710	-
H75-60	Sept. 12, 1975	1145	LL	62°40.6'N	59°22.4'W	700	-
H75-61	Sept. 12, 1975	1473	CF	62°18.7'N	59°36.1'W	819	-
H75-62	Sept. 13, 1975	1520	CF	62°23.7'N	59°18.1'W	798	-
H75-28	Sept. 7, 1975	3093	ER	57°36.6'N	45°05.1'W	627	-
H75-29	Sept. 7, 1975	2395	ER	58°00.2'N	45°00.4'W	912	-
H75-30	Sept. 7, 1975	2230	ER	58°11.9'N	45°40.3'W	900	-

Key: H - C.S.S. Hudson
V - R/V Vema
A - R/V Atlantis
T.W. - Trigger Weight

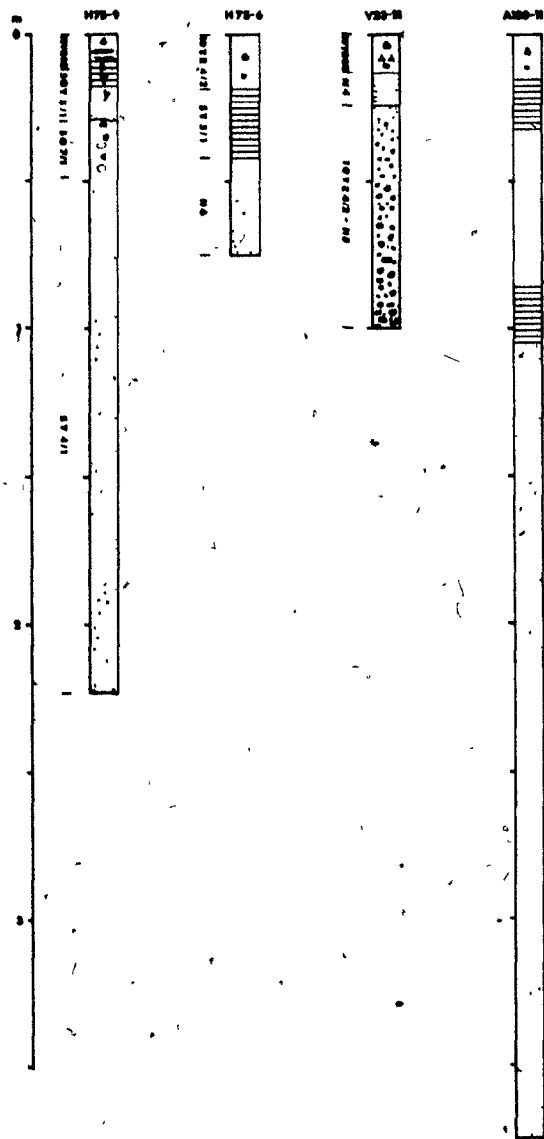
CF - Channel floor
CM - Channel wall
RL - Right levee

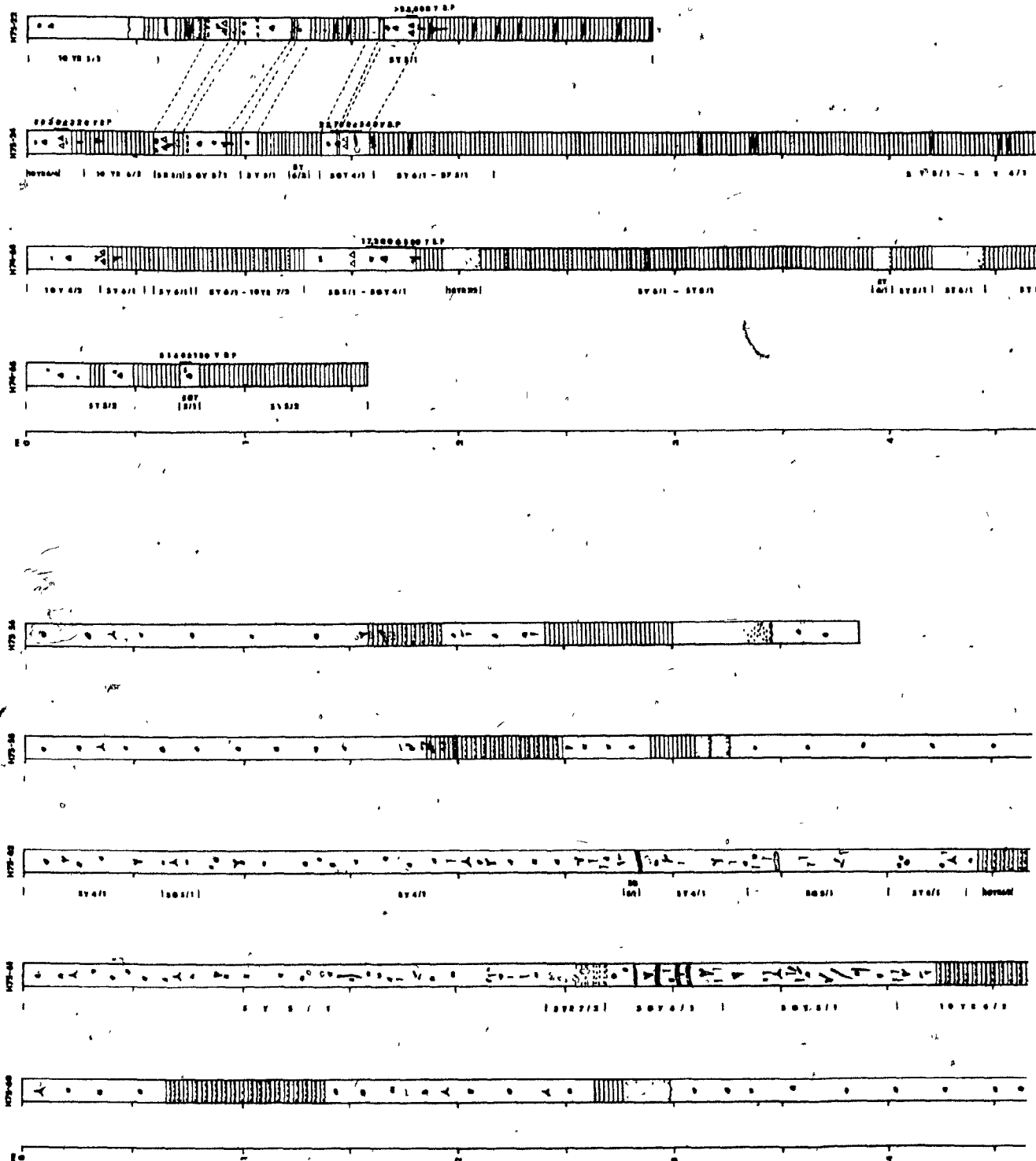
LL - Left levee
ICF - Imarssuak Channel Floor
ICL - Imarssuak Channel Levee
ER - Eirik Ridge

Appendix 4. Core Descriptions



Appendix 4. (Cont'd)







0 7 5 / 1 - 8 7 4 / 1



0 7 4 / 1

0 7 4 / 1

0 7 4 / 1

0 7 4 / 1

0 7 4 / 1

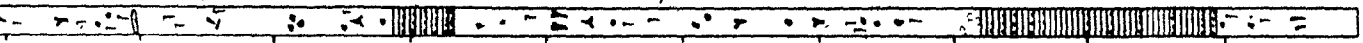
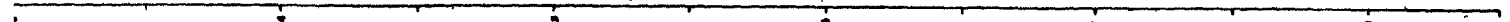
0 7 4 / 1

0 7 4 / 1

0 7 4 / 1

0 7 4 / 1 - 0 7 4 / 1

0 7 4 / 1



0 7 4 / 1

0 7 4 / 1

0 7 4 / 1

0 7 4 / 1

0 7 4 / 1

0 7 4 / 1

0 7 4 / 1

0 7 4 / 1

0 7 4 / 1

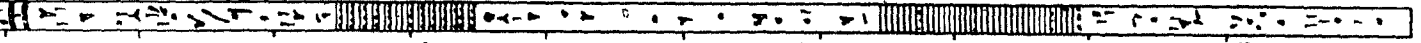
0 7 4 / 1

0 7 4 / 1

0 7 4 / 1

0 7 4 / 1

0 7 4 / 1



0 7 4 / 1

0 7 4 / 1

0 7 4 / 1

0 7 4 / 1

II

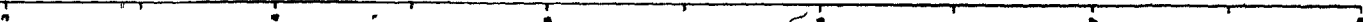
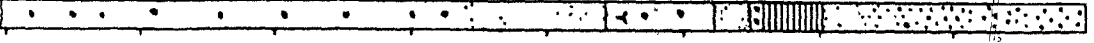
0 7 4 / 1

0 7 4 / 1

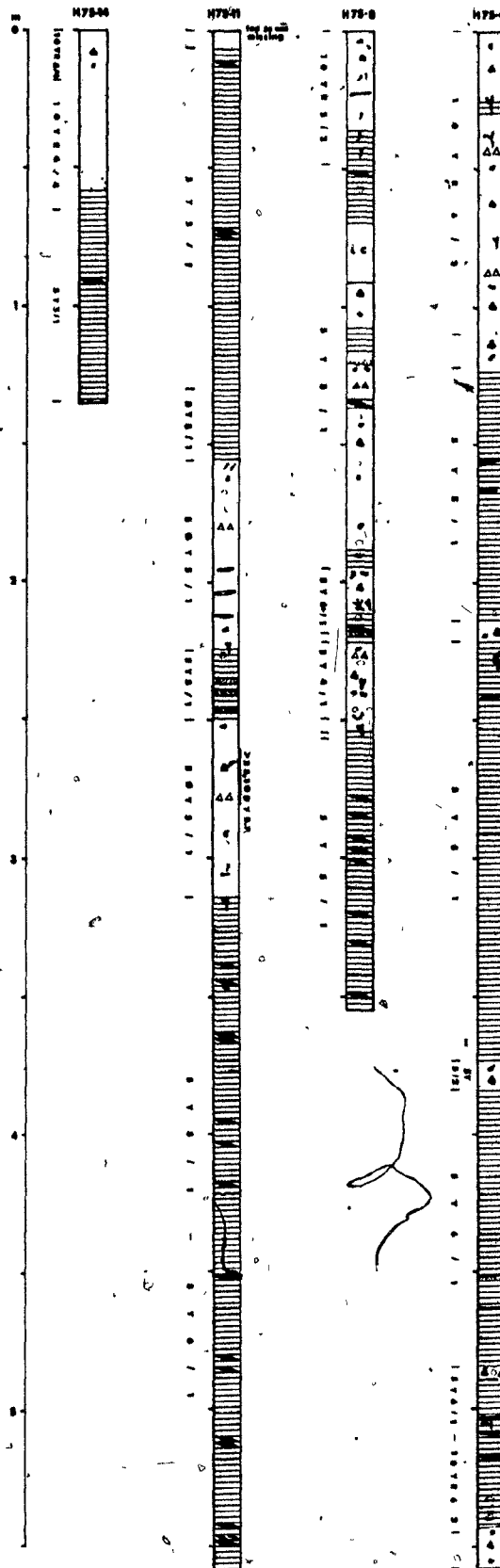
0 7 4 / 1

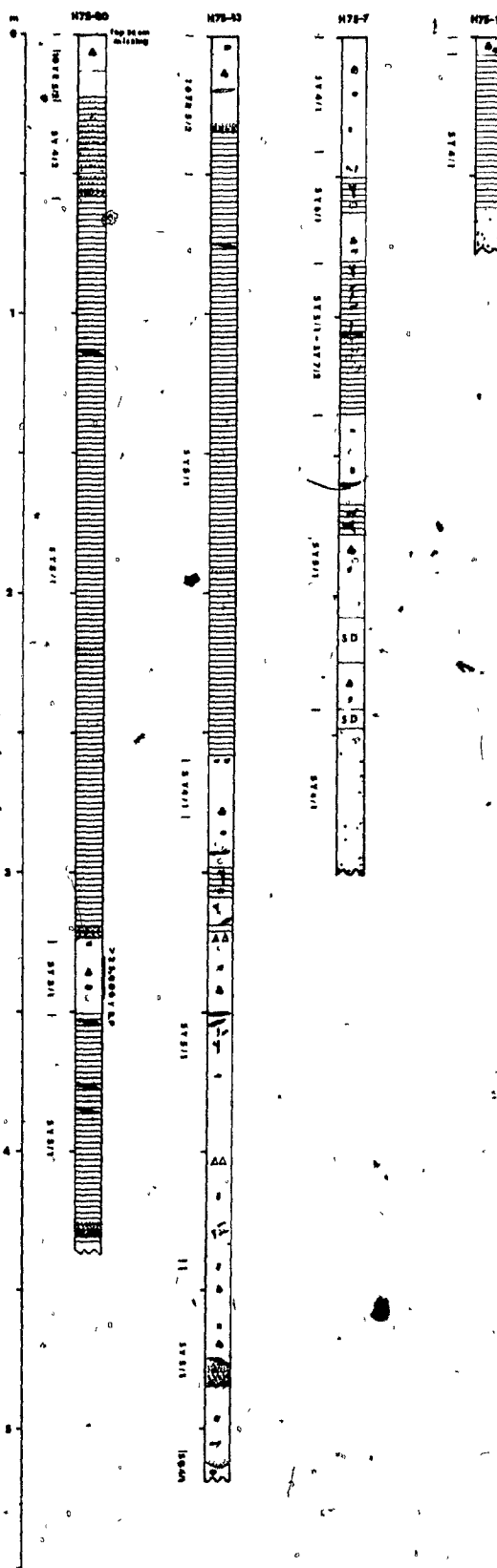
0 7 4 / 1

0 7 4 / 1



Appendix 4. (Cont'd)





Appendix 5. Grain Size Parameters

Core No.	Core Depth (cm)	Bottom (Turbidite) Division	Median (ϕ)	Mean (ϕ)	Inclusive Stand. Dev. (σ_2)	Graphic Skewness (S_{k_2})	Kurtosis (K_2)	Max. Size (ϕ)	ϕ	ϕ (ϕ)	SI	C
I. Channel-Fill Facies												
H75-25	100-110		-1.3	-1.2	2.69	+0.24	0.77	-4	53.75	42.15	1.90	2.20
	140-160		-2.2	-1.37	2.55	+0.46	0.77	-4	58.22	37.50	1.97	2.31
	180-190		-2.9	-1.57	3.28	+0.46	0.88	-4	62.79	28.55	4.73	3.93
V23-21	60-65		-2.2	-	-	-	-	-2	92.08	6.59	0.86	0.08
II. Spill-over Facies												
A. Right levee												
H75-22	60-70	E	8.8	8.56	1.71	-1.06	0.9	1.23		0.07	36.2	62.1
	70-73	D	8.6	8.40	1.90	-0.13	0.7	1.23		0.08	44.0	56.0
	73.5-75	D	7.0	7.86	2.75	+0.52	1.0	1.5		0.6	63.7	36.8
	75-75.5	C	5.5	5.53	0.99	+0.24	1.55	1.0		4.6	89.4	6.10
	75.5-77.5	"A"	6.5	6.70	3.27	+0.11	0.93	-1.24	0.25	25.51	43.34	31.0
H75-22	269-270	D	9.2	-	-	-	-	3.74		0.001	33.0	67.10
	271-272	D	8.2	8.30	1.99	+0.04	0.61	2.74		0.006	46.7	53.50
	272-273	D	7.1	7.77	2.20	+0.38	0.68	2.41		0.02	61.3	38.40
	274-275	C	5.4	5.46	0.99	+0.30	1.60	2.47		0.39	94.6	5.40
	785.5-786.4	D	7.6	8.43	2.91	+0.43	0.82	2.47		0.098	55.68	44.22
H74-68	787.5-788.5	D	7.1	7.97	2.77	+0.54	0.82	1.74		0.75	59.58	39.67
	791-792	C	5.3	6.03	2.36	+0.64	1.76	1.23		3.80	78.32	17.88
	792-793	C	4.8	5.33	2.16	+0.65	2.14	1.74		13.63	73.77	12.60
	793-794	C	4.5	4.80	1.97	+0.58	3.14	-0.24		20.54	69.43	10.03
	489-495	D	9.0	-	-	-	-	1.5		0.09	36.86	62.93
H74-68	496-500	C	4.7	4.97	1.37	+0.37	2.08	1.23		8.72	84.13	7.15
	500-504	C	4.7	4.87	1.29	+0.45	2.01	1.23		17.06	76.50	6.45
	504-506	"A"	7.3	6.77	4.53	-0.08	1.12	-1.0		21.61	36.65	41.74
	506-508	"A"	7.3	-	-	-	-	-1.24	0.30	23.80	34.59	41.31
B. Left levee												
H75-13	476-477	D	5.2	5.9	2.38	0.69	1.99	-		2.72	79.81	16.47
	477-480	C	4.9	4.96	1.10	0.11	2.05	-		5.84	88.77	5.39
	480-481	B	4.4	4.60	1.55	0.62	3.64	-		16.28	75.51	7.21
	481-483	A	0.8	1.60	1.76	0.63	0.73	-4	1.88	86.01	11.64	2.33
H75-20	426-427	B	1.0	1.80	2.32	0.72	2.20	-		81.48	13.34	5.18
	427-429	B	1.0	-	-	-	-	-		88.95	2.47	8.48
III. Pelagic Facies												
H74-68	145-146	F	7.7	8.23	3.05	+0.27	0.90	1.23		4.71	50.29	95.00
H74-66	445-446	F	10.3	10.1	2.52	-0.10	0.81	1.74		0.37	20.59	79.40
	460-461	F	7.9	-	-	-	-	1.5		1.85	50.02	48.12
	480-481	F	7.6	8.13	2.83	+0.29	0.84	1.5		0.21	53.96	46.04
H75-4	115-122	F	5.7	5.63	2.73	-0.04	0.61	-4	0.94	33.04	32.35	33.57
	211-216	F	7.2	6.83	3.54	-0.20	0.70	-4	2.89	24.47	39.93	32.71
H74-65	20-21	F	7.2	7.1	3.85	+0.03	0.96	-1.24	0.23	20.21	46.27	33.29
H74-77	0-10	F	8.9	8.43	1.29	-0.49	0.80	1.0	1	0.43	34.49	65.07
H74-78	0-10	F	6.5	6.27	2.85	-0.09	0.72	0.0		37.02	43.53	30.62
IV. Contourite Facies												
H75-29	48-58	sporadic bioturb.	8.0	-	-	-	-	-		7.43	44.76	47.81
H75-30	185-192	v. strongly bioturb.	6.9	7.8	2.85	0.51	1.01	-		2.48	60.19	37.33
H75-30	473-480	mottled	6.0	-	-	-	-	-		5.07	67.10	27.83

G- Gravel, S- Sand, SI- Silt, C- Clay

Appendix 6. Lithology of Channel-fill Pebbles
(in percent)

Core No.	Core Depth (cm)	Carbonate	Granite Gneiss	Sandstone	Amphibolite	Gabbro	Basalt	Anorthosite	Others	Total No.
V17-196	500-600	54.3	43.3	1.0	0.5	0.5	0.5	-	-	210
H75-25	100-110	54.4	31.3	6.5	2.3	1.4	2.3	0.5	Ironstone (1.4)	217
H75-25	140-150	46.5	44.8	1.2	1.2	1.7	2.3	1.7	Sillimanite-schist (0.6)	172
H75-25	180-190	49.5	32.0	7.0	2.0	3.0	4.5	0.5	Sillimanite-schist (1.5)	200
H75-21	150-160	47.9	22.9	20.8	2.1	4.2	2.1	-	-	48
H75-21	210-225	52.4	31.7	8.5	3.7	1.2	2.4	-	-	82
H75-14	53-57	23.0	20.5	46.2	2.6	5.1	2.6	-	-	39
H75-13	480-483	40	60	-	-	-	-	-	-	5
V23-21	60-65	48.8	40.8	4.8	1.6	1.6	-	1.6	Ironstone (0.8)	125
		46.3	36.4	10.6	1.7	2.1	1.9	0.5		1098

Appendix 8. Abundance of Ice-rafted Tephra and
Ice-rafted Debris (IRD)

Core No.	Core Depth (cm)	Tephra grains/g, > 63 μ	IRD grains/g, total sample
H75-61	9-12	-	8,611
	18-20	-	21,106
	49-52	-	6,466
	89-92	-	15,937
	119-122	-	18,540
	159-162	-	4,592
H74-68	33-34	10	6,244
	142-143	4	1,782
	145-146	4	911
	148-149	3	5,565
	151-152	4	147
	155-156	1	950
H75-25	3-6	-	18,408
	17-20	-	
H75-24	9-12*	-	30,502
	14-17	6	7,063
	59-62	11	8,238
	64-67	8	6,818
	79-82	4	2,524
	84-87	7	10,208
	99-102	5	9,125
	139-142	7	17,982
	144-147	25	1,222
	149-152	6	2,867
	154-157	5	606
H75-22	14-17	-	8,238
	79-82	2	8,988
	89-92	22	3,299
	109-112	8	3,299
	164-167	2	761
	169-172	1	4,177
	172-182	17	2,682
H75-21	10-13	-	820
	17-20	-	2,603

Appendix 8 (Cont'd)

Core No.	Core Depth (cm)	Tephra grains/g, > 63 μ	IRD grains/g, total sample
H75-13	16-19	-	33,244
	267-270	-	11,337
	310-313	-	731
	320-323	1	4,180
	337-340	-	4,149
	350-353	-	491
	376-379	-	563
	390-393	-	435
	402-405	60	315
	449-452	-	7,045
H75-11	175-178	19	5,327
	184-187	12	2,013
	274-277	44	504
H75-8	10-13	-	813
	22-25	-	1,006
	223-226	2	269
	242-245	-	-
H75-4	10-13	-	8,164
	44-47	3	1,205
	67-70	-	2,182
	86-89	1	12,986
	94-97	-	18,002
	107-110	-	9,663
	115-122	-	96
	211-216	-	175
	545-558	-	81

Appendix 9 Organic Carbon and Carbonate Contents

Core No.	Core Depth (cm)	Organic Carbon (%)	Carbonate (%)	Total Carbon (%)
H74-66	50-51	0.61	3.17	3.78
	98-100	0.67	2.76	3.43
	191-192	0.68	2.47	3.15
	301-302	0.51	2.01	2.52
	441-442	0.56	0.73	1.29
	450-451	0.30	0.43	0.73
	455-456	0.55	1.97	2.52
	490-492	0.85	3.20	4.05
H74-68	38-39	0.57	2.73	3.30
	141-142	0.19	1.14	1.33
	171-172	0.23	1.59	1.82
	210-211	0.97	3.97	4.94
	484-485	1.05	3.12	4.17
	620-621	1.00	4.00	5.10
	801-802	0.79	3.41	4.20
H75-62	10-12	0.39	1.12	1.51
	195-197	0.36	2.10	2.46
	410-412	0.54	0.69	1.23
	690-692	0.73	4.69	5.42
	760-762	0.38	0.93	1.31
H75-24	0-4	0.42	4.05	4.47
	80-82	0.35	0.85	1.20
	156-158	0.30	1.57	1.87
	350-352	0.89	2.13	3.02
	550-552	0.83	4.35	5.18
	750-752	0.92	4.74	5.66
H75-22	68-70	0.48	3.66	4.14
	195-197	0.69	3.94	4.63
	233-235	0.88	4.18	5.06
	283-285	0.96	4.31	5.27
H75-13	10-12	0.49	4.41	4.90
	50-52	0.65	2.93	3.58
	200-202	0.88	2.66	3.54
	260-262	0.43	1.59	2.02
	330-332	0.29	1.27	1.56
	430-432	0.50	1.77	2.27

Appendix 9. (Cont'd)

Core No.	Core Depth (cm)	Organic Carbon (%)	Carbonate (%)	Total Carbon (%)
H75-4	5-7	0.19	2.82	3.01
	100-102	0.33	2.66	2.99
	250-252	0.93	3.09	4.02
	470-472	0.92	2.16	3.08
H75-25	5-10	0.34	3.03	3.37
	30-32	0.38	2.72	3.10

Appendix 10. Method to Impregnate Mud for
Thin Section Preparation

I. Replace water with acetone in vapor tight container.

- a. 75% chloroform, 25% acetone for 1 day;
- b. 50% " , 50% " " 1 " ;
- c. 25% " , 75% " " 1 " ;
- d. 0 " , 100% " " 2 days.

Decant fluid.

II. Replace acetone with epoxy in vapor tight container.

100 parts	araldite resin (No. 6010)	
28 "	hardener (No. 972)	for 3 days
47 "	acetone	

III. Cure specimen.

Remove cover of container to allow evaporation of acetone for 3 days.

Place in oven at 30-40°C for 1 day.

Place in oven at 60°C for 1 day.